EFFECT OF MAGNETIZATION ON MECHANICAL PROPERTIES AND FORMABILITY OF STEEL SHEETS

by

RAVI DATT YADAV
(2K18/PHDME/511)

Under the Supervision of
Prof. Vijay Gautam

Department of Mechanical Engineering

Submitted
in fulfillment of the requirements of the degree of
Doctor of Philosophy
to the

DELHI TECHNOLOGICAL UNIVERSITY

APRIL 2024

CERTIFICATE

This is to certify that the thesis entitled "**Effect of Magnetization on Mechanical Properties and Formability of Steel Sheets**" being submitted by **Mr. Ravi Datt Yadav** to the **Delhi Technological University, Delhi** for the award of the degree of **Doctor of Philosophy** in the Department of Mechanical Engineering is a bonafide research work carried out by him under my supervision and guidance. To the best of my knowledge the thesis has reached the requisite standard. The research reports and the results presented in this thesis have not been submitted in parts or in full to any other University or Institute for the award of any degree or diploma.

(**Dr. Vijay Gautam**)
Professor
Department of Mechanical Engineering
Delhi Technological University
Delhi-110042

Date: 12.04.2024

ACKNOWLEDGEMENTS

I would like to express my profound appreciation and heartfelt thanks to **Prof. Vijay Gautam** for providing me with the chance to cooperate with him on this research project. Throughout this effort, I have gained a great deal of knowledge from his exceptional intellect, passion, leadership, focus, and perseverance, all of which made it almost challenging for the thesis to be completed on time. Really few words are used to request his cooperation and favour. He has my sincere gratitude in every way.

I express my deep sense of gratitude to **Prof. D. Ravi Kumar (IIT Delhi), Prof. Surendra Kumar Rathore (RTU Kota), Prof. R.C Singh (MED DTU) and Prof. Amit Kumar Shrivastava (CED DTU)** for being part of my thesis committee. Their questions and valuable suggestions during my presentations and examinations have been very useful in providing direction to my research work. I have been fortunate enough to interact with **Prof. A. K. Agrawal** who gave me valuable suggestions to complete my thesis work. I am also grateful to **Prof. S. K. Garg**, Head of Department of Mechanical Engineering and other faculty members for their kind support in carrying out my research work.

My special thanks to my younger brother **Mr. Rakesh Kumar** for his constant encouragement and unconditional support. Thanks to my senior and fellow research scholars **Dr. Pankaj Kumar Sharma, Dr. Nanak Ram, Mr. Subhjit Konar, Mr. Bijendra Kumar, Mr. Praveen Kumar Singh, Mr. T. Sankar Ram** and **Mr. Akash** for their fruitful and productive association that made my each and every visit to DTU Delhi full of pleasant and memorable experiences.

I would like to thank **Mr. Om Parkash** and **Mr. Takchand** for their kind support for the experimental work carried out at DTU Delhi.

ABSTRACT

The current study discusses how a change in tensile characteristics with an applied magnetic field improves the formability of a dual phase steel sheet. The work also reports a novel design of an electromagnetic uniaxial tensile test tool and its performance analysis to assess the effect of magnetic field on tensile properties. The electromagnetic tool is developed as an external attachment to a conventional uniaxial tensile test specimen while testing in a universal testing machine. For the simulations, five different configurations of electromagnetic tools are modelled with different magnetic flux density. Based on the predicted results of magnetic flux density distribution, obtained from simulations and analytical model, the electromagnetic tools are designed and fabricated. Furthermore, uniaxial tensile tests were performed with electromagnetic tools to analyze the tensile properties, and the optimal tool was identified based on the results. For the effect of magnetization on the steel sheet two grades of steels were select DP590 and ZC440 in three different directions.

The experimental results obtained from tensile tests show a significant improvement in the tensile strength and normal anisotropy due to magnetic field. A negligible change in strain hardening exponent with a slight decrease in percentage elongation was also observed due to the magnetic field. The effect of magnetic field was observed in the higher thicknesses of both steels in term of ultimate tensile strength and anisotropy. It was observed that higher magnetization of material ZC440 steel gives the better results when compared to the DP590 steel sheet. The samples for microstructural investigations using electron backscattered diffraction technique were taken from the middle of the specimens tested with 20% of plastic strain in all the cases of experiments performed with and without the magnetic field. The magnetic force microscopy frequency analysis was also performed to evaluate the evidences of magnetic field on the tensile tested specimens. A significant increase in the values of strengths and anisotropy but a slight decrease in ductility and strain hardening exponent were observed

in the specimens tested with the magnetic field. A modified electromagnetic tool was also developed as an attachment with sheet samples for conducting experiments on an Erichsen cupping machine to evaluate the forming behavior of the sheet. The results of Erichsen cupping experiments were obtained with and without magnetic field and it is observed that the magnetic field increases the values of Erichsen Index suggesting an enhanced formability. The value of Erichsen Index increased in both material but the value of ZC440 Erichsen index was higher when compared to the DP590.

Numerical simulations were carried out using a finite element (FE) method-based software to simulate Erichsen cupping test and predict punch force and Erichsen Index in both parent of ZC440 and DP590 sheets. The predicted results were validated with experimental work. The FE results showed a value of reduction in sheet thickness during stretching was validated with the experimental data. The experimental reading of sheet thickness was measured by the Creo software by putting the image of the samples. The increasing value of punch force was validated in the FE results. Comparison of the experimental versus simulation results of the Erichsen cupping test confirmed that the MF increased the formability of the sheet. It was also confirmed that the MF has more effected on the ZC440 material as compared to the DP590 material. This newly developed electromagnetic tool setup worked on the basic of the magnetization behaviour of the material as well the sheet thickness of the material.

Keywords**:** *Magnetic field, Magnetostatic Finite element analysis, Magnetic flux density, Ultimate tensile strength, Yield strength, Strain hardening exponent, Normal anisotropy, ductility, Electron backscattered diffraction*

TABLE OF CONTENTS

LIST OF FIGURES

LIST OF TABLES

ABBREVIATIONS

OSU	Ohio State University
LDR	Limiting Draw Ratio
LDH	Limiting Dome height
RD	Rolling Direction
BCC	Body Centered Cubic
XRD	X-ray diffraction
EBSD	Electron backscattered diffraction
SEM	Scanning electron microscopes
TD	Transverse direction
ND	Normal direction
ODF	orientation distribution function
UTS	Ultimate Tensile Strength
DSM	Domain Structure Model
ZC440	High Strength C-Mn Steel Sheet
DP590	Dual Phase
EMUTT	Electromagnetic Uniaxial Tensile Test Tool
CAD	Computer Aided Design
FEA	Finite Element Analysis
VSM	Vibrating Sample Magnetometer
UTM	Universal Testing Machine
FEG	Field Emission Gun
IE	Erichsen Index
FEM	Finite Element Method
LAGB	Low Angle Grain Boundaries
HAGB	High Angle Grain Boundaries
KAM	Kernel Average Misorientation

NOMENCLATURE

n	Strain hardening exponent
$\bar{R}$	Normal anisotropy
m	Strain rate sensitivity index
σ	True stress
ε	True strain
ε_w	Strain in width of tensile specimen
ε_t	Strain in thickness of tensile specimen
ε_l	Strain in length of tensile specimen
R	Plastic strain ratio
ΔR	Planar anisotropy
B	Magnetic flux density
M	Magnetising force
tool-A, tool-B, tool-C, tool-D, tool-E	Electromagnetic Uniaxial Tensile Test ToolS
Le	Length of the electromagnet coil
dc	Diameter of the enabled copper wire
r	radius of coil
I	Current
V	Voltage
$\vec{S}$	Distance vector
$\vec{P}$	Position vector
$\vec{\imath}, \vec{\jmath}\ \vec{k}$	Unit vector in X, Y and Z axis
R'	Distance between the center of the coil and the point P (x, y, z)
H_{1x}, H_{1y}, and H_{1z}	Magnetic field strengths in X, Y, and Z directions

R_p	Distance measured from a point O to a point P
j	Represents the number of turns of coil radially
i	represents the number of turns of coil in the longitudinal
r_{1x}, r_{1z} and y	Initial points in Cartesian coordinates
H_t	Total magnetic field strength
μ_0	Permeability of air in free space
B_f	Final magnetic flux density
M_{TS}	Value of the magnetization taken from the B-M plot
σ_e	Engineering stress
ε_s	Engineering strain
K	strength coefficient
w_0, l_0	Initial width and length of tensile specimen
w_f, l_f	Final width and length of tensile specimen
$s(R)$	Standard deviation of the plastic strain ratio
$s(\varepsilon_w)$ and $s(\varepsilon_l)$	Standard deviation in values of true strains in width and length
$v(R)$	Coefficients of variation
R_{11}, R_{22}, R_{33}, R_{12}, R_{13} and R_{23}.	Anisotropic yield stress ratios

CHAPTER 1

INTRODUCTION

It is interesting to note the correlation between magnetic fields and alloy plasticity, especially in high silicon Fe-Si alloys [1,2]. Increasing silicon content in Fe-Si alloys can lead to deterioration in their plastic deformation capacity, which impacts their processing and application potential [3-5]. It seems that the impact of magnetic fields on the properties of materials, such as plastic deformation and dislocation dynamics, is a complicated and diverse subject that needs in-depth research. Magnetic fields influence various characteristics of solids, including grain boundary structure [6,7], residual stress [8], and atomic diffusion within alloys [9]. High gradient magnetic fields can affect the diffusion of elements like silicon, altering phase nucleation and growth within alloys [10]. Magnetic fields can modify the spin state of electrons, reducing the energy required for dislocation motion. This phenomenon, known as magneto-plasticity effect, can enhance the plastic deformation capacity of materials [11-13]. External magnetic fields can alter the stress fields around ferromagnetic phases, influencing dislocation emissions and thereby changing dislocation configurations in alloys [14,15].

The impact of magneto-plasticity was observed in single crystals of hydronium and metals [16-19], including LiF, Al, and Fe. An external magnetic field may alter a material's plasticity; in this case, the ferromagnetic Fe-Al phase's residual stress field was altered by applying a static magnetic field. This resulted in the Fe-Al phase emitting dislocations around it, changing the dislocation configurations in Al alloys [20]. Dislocation movement, slip system operation, and crystal anisotropy may all work to influence an alloy's plasticity because the movement of dislocation along slip orientations in glide planes is the primary regime of plastic deformation. However, polycrystal plasticity and polymorphic deformation of alloys are

complex, the relationship between slip systems, crystal orientation, and magnetoplasticity has not been explored or documented in literature. The multifaceted impact of magnetic fields on alloy properties, particularly plasticity, and suggests the necessity of further research, especially focusing on the relationship between crystallographic features, dislocation dynamics, and magnetic influences to advance the understanding and utilization of alloys in various applications.

1.1 Magnetization

The magnetic fields required to magnetise individual domains to saturation are modest in ferromagnets, hence it is possible to suppose that in a zero applied field, individual domains are fully magnetised while the net magnetization of the entire specimen is zero [21]. When an external magnetic field is applied, domains oriented in the field begin to expand at the expense of other domains. This is achieved by domain wall motion as shown in Figure 1.1 [22].

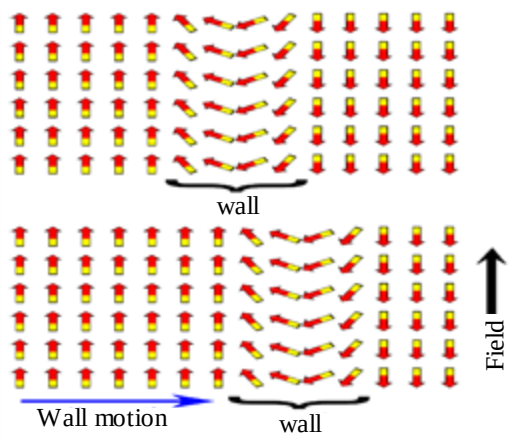

Figure 1.1 Schematic diagram of domain wall motion [22].

The domain magnetization will eventually be reoriented in the direction of the easy axis that is closest to the applied field's direction if the applied magnetic field is strong enough to overcome the anisotropy energy. The domain walls and the direction of the domain magnetization will be difficult to move if the anisotropy energy is large, which results in a high coercive field. As a result, the material will be challenging to magnetise to saturation and

challenging to demagnetize back to zero magnetization [21]. Additionally, anchoring the domain walls might strengthen the coercive field. Imperfections, inherent stresses, and defects prevent the domain wall from moving freely, which increases coercivity.

Magnets are known to be indifferent to certain materials; for example, they will fall straight down a wooden wall. Iron, nickel, and cobalt-based items typically draw magnets materials as ferromagnetic materials [23]. These metals have unique atoms that are the reason magnets are drawn to them. The magnetic moments of the atoms within the majority of other non-magnetic materials are all oriented in random directions and cancel each other out. Atoms arrange themselves into formations known as domains in ferromagnetic materials. As seen in Figure 1.2, a domain is an area inside a material where groups of magnetic moments naturally align in the same direction.

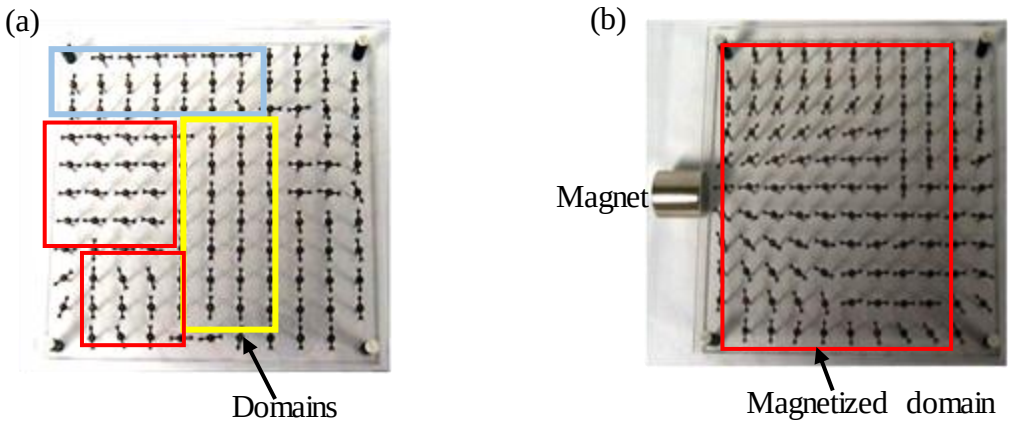

Figure 1.2 Domain boundary representation in ferromagnetic material (a) without magnetization (b) with magnetization [24].

An object can contain many domains. As illustrated in Figure 1.2 (a), the domains are likewise randomly orientated in the absence of an external magnetic field to produce a net magnetic field. On the other hand, as Figure 1.2 (b) illustrates, the domains will spin and align with the external magnetic field when it exists. The entire thing gets magnetised in that direction and turns into a magnet when all or most of the domains are aligned in that direction. Induction is the process of magnetising another object with the help of a magnetic field. As long as the

magnet's domains remain aligned, once it has been induced, it will produce its own magnetic field [25].

However, the domains can also exist in other configurations where their magnetization is generally pointing in the same direction, resulting in an external magnetic field, as shown in Figure 1.3 [26]. Although these are not minimum energy configurations, due to a phenomenon in which the domain walls become "pinned" to defects in the crystal lattice, they can be local energy minimums and hence very stable [26].

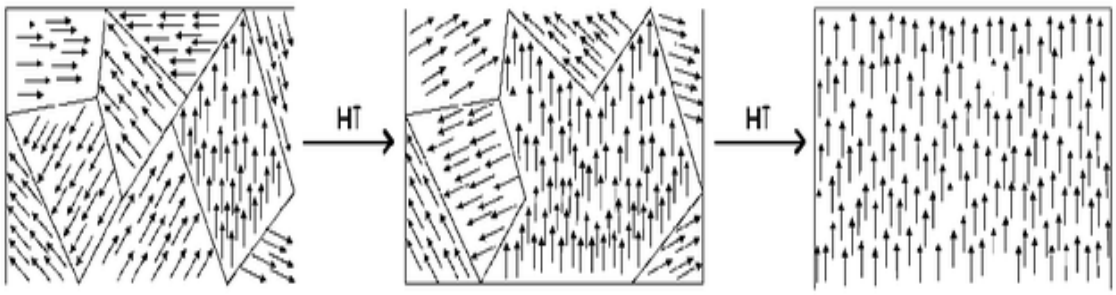

Figure 1.3 Magnetic domains orientation rotation and enlargement in response to an applied external field [26].

When an external magnetic field is applied to the material, the domain walls can move, leading to the growth of domains aligned with the field and the shrinkage of opposing domains. The domain walls stay stuck in their new orientation when the external field is withdrawn, and the aligned domains generate a magnetic field. A chunk of ferromagnetic material that has been "magnetised" to the point of becoming a permanent magnet looks like this [27].

1.2 Sheet metal forming

In order to manufacture complicated components for the automotive industry, home appliances, aviation parts, etc. with the least amount of material waste and energy consumption while allowing the designer to take advantage of the inherent qualities of the

material, sheet metal forming is crucial. It includes applying external forces that create significant plastic deformation in the material to flat sheet metal blanks in order to shape them into components of the required forms, either in one step or in numerous phases. Applying a compressive load, tensile force, or a combination of both compression and tensile load causes the plastic deformation. Figure 1.4 illustrates a few of the frequently used sheet metal forming techniques, including stretch forming, deep drawing, and bending.

During a stretch forming process, a punch or rigid tool is used to distort the material into the desired shape after the edges of a sheet metal blank are clamped using a strong blank holding force as shown in Figure 1.4 (a). The material is exposed to only tensile pressures throughout the stretch forming process. Compared to rolled or drawn parts, this method offers superior surface quality and shape control [28]. The aerospace industry mostly uses this method to create aeroplane skin panels.

The first step in the sheet metal forming process is deep drawing, which involves pulling material into a die with the right geometry as shown in Figure 1.4 (b). As opposed to stretching, this method involves drawing material into the die from the outer flange area to create the required form. Large-depth pieces are mostly produced using this procedure through one or more operations. Tensile and compressive stresses are combined during the deep drawing process. Compressive hoop stress and radial tensile stress are applied to the flange region; a high compressive hoop stress results in wrinkling. By using enough blank holding force, this can be prevented. Significant thinning was caused by the material being subjected to plane strain straining in the cup wall region. Contact with the bottom punch causes biaxial tensile stress to be applied to the metal in the blank's center [29].

Bending is a shaping process where bending force is applied to a sheet of metal to create curved sections. V-bending, U-bending, and other bending operations are frequently performed as shown in Figure 1.4 (c). When a sheet bends, the inner part experiences

compressive stress while the outer part experiences tensile stress. Springback, or the change in bend angle caused by the material's elastic recovery after bending, can be corrected for by making the appropriate tool allowances. The aforementioned procedures are combined in complex sheet stampings. Stretching and drawing, together with related bending, unbending, and flanging, are required in the manufacturing of the majority of automotive and aerospace parts [30].

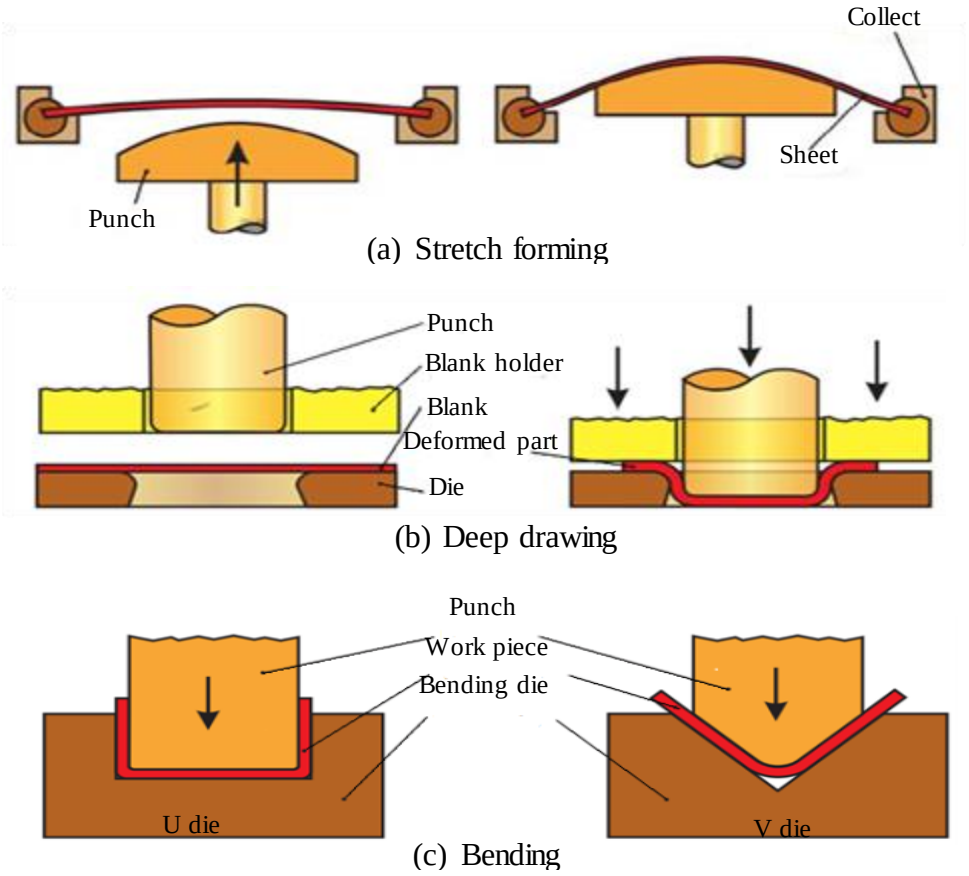

Figure 1.4 Standard processes for sheet metal forming [31].

1.3 Formability assessment

In sheet metal forming processes, the shape of flat sheets is altered in sheet metal forming operations by applying punch force in relation to the dies design. The applied force to the metal that is greater than its yield strength, results in plastic deformation without failure or cracking. This allows the sheet to be stretched or bent into a wide range of intricate shapes.

The thickness of sheet metal normally ranges from 0.4mm to 5mm. Sheet metal formability can be evaluated through multiple methods such as the Swift cup drawing test, the Erichsen cupping test, the Fukui's conical cup drawing test, the Ohio State University (OSU) formability test and the Hydraulic bulge test. These tests are extensively used to assess the formability of various sheet metals.

1.3.1 Swift cup drawing test

A common technique to assess a sheet's drawability is the Swift flat bottom cup test [32]. In this test, circular blanks with varying diameters are drawn into the die using a flat bottom punch with a 50mm diameter as shown in Figure 1.5. The limiting draw ratio (LDR), which is the ratio of the punch diameter to the maximum blank diameter that may be drawn without failure, is found by progressively increasing the blank diameter.

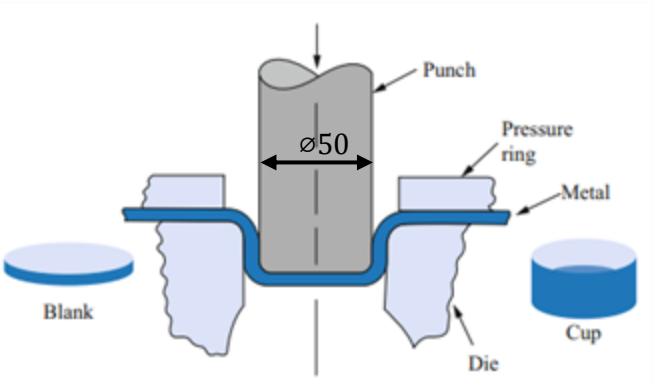

Figure 1.5 Schematic diagram of Swift cup drawing test [33].

1.3.2 Erichsen cupping test

The Erichsen cupping test, also known as the Erichsen test, is a standardized test method used to evaluate the deep-drawing and stretch-forming properties of sheet metals. The test measures the ability of a sheet metal to undergo plastic deformation without cracking or failure [34]. It is widely used in the metalworking industry to assess the formability and ductility of sheet metal materials. In this test, a circular disc-shaped specimen is cut from the sheet material. The diameter of the specimen is typically standardized. The specimen is clamped over a circular die with a hemispherical cavity. A hemispherical punch is pressed into the center of the specimen at a controlled rate, causing the metal to deform into the die as shown in Figure 1.6. The depth of the cup or the height of the formed dome is measured after the test. This measurement indicates the maximum deformation the material can undergo before failure. Failure is often defined as the occurrence of cracks, fractures, or any other visible defects on the surface of the formed cup.

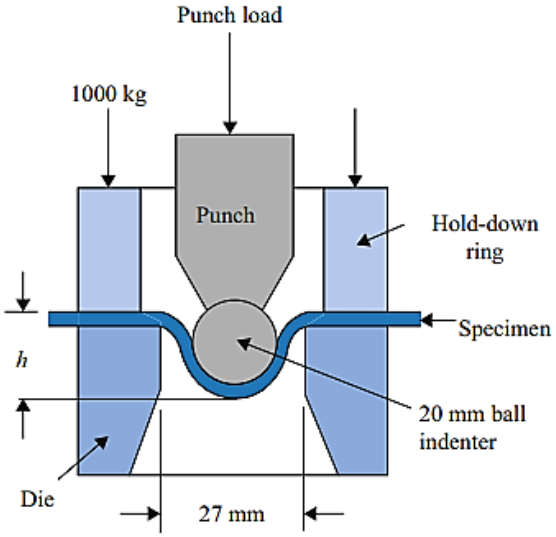

Figure 1.6 Schematic diagram of Erichsen cupping test [33].

1.3.3 Fukui's conical drawing test

To assess formability in a mixed mode of deformation (stretching and drawing), Fukui [35] presented an additional testing technique. Figure 1.7 shows the test setup, which consists of a conical die with a 60° included angle and a spherical ball with a diameter of 22mm. Till the failure in the sheet is noticed, the punch forces the ball to deform the supporting circular blank. Drawn from the flange area, the material experiences distortion. It results in a conical cup since the opening is substantially bigger than the ball. Based on the cup's base diameter, formability is assessed.

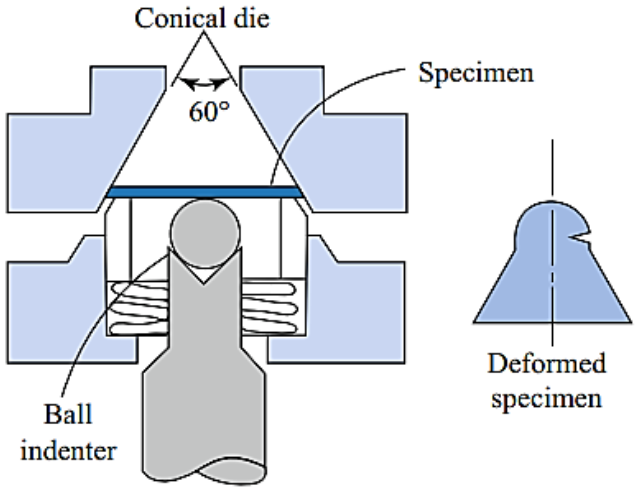

Figure 1.7 Schematic diagram of Fukui conical cup test [33].

1.3.4 Ohio State University (OSU) formability

Another technique to ascertain the limiting dome height under plane strain conditions was presented by Wagoner et al. [36] and is referred to as the Ohio State University (OSU) test. An elliptical punch has been substituted for the hemispherical punch utilised in the limiting dome height (LDH) test in the test configuration as shown in Figure 1.8. Formability is measured by the punch height at failure. It takes only 124mm of specimen width to induce a plane-strain failure, making this test quick to do. With the use of the hemispherical and flat

elliptical punches, several coated and uncoated sheet materials were tested [36], and the outcomes were discussed. When comparing OSU testing to LDH tests, the former produced more consistent and reliable results.

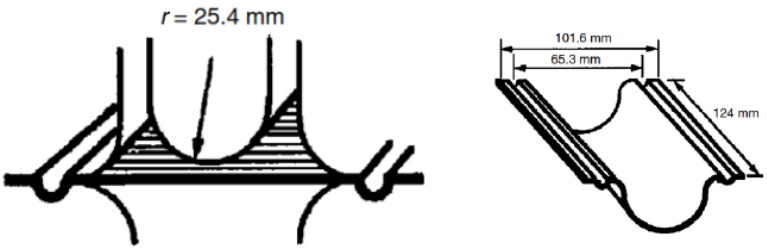

Figure 1.8 Schematic of OSU test and a tested blank [35].

1.3.5 Hydraulic bulge test

The hydraulic bulging test is an additional technique for assessing the formability of a sheet that has undergone biaxial stretching [37]. A pressure chamber and clamping mechanism make up the arrangement. It is possible to increase pressure by utilising gas or fluid (Figure 1.9).

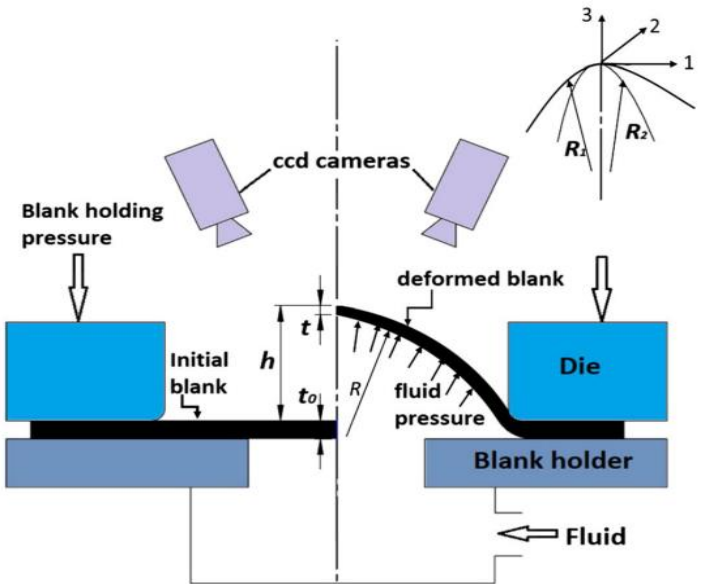

Figure 1.9 Schematic of hydraulic bulge test [38].

To assess formability, one uses the bulge height at which the material fails. This test has the advantage of not requiring friction to occur between the tool and the workpiece, which allows for equibiaxial stretching and ultimately higher overall strain.

1.4 Factors affecting formability

Formability is a key mechanical property of materials that describes their ability to undergo deformation processes without wrinkling, cracking, or localised necking. In the context of manufacturing and engineering, formability is crucial for shaping materials into desired geometries through processes such as bending, stretching, drawing, stamping, and other forming operations as discussed above in this chapter. The evaluation of formability helps ensure that materials can be successfully processed into components with complex shapes without failure. Various tests, such as the Erichsen cupping test, Swift cup drawing test, and others, are used to evaluate the formability of sheet metal [39]. Computational tools are often employed to simulate and predict the formability of materials under different processing conditions. In summary, formability is a critical property that influences the manufacturing and shaping of materials in various industries. The successful implementation of forming processes relies on selecting materials with suitable formability characteristics and optimizing process parameters to achieve desired shapes and components. Sheet formability is determined by a vast number of variables that interact in a complex way. These factors are divided into three categories: (a) process variables, (b) design parameters, and (c) material properties.

The process variables that significantly affect the formability by various parameter like mode of deformation, strain path, and lubrications. The design parameters are most important factor that affect the formability of sheet like punch corner radius, die entry radius and punch and die clearance. The materials properties such as strength and ductility, strain hardening

exponent (n), normal anisotropy ($\bar{R}$), crystallographic texture, and strain rate sensitivity index (m) influencing formability.

1.4.1 Strain hardening exponent

The strain hardening exponent (n-value) is a crucial parameter that significantly affects the formability of materials, particularly in metal forming processes. The strain hardening exponent is a measure of how a material's strength increases as it undergoes plastic deformation. It is a key factor in understanding the stress-strain behaviour of a material during plastic deformation. The strain hardening exponent [40] is often associated with the power-law relationship between stress (σ) and strain (ε) in the form of $\sigma = K \times \varepsilon^n$, where: σ is the true stress, ε is the true strain, K is a constant, and n is the strain hardening exponent.

1.4.2 Normal anisotropy

Normal anisotropy ($\bar{R}$) is a phenomenon that occurs in materials where the mechanical properties, such as yield strength, tensile strength, and elongation, vary with the direction of testing or deformation. This directional dependence of mechanical properties can significantly impact the formability of materials, especially in sheet metal forming processes. Normal anisotropy specifically refers to the variation of properties in the plane normal to the rolling or forming direction. Normal anisotropy can have a significant impact on the formability of materials, especially in sheet metal forming. Engineers need to carefully consider the directional dependence of mechanical properties when designing components or selecting materials for applications involving significant plastic deformation. Optimization strategies and informed material selection can help achieve the desired balance between anisotropy and formability.

The mechanical properties of sheet metals vary depending on the rolling direction (RD). This dependency of mechanical properties on orientation is referred to as anisotropy. The plastic

strain ratio (R) is defined as the ratio of strain in width (ε_w) to strain in thickness (ε_t), and it is used to analyze anisotropy in sheets. The plastic strain ratio (R) [41] defined as:

$$R = \frac{\varepsilon_w}{\varepsilon_t} \tag{1.1}$$

The plastic strain ratio (R) is calculated by using experimental results from tested specimens cut at 0°, 45°, and 90° to the RD. The determined values of R, are $R0$, $R45$, and $R90$, respectively. Planar anisotropy (ΔR) is best measured by the average variation [41], which may be written as:

$$\Delta R = \frac{R0 - 2R45 + R90}{2} \tag{1.2}$$

The normal anisotropy ($\bar{R}$) or average plastic strain ratio is written as:

$$\bar{R} = \frac{R0 + 2R45 + R90}{4} \tag{1.3}$$

When R is larger than '1' in any direction, it means that the thickness direction has a higher strength value than the other directions. The drawability is improved and the thinning impact is lessened when R is higher. It also prevents the creation of a neck at stressed notices in the sheet.

A sheet metals anisotropy results from the generation of a crystallographic texture during plastic deformation, such as cold rolling, annealing, and mechanical fibering [42]. Anisotropy is substantial decreased, during plastic deformation in rolling because it alters the material's crystallographic structure. The strength of a single crystal is extremely anisotropic, and large deformation causes polycrystalline sheets to approach single crystal anisotropy. As a result, the polycrystalline sheet also exhibits strong anisotropic behaviour under large deformation. The slip system of the BCC lattice structure of the sheet material is the basis for this behaviour. By merging the family of slip directions <111> and advantageous slip planes like ({110}, {112}, or {123}) together, the BCC lattice structure exihibt total of 48 slip systems. Because of this characteristic of the slip systems, the orientation of the grains determines how much a

grain will deform at a given stress level [43]. The fundamental cause of anisotropy resulting from mechanical fibering or intergranular substructure is the preferential alignment of structural discontinuities in the working direction, such as inclusions, void segregation, and phase [44].

1.4.3 Crystallographic texture

Texture analysis is a crucial aspect of understanding the properties and behaviour of polycrystalline materials in the field of material science and engineering [45]. Various methods are employed to analyze texture, providing insights into the distribution of crystallographic orientations within a sample [46]. The X-ray diffraction (XRD) is a widely used technique to study the crystallographic orientation of polycrystalline materials. It involves exposing a sample to X-rays and analyzing the diffraction pattern produced. The intensity and position of diffraction peaks provide information about the crystallographic orientations present in the material. The electron backscattered diffraction (EBSD) is a scanning electron microscopy technique used to obtain crystallographic information from a polished surface of a material [47]. It provides data on grain orientations, grain boundaries, and other microstructural features. EBSD can be used to create orientation maps and quantify texture in terms of crystallographic orientation distribution functions. Here are some common methods for texture analysis:

1.4.3.1 Crystallographic texture analysis

Texture can be investigating by various methods in polycrystalline materials namely a comprehensive overview of both quantitative and qualitative methods used in texture analysis [48]. It is a powerful technique for quantitatively analyzing texture. Texture goniometry involves measuring the intensity of diffracted X-rays at different angles to determine crystallographic orientations. EBSD is a quantitative method that provides detailed information at the microscale [49]. It is commonly using an attached to a scanning electron

microscopes (SEM) to map crystallographic orientations, grain boundaries, and phases. Texture is commonly represented using pole figures. In a stereographic projection, pole figures show a specified crystallographic axis (pole) with plotted crystallites, providing a visual representation of texture [50]. The sample reference frame is defined by specific crystallographic directions relevant to the material's processing history. Cold working of metals often involves the rolling direction (RD), transverse direction (TD), and normal direction (ND) as key reference directions, are commonly used in the study of metal textures [51].

1.4.3.2 Orientation distribution function (ODF)

The orientation distribution function (ODF) represents the volume fraction of grains with a specific orientation in a polycrystalline material. It described using three Euler angles, which define the transition from the sample's reference frame to the crystallographic reference frame of each grain [52], [53]. The ODF cannot be measured directly by any technique. It is derived from the evaluation of a set of pole figures or diffraction spectra. ODF can be represented as a function, a sum of functions, or expanded in a series of harmonic functions [53]. Discrete methods divide the ODF space into cells and focus on determining the value of the ODF in each cell. Understanding the ODF is crucial for characterizing the full 3D crystallographic texture of polycrystalline materials. The combination of techniques such as X-ray diffraction and EBSD, along with various mathematical representations, allows researchers to gain valuable insights into the distribution of crystallographic orientations in a material.

1.4.4 Strain rate sensitivity index

The strain rate sensitivity index (m-value) is a crucial parameter that influences the formability of materials. It characterizes how the material's flow stress changes with variations in strain rate, providing insights into its deformation behaviour under different conditions. The index is often incorporated into constitutive models to predict material

behaviour during forming processes. Materials with higher strain rate sensitivity indices have flow stresses that are more sensitive to changes in strain rate. A positive strain rate sensitivity ($m > 0$) is generally associated with improved formability. Materials with positive m-values tend to exhibit higher ductility and are more conducive to deformation processes like rolling, extrusion, and drawing. Negative strain rate sensitivity ($m < 0$) can lead to dynamic strain aging phenomena, affecting material behaviour during forming. The dynamic strain aging can result in serrated flow, localized necking, and reduced formability. The strain rate sensitivity index is often temperature-dependent, and the temperature at which forming processes occur can significantly influence formability. The elevated temperatures can alter the m-value, affecting material flow behaviour and formability [54].

CHAPTER 2

LITERATURE REVIEW

In this chapter, a detailed review of available literature on factors affecting the formability under magnetic field of steel sheet is carried out. This is reviewed in this chapter for understanding the magnetization behaviour of metals during operations. Both experimental and numerical studies are investigated.

2.1 Magnetic field effect on tensile properties

In the recent years, a uniaxial tension test assisted with a weak constant magnetic field has been employed to investigate the effects on the tensile properties of a sheet in order to enhance its formability. The modulus of elasticity, upper and lower yield points, ultimate tensile strength and percentage elongation of the different steel grades observed a small change in the tensile properties under the effect of transverse magnetic field during the tensile tests [55,56,57]. A summary of the work done by researchers in the recent years on magnetic field effect on tensile properties of steel sheets as follows:

Kraiev [58] performed tensile tests on some steel specimens with an external magnetic field of 1.2T in the transverse direction and reported the magnetoplasticity effect on flow stress and dislocation density in term of energy absorptions spectrum.

Hou et al. [59] studied the effects of pulsed magnetic fields on the residual stress, hardness and dislocation density of Cr4Mo4V steel, at different intensities varying from 1.0 to 2.5T. It was observed that the compressive residual stress, hardness and dislocation density decrease at lower magnetic field (1.0T to 1.3T) but these may increase at a higher value of magnetic field (2.0T to 2.5T).

Wang et al. [60] studied the effect of magnetic field of 1.5T on the mechanical properties of the Eurofer-97 structural steel at room temperature. It was noticed that the magnetic field increases the proportionality limit by 2.6% thereby increasing the yield strength by 14 MPa. It was also observed that the magnetic field enhances the ultimate tensile strength (UTS) by <1% only and has marginal effect on the elongation. Authors also stressed the need of further studies on the effect of applied magnetic field on fatigue and creep behaviour of the material.

Zagulyaev et al. [61] investigated the influence of a constant magnetic field of 0.3T and 0.6T on plastic properties of non-magnetic materials (like titanium and aluminium) in creep experiments. It was observed that creep rate increases with an applied magnetic field of 0.1T and thereafter, it decreases with increase in the magnitude of magnetic field. Author has also suggested a further study to understand the effect of magnetic field on creep phenomenon.

Zhang et al. [62] studied a structural steel that has not been quenched but tempered for one hour at 600 and 650 degrees Celsius both with and without a 14T magnetic field. By raising the cementite/ferrite interfacial energy and the magnetostrictive strain energy, the magnetic field can successfully stop the directed growth of cementite along martensite plate borders and twin boundaries. Cementite that resembles particles is finally produced. Furthermore, it is evident that the magnetic field can impede the development and expansion of "distortion-free" regions inside the matrix, even while it does not significantly alter the "distortion-free" portion's orientation distribution. Research on this topic advances our knowledge of how a magnetic field affects the phase transition of solid metallic materials.

Goins et al. [63] carried out numerical simulations on tailoring of a microstructure with the use of various external forces like magnetic, electrical and mechanical to control material properties and performance through microstructure engineering. Time dependent magnetic fields were applied to control the texture. It was concluded that a dynamic field

application of the magnetic field, through a changing field direction over time, can create a new microstructure feature and the temperature plays an important role in the evolution as well.

Sidhom et al. [64] studied the effect of magnetic field (in the range of 0.04T to 0.08T in longitudinal direction) on mechanical properties and microstructure in plain carbon steel specimens. It was concluded that the magnetic field decreased the ductility but slightly affected the grain size and hardness of the material.

Domenjoud and Daniel [65] reported a comprehensive magneto-mechanical characterization of an electrical steel (DC04) under various applied tension stress and plastic deformation levels, both hysteretic and anhysteretic. Two hardening stages were identified as a result of the material's mechanical characterization: a first stage that is linked to the generation of long-range internal back stress, and a second stage that is dominated by intragranular stresses related to the formation of dislocation structures. The magnetic characterisation demonstrates that plastic strain entails a notable loss of magnetic behaviour in the absence of applied stress. A portion of the virgin material's magnetic characteristics can be recovered through mechanical reloading. For the magneto-mechanical behaviour, including the impacts of internal stress and dislocation density, a simplified multiscale modelling method was proposed.

Zhang et al. [66] applied transverse static magnetic field to experimentally study the magneto-plasticity behaviour of Fe-3.2 wt.%Si single crystal along various crystal orientations. The application of a magnetic field resulted in a significant decrease in the yield and tensile strength of Fe-3.2 wt.%Si single crystal, demonstrating a magneto-plasticity effect. This effect varied with the crystal orientation, and the greatest decrease in the yield strength and tensile strength was observed along the [110] crystal direction.

2.2 Magnetoplasticity

The various effects of the magnetic field are initiated by the static, pulsed, and microwave nature of the field and are supported well by magnetoplasticity. An external magnetic field affects the mobility of individual dislocations, phase transformation, microstructure, spin, and electron [67,68]. A summary of the work done by researchers in recent years on the magnetoplasticity of steel sheets is descried as follows:

Muller et al. [69] performed a series of compression tests on the specimens of single crystals of Ni-Mn-Ga in the presence of a transverse magnetic field to study the relationship between microstructure and magneto-mechanical properties. A detailed discussion of the microscopic mechanisms involved in magnetic-field-induced deformation is provided in order to comprehend the relationship between the magneto-mechanical characteristics and the microstructure. The spatial distribution of martensite domains inside the microstructure is what determines the magnetic work per unit volume and, to a lesser extent, the macroscopic magneto-stress. The interplay between twinning dislocations and their interactions with the surface determines the magnetic threshold field needed to initiate magnetoplasticity, which is dependent on the twin thickness. This microscopic technique fully describes the threshold field when considering the twinning dislocation, which is the elementary carrier of magnetoplasticity.

Molotskii [13] reported that the energy of the dislocation bonds depends on the spin multiplicity of radical pairs either in singlet or triplet spin states, and a magnetic field induced between the spin states rapidly increases the dipping of dislocations. When dislocation bonds to paramagnetic barriers, the radical pairs created by these entities' orbitals determine their spin multiplicity. It is possible for the radical pairs to have significantly different binding energies in singlet or triplet spin states. The singlet and triplet states can change when subjected to a magnetic field. The triplet states with a lower binding energy than the singlet

states may form in addition to the singlet state population as a result of these transitions. There is an increase in flexibility in a magnetic field as a result of the depinning of the dislocations from barriers. One can explain the magnetoplasticity effect's main characteristics using this method.

Kovaleva and Shevchuk [70] experimentally studied the effect of magnetic field on the modulus of elasticity and Poisson's ratio of alloy steels. It was concluded that effect of a magnetic field with a magnitude of 0.04T applied in the transverse direction affects the Young's modulus and Poisson's ratio, however a marginal change in the properties of structural steels is observed. Elasticity properties are significantly impacted by a continuous magnetic field. The development of the $\Delta\mu$ effect is significantly stronger than that of the ΔE effect for every test material. The ΔE and $\Delta\mu$ effects are significantly enhanced when NP2 alloy (Ni>98%) is annealed at 800°C.

Osinskaya et al. [71] used the microhardness method to experimentally study the magnetoplasticity effect caused in the beryllium bronze BrB2 aged in magnetic fields of up to 1T. The fluctuation in neutron scattering throughout the ageing of BrB2 beryllium bronze samples has been shown by neutron studies to coincide with magnetic field modulation. The main outcome of this experimental work is the proof that thermomagnetic treatment in the presence of a continuous and pulsed magnetic field activates the MPE, causing the BrB2 beryllium bronze alloy to harden and plasticize. This opens the door to the development of materials with predictable functional properties. Research using neutrons has demonstrated that changes in neutron scattering during the ageing process of BrB2 beryllium bronze samples are correlated with changes in magnetic field. The structure of magnetically active centres and the makeup of the MPE in this alloy may become clearer with the addition of this information.

Verzhakovskaya et al. [72] used an X-ray diffraction technique to measure the diffusion process of aluminium diffusion in α-Fe for the first time utilising a pulsed magnetic field. It was established that the diffusion process is strongly influenced by the frequency and amplitude of magnetic field pulses. To clarify the process of Al diffusion in α-Fe when a pulsed magnetic field is present, all potential defect kinds in the diffusion zone must be taken into account. Their energy of interaction with the magnetic field and the moving domain walls must also be assessed, and their motion kinetics in the pulsed magnetic field must be examined. These kinds of studies are crucial to understanding the physics of strength and the defect spin response issue.

Huber et al. [73] examined how the material behaved mechanically and assessed the internal stresses brought on by strengthening. The alloy displays three stages of stressing and isotropic mechanical behaviour. At greater degrees of plastic strain, the internal stresses are associated with the heterogeneous dislocation structures and the stress drop during the early stages of deformation. An appropriate magnetic frame has been produced. Either the tensile or cross directions are used to study magnetic properties. From the onset of the plastic strain, the magnetic characteristics sharply diminish. Comparing the crossing trials to the colinear observations, the impact of the plastic strain on the magnetic characteristics is lessened.

Wang et al. [74] examined the mechanical properties and microstructure of the Ti-48Al-2Cr-2Nb alloy, which was made via powder-hot isostatic pressing and then treated with a strong magnetic field. The findings demonstrate that applying a high magnetic field treatment enhances the duplex microstructures and raises the percentage of CSL boundaries for the phase, which in turn enhances the Ti-48Al-2Cr-2Nb alloys strength and elongation. More specifically, after holding for three hours at 1260°C in the 10T magnetic field, the ultimate tensile strength improves to 440 MPa and the room elongation increases from 0.4% to 1%. The increase of mechanical properties of TiAl alloys and the alteration of

microstructure features are well explained by the magnetoplasticity effect, which modifies the dislocation characteristics due to the transformation of electron spin state.

Atherton et al. [75] report assessing the stress effects on the reversible component and the initial magnetization curve of a 1% Mn pipe line steel sample. The reversible and irreversible magnetization components change under stress. Magnetization shifts caused at different fields and with varied amplitudes by compressive and tensile stress cycles are provided. The magnetostriction measurements obtained along an initial magnetization curve and a hysteretic stress curve using the same sample under different tensile and compressive conditions are also studied. A straightforward explanation is offered, assuming that stress alters the alignments of magnetic domain easy axes concerning strain. The compressive force caused domain magnetizations to align preferentially perpendicular to the direction of stress. When the magnetization vectors are distributed in a way that is characterised by preferential magnetization orientation along the direction of tensile stress, rotating processes are more prone to alter this distribution at higher fields. It noticed that, in comparison to compression, tension appears to have a greater influence on both magnetization and magnetostriction.

Silva et al. [76] discovered the magnetic domains' easy orientation in a SAE 1045 steel sample. In order to identify the magnetic easy direction, induced magnetic fields were applied to samples of rolled SAE 1045 steel (formed by ferrite and perlite microstructures) in the reversibility zone of magnetic domains. The non-destructive method can be applied to the investigation of steel's magnetic characteristics as well as local magnetic properties based on various directions of magnetization. With samples of varying sizes and even varied geometries, this method was also successful in determining the magnetization easy direction of the steel under investigation. An external magnetic field was produced by the direct current and applied in the magnetic reversibility region. Unlike prior works that exclusively published

data in the high induced losses zone, this region, which is part of the low induction loss region, has shown to be sensitive to magnetic anisotropy.

Mian et al. [77] measured the non-saturated hysteresis loop under externally applied stress in order to examine the impact of stress on the magnetization process for Ni-Cu-Zn ferrite. To calculate the impact of stress during the reversal magnetization process, a weak field was used. The experimental results indicate that the compressive stress in the applied field from 0.20 to 0.84 Oe has a significant impact on the non-reversible reversal magnetization process. The toroidal shape of the sample was intended to measure the variation in the stress effect between the radial direction perpendicular to the detecting direction and the detecting direction. For the Ni-Cu-Zn ferrite with negative magnetostriction, the effect of stress in the detecting direction is greater than in the radial direction. Stress has a greater effect in a weak field with an applied field that is larger than the material's coercivity. In comparison to the detecting direction, the effect of tensile stress on magnetostriction in the perpendicular direction is less. A physical calculation that demonstrates the two- and one-dimensional effects of stress on magnetization in directions perpendicular to and parallel to the detecting direction can be used to produce this experimental result.

Mishra [78] presented a theoretical investigation of the fracture-induced magnetic phenomenon, in which low carbon iron tensile specimens fracture and produce a temporary magnetic field that causes the broken fragments to become magnetised. The research suggests a novel ductile fracture property for ferromagnetic materials: at the moment of fracture, the specimen's surface thin layer acts as a magnetic thin film with a Neel wall configuration, which allows for the fracture to occur.

The short-range exchange forces resulting from spin-spin coupling and the long-range internal magnetic forces resulting from dipole-dipole coupling make up the majority of the energy of

the domain configuration when mechanical loads and external magnetic fields are absent. Initially ascribed to the Weiss molecular field, the spontaneous magnetization M 5(T) is currently ascribed to quantum-mechanical exchange forces that have the tendency to align adjacent electron spins parallel. Saturation magnetization M5 (T) at a given temperature T is thus a function of strain (and hence of stress) in a specimen. The exchange force depends on the distance between the atoms whose spins it couples, and so it depends on the strain.

Permiakov et al. [79] investigated the non-oriented steels' stress dependency of their magnetic characteristics at one- and two-dimensional magnetization. In electrical steels, mechanical stress has a significant impact on magnetization. The application of the unique magnetic measurement's method combines 2D magnetic measurements with uniaxial stress measurements. Ten MPa of compressive stress and one hundred MPa of tensile stress are the ranges of uniaxial stress. A useful tool for predicting and providing a physical explanation for stress dependency in grain-oriented steel is a domain theory. When it comes to rotational magnetization, the 90° domain wall movement has a greater impact on the magnetization processes than in the alternating 1D scenario.

Matsuo (2011) [80] reported that simplifying the domain structure model (DSM) allows for the analytical revelation of the fundamental mechanism behind the mesoscopic magnetization process. To compare the influence of individual energy components explicitly, the anisotropic energy is used to normalise the magnetic energy components. The product of averaged magnetization and demagnetizing components approximates the magnetostatics field. The domain wall motion, nucleation-type hysteresis, and magnetization rotation are represented by a straightforward two-domain model. The magnetization curves produced by the periodic micromagnetic simulation and the simplified DSM agreement. The discontinuous magnetization-state transition seen in a magneto-impedance sensor is represented by the simplified DSM. The DSM makes essential mechanisms of the mesoscopic magnetization

process, including domain wall motion, which are not well-represented by single-domain models, simpler through analytical revelation. By applying the model parameters, magnetic energy components are normalised so that the influence of each individual energy component may be directly compared.

Ito et al. [81] studied a six-domain simplified domain structure model (SDSM) and proposed mesoscopic magnetization under cubic anisotropy. By using the volume-ratio variations of domains, the six-domain model represents 90° and 180° domain-wall motions. Six-domain models weree assembled to represent the magnetization process of grain-oriented and non-oriented silicon steel sheets. The effect of compressive stress was successfully reproduced, and the simulated magnetization curves correlate well with the experimental characteristics. The assembly of SDSMs with six domains effectively reflected the magnetic properties of grain-oriented and non-oriented silicon steel sheets, reconstructing the degradation of the properties due to compressive stress.

Jiles [82] studied a model theory of how an applied uniaxial stress causes a ferromagnetic material to alter in magnetization. The description of these effects is completely different from the explanation of the changes in the hysteresis curve under a series of applied stresses that are constant. Under the suggested model theory, the primary process is the application of stress that unpins domain walls, allowing the walls to move and altering the magnetization. As a result of this magnetization shift, the displacement from the anhysteretic magnetization is decreased. Furthermore, stress is applied through the magnetoelastic coupling, which modifies the anhysteretic magnetization itself. It was demonstrated that the effect can be explained by an equation where the displacement of the magnetization from the anhysteretic magnetization is proportional to the rate of change of magnetization with elastic energy. This law appears to be applicable when the material is in a significant hysteresis loop at the beginning.

Birss et al. [83] investigated the variation in magnetization of a variety of iron-carbon alloys treated to different metallurgical procedures by applying compressive and tensile stresses and magnetic fields simultaneously. The magnetization-stress curves for low carbon content, annealed materials are asymmetrical in tension and compression when exposed to a tiny magnetic field. Curves that are sensibly symmetrical are obtained for cold-worked, high carbon content materials as the asymmetry becomes less noticeable in the applied fields and stresses utilised, as well as for an increase in residual internal stress and carbon content.

Craik and Wood [84] conducted research on magnetization curves that were produced by applying stresses to several types of polycrystalline magnetic materials while they were exposed to a tiny, steady magnetic field. The materials that were investigated were silicon iron with both cube and isotropic textures, nickel, and mild steel. A thorough compensation was made for residual stray fields. The range of 0 to 10 kg/mm^{-2} was used for both compressive and tensile loads. Stress-related outcomes defied any hypothesis predicted only on the shifting of already-existing domain walls. However, it seems rather certain that in both isotropic and oriented polycrystalline materials, discontinuous changes of domain structure occur under stress, and they must be included in any theory of magnetization under stress.

Saka et al. [85] conducted research on simulating domain structures in applied fields by minimising the total energy in two dimensions. The balance between the Zeeman energy E_m and the magnetostatic energy E_s determines the magnetization orientations and wall positions in the applied field. Conversely, the balance between wall energy and anisotropy energy determines the number of domains. It was discovered that the film form appeared to govern the energies E_s and E_m regardless of the number of domains, and that the ratio of E to E_m is roughly 1 to 2. Furthermore, observations made with a Kerr microscope accord with the change in domain structure caused by the applied field.

Ren and Ren [86] studied the metal magnetic memory (MMM) testing technique, a unique testing method that can assess the stress concentration state of ferromagnetic components early on. The association between the leaking magnetic field of a specific spot on a cold-rolled steel specimen and the tensile stress was measured repeatedly while loading and unloading the specimen under various maximum tensile stresses. It demonstrated the connection between the magnetic induction intensity and that the stress is linear when the maximum tensile stress is less than 610 MPa. The connection between the magnetic induction intensity and the tensile becomes bending line as the maximum tensile stress increases from 610 MPa to 653 MPa of yield point. As the magnetic induction intensity varies quickly, the location of the bending line's extreme point will shift quickly from the position of lower stress to the position of greater stress. When the yield point's 653 MPa, maximum tensile stress is exceeded, there is minimal movement in the extreme point's position and a significant fluctuation in the magnetic induction intensity. In terms of theory, there are two types of tensile stresses: ordered and disordered. The order stress magnetization in the elastic stress stage is modelled microscopically, and the results show good agreement with the experimental data. At the plastic deformation stage, a microscopic model of disordered stress magnetization was developed, and the results show good agreement with the experimental data. In order to accurately detect and evaluate metal magnetic memory testing technology, the research results can be used as a reference.

Perevertov [87] conducted a thorough investigation on the impact of residual stress on the mild steel hysteresis characteristics. It was discovered that the material's magnetic qualities were diminished by the stress. Anisotropy generated by stress was noted, with the easy direction parallel to the tensile tension that had been applied earlier. Compared to the hard axis, the changes in the hysteresis loops recorded along the easy axis were substantially less. The coercivity and remanence were the most delicate characteristics. As is typical for

loops measured along the hard axis of anisotropic polycrystalline materials, the loops measured in the stressed direction were bulged. On distorted samples, loops measured in any fixed direction crossed at two locations known as coincident points in the second and fourth quadrants. Using the effective field concept—in which the stress-induced field is the result of two independent functions of stress and magnetization—simple hypotheses allow for the modelling of this occurrence. Then, from experimental data, the normalized function of stress may be learned.

Li et al. [88] created an integrated model based on the Sablik-Landgraf model that describes how plastic deformation affects magnetization. The modelling strategy takes into account how plastic deformation affects both the effective field and the model parameters. The contributions of plastic deformation, stress demagnetization term, and residual stress are integrated into the effective field. The impact of plastic deformation on the interdomain coupling coefficient, scaling constant, and pinning coefficient of the model is also taken into account. In keeping with the experimental findings, the computed magnetization shows a rapid change in the early stages of plastic deformation and then gradually declines as plastic strain increases. The relationship between magnetization and plastic strain in the modified model is nonlinear. The magnetization drastically drops during the initial stages of plastic deformation. The magnetism gradually decreases with increasing plastic deformation. Results from the new model equation show good agreement with experimental observations.

Langman [89] studied the magnetization of mild steel under both hysteretic and anhysteretic conditions, at field strengths ranging from 100 A/m to 1200 A/m. A uniaxial load was applied and the magnetization was either parallel or perpendicular to it. The experimental results demonstrated that whereas parallel compression or perpendicular tension significantly decreased the flux density, tension parallel to the field and compression perpendicular to the field had comparatively little influence on the flux density. The borders between grains inside

a distinct polycrystalline ferromagnetic area with varying easy-magnetization directions. The domains were misaligned with the surrounding grains and point in these directions at medium field strengths. The component of magnetization normal to the border thus exhibits a discontinuity at the grain boundaries. A polycrystalline ferromagnetic distinct zone with distinct easy-magnetization directions where the grain boundaries are located. The domains point in these directions at medium field intensities and are out of alignment with neighbouring grains' domains. As a result, the magnetization component normal to the boundary exhibits a discontinuity at the grain boundaries. Demagnetizing energy is related to the presence of magnetic poles there. If reverse magnetization domains exist and result in a pole distribution with the opposite sign, this energy will be diminished. If the resulting energy decrease was greater than the energy needed to build the domains, this would happen.

Kusanagi et al. [90] examined how stress affected the amount of acoustic emission when nickel and mild steel were magnetised. It is now evident that there is a significant stress dependence on the acoustic emission magnitude during magnetization. Field inspection-appropriate non-destructive testing applications ought to benefit from this effect. Non-destructive testing (NDT) applications that are appropriate for field inspection, including the assessment of residual surface stress, should benefit from this impact. We are developing a NDT approach based on the phenomenon of abrupt and discontinuous movements of magnetic-wall Barkhausen noise analysis (BNA). Barkhausen noise can be distinguished from AE signals during magnetization based on the type of measurement used: stress pulses picked up by a piezoelectric transducer for the former, and discontinuous magnetization picked up by a coil for the latter. One characteristic of the AE's dependence on stress during magnetization that differs from Barkhausen noise's dependency on stress may be the broader stress-dependent region. A NDT technique that is more broadly applicable than BNA could result from more investigation into the variance of AE signals during magnetization.

Atherton and Jiles [91] studied domain walls fracture under stress and separate from their pinning sites, stress cycling applied to 1% manganese steel at low magnetic fields results in an irreversible change in the magnetization towards the anhysteretic. It was determined that the difference between the initial flux density and the anhysteretic flux density at the same field, H, is proportional to the change in flux density brought on by a single stress cycle of fixed amplitude. It was discovered that the variation in flux density as a function of stress is roughly proportionate to stress.

Permiakov et al. [92] examined the effects of uniaxial mechanical stress on magnetisation processes and energy losses in non-oriented Fe-Si steels under alternating and circular rotating flux. Any type of magnetic flux can be created, from alternating in all directions to various elliptical and circular rotational fluxes, thanks to the sophisticated waveform control and measurement technique. Rotational magnetization under uniaxial stress provides a fresh insight into how applied compressive or tensile loads, as well as plastic deformation, alter a material's anisotropy. Since non-oriented steel is widely used in situations of rotational magnetization, mechanical stress, and deformation, there may be many practical uses for this new research. When comparing rotating magnetization to alternating longitudinal and transverse magnetization, the magnetic characteristics of non-oriented Fe-Si steel under uniaxial stress deteriorate significantly. Under alternating magnetization, the magnetic characteristics exhibit varying behaviours depending on the rotational flux, either slightly improving or worsening.

Lihong et al. [93] looked into the possibility of using stress alone to generate weak magnetic signals on the surfaces of ferromagnetic materials. These signals might be used to gauge the extent of damage to ferromagnetic components. The normal component of the stress-induced magnetic field, Hp(y), was measured during tensile testing on the surfaces of sheet specimens made of three different ferromagnetic materials. It has been determined that

Hp(y) is dependent on the applied stress and exhibits distinct properties on the elastic and plastic deformation phases, in that order. A ferromagnet's interaction energy was taken into consideration when discussing the phenomena of abrupt changes in magnetic signals that occur at the moment of fracture.

2.3 Research gaps and motivation for the present work

After an extensive literature survey on the topic of magnetization effect on mechanical properties of steel sheets, it was observed that the following issues have not been researched and addressed in the domain of sheet metal forming:

1. Several methods are discussed for evaluating the formability of different grades of various steels in literatures but minimal research is done on the effect of magnetization on forming behavior of sheet metal.
2. Effect of varying magnetic field on mechanical properties of steels limited work has been studied.
3. Effect of magnetic field on formability of varying sheet thickness limited work has been studied.
4. Effect of change of stress for the change of magnetization properties during uniaxial testing is studied for hysteresis curves. This method has not been studied for its effect on the formability for the steel sheets.
5. Effect of magnetization on the domain wall is available in the literature, but its effect on the mechanical behavior of material is not studied so far.

2.4 Research objectives

Suitable grades of steel sheets are chosen for manufacturing components for automotive and aerospace industries. The study of magnetization effect on the formability of steel sheets and change in their mechanical properties is more challenging as compared to the other conventional and non-conventional process. In the view of the above-mentioned challenges and the research gaps in prediction of mechanical properties with the varying of magnetization of steel during forming, objectives of the proposed research have been broadly formulated as below:

1. Characterization of tensile properties of ZC440 and DP590 steel sheets of different thicknesses with and without magnetic field.
2. Formability assessment of ZC440 and DP590 steel sheets with and without magnetic field.
3. FE simulation of effect of magnetization on formability of ZC440 and DP590 steel sheets during forming and experimental validation of predicted results.

CHAPTER 3

DESIGN AND DEVELOPMENT OF ELECTROMAGNETIC TOOL FOR UNIVERSAL TESTING MACHINE

In the sheet metal forming industry, meeting customer needs as quickly as possible is a major difficulty. These days, one of the most important considerations when developing vehicle structural components for improved crashworthiness and fuel efficiency is the selection of steel sheets with a high strength-to-weight ratio. The high yield and tensile strengths of an advanced high-strength steel sheet come at the expense of its ductility, strain hardening exponent, and normal anisotropy, which highly impact its formability [94-96]. Tensile and yield strengths, ductility, strain hardening exponent, and anisotropy are the material characteristics that affect a sheet metals formability.

3.1 Selection of materials

In the present work, a high strength C-Mn steel sheet (ZC440) with a sheet thickness of 1.0, 1.2 and 1.4 mm and dual phase (DP590) steel sheet with a sheet thickness of 1.0, 1.2 and 1.6 mm is selected for the experimental work. The selected steel sheet possesses a combination of high strength and ductility and is commonly used in the skin panels and white body components in the automotive industry. It is a ferromagnetic material that can be magnetised with the help of an electromagnetic uniaxial tensile test (EMUTT) tool. The chemical composition of steels was determined using the spark test technique and is presented in Table 3.1and Table 3.2.

Table 3.1 Chemical composition in wt. (%) of ZC440

Sheet thickness	C	Si	Cr	Mn	Ni	S	P	Sn	Al	W	As	Fe
1.0 mm	0.09	0.12	0.07	0.99	0.03	0.02	0.04	0.02	0.05	0.01	0.01	98.55
1.2 mm	0.12	0.12	0.06	0.97	0.05	0.04	0.05	0.04	0.04	0.02	0.01	98.48
1.4 mm	0.10	0.13	0.08	0.93	0.02	0.02	0.05	0.03	0.04	0.01	0.01	98.40

Table 3.2 Chemical composition in wt. (%) of DP590

Sheet thickness	C	Si	Cr	Mn	Ni	S	P	Ti	Al	W	As	Fe
1.0 mm	0.16	0.26	0.10	1.30	0.06	0.04	0.05	0.02	0.06	0.01	0.03	97.9
1.2 mm	0.15	0.22	0.11	1.35	0.07	0.04	0.07	0.07	0.01	0.04	0.06	97.8
1.6 mm	0.17	0.24	0.12	1.31	0.06	0.05	0.04	0.01	0.06	0.01	0.08	98.1

3.2 Design of electromagnet uniaxial tensile test (EMUTT) tool

As it has been studied in the previous chapter and found that there are numbers of magnetoplasticity methods that are applied for enhancing the formability of sheet. Also, a number of researches were carried out based on the transverse direction magnetic field (MF) applied on the tensile specimen for improving the tensile properties. It has been proven that the MF affects the ferromagnetic material properties in term of tensile properties and texture of the deformed sheet. The MF based tensile test is the new concept for improving the tensile properties. The main aim for the development of this electromagnetic uniaxial tensile test tool (EMUTT) is to enhance tensile properties with weak MF during tension test and then compare the results of tensile properties of tested specimens without MF. To produce an electromagnetic tool, a finite element analysis was performed on the tool, and then a final computer aided design (CAD) model was created to fabricate the tool design. Based on the distribution of magnetostatics MF, the tool was designed. The tool was designed in such of

way that the it can uniformly distribute the magnetic flux along the gauge length of the tensile specimen. The uniformity of MF is the best studied for designing and implementation of the novel electromagnetic uniaxial tensile test tool.

It was decided to develop five electromagnet tools, in which the tools diameter is the only parameter that varies in response to variations in the coils number of turns while the current remains constant. These input parameters directly affect the magnetic flux density distribution. The change in magnetic flux density distribution is useful in determining the degree of improvement in the specimens' tensile properties. The CAD model of EMUTT tools was finalized and built to conduct experiments based on magnetostatics simulations.

3.2.1 Electromagnetic model for finite element analysis

The finite element analysis (FEA) of electromagnetic uniaxial tensile test (EMUTT) tool performed in Maxwell Ansoft V13 was used to study in the tensile specimen. The pre-CAD model of EMUTT tool was made based on the earlier study shown in Figure 3.1. The magnetostatics FEA simulation was performed to analysis the MF with the surface of the tensile specimen with in the parallel length. By assigning materials, boundaries, and source conditions and using Maxwell equations over a specific region or space, Maxwell Ansoft V13 was used to solve the electromagnetic field problem of the given model. The CAD model was imported to the software for checking the feasibility of the tool by plotting magnetic flux distribution of the specimen surface. The assigned properties of tensile specimen for the model were generated from a B-M characteristic plot for DP590 and ZC440 steel sheet in powder form using a vibrating sample magnetometer (VSM), as seen in Figure 3.2. The value of bulk conductivity assigned for DP590 and ZC440 steel is 2000000 siemens/meter. The graph that is drawn between magnetic flux density (B) and magnetising force (M) is called the B-M curve, or magnetization curve. The copper wire utilised in the EMUTT tool model has a relative permeability of 0.99 and a bulk conductivity of 58000000 siemens/meter. The

bobbin has a relative permeability of 1.09 and a bulk conductivity of 1100000 siemens/meter. A set of Maxwell equations with specified material parameters, source, and boundary conditions are used in the simulation over a finite region.

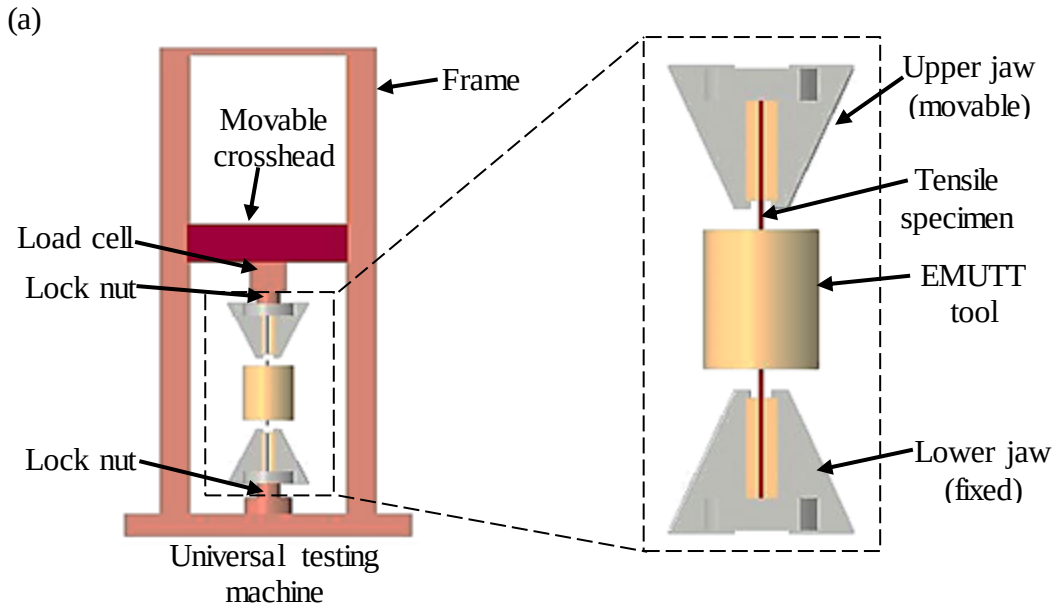

Figure 3.1 CAD model of electromagnetic uniaxial tensile test tool along with ferromagnetic tensile specimen prepared for magnetostatic simulation on Creo 5.0.

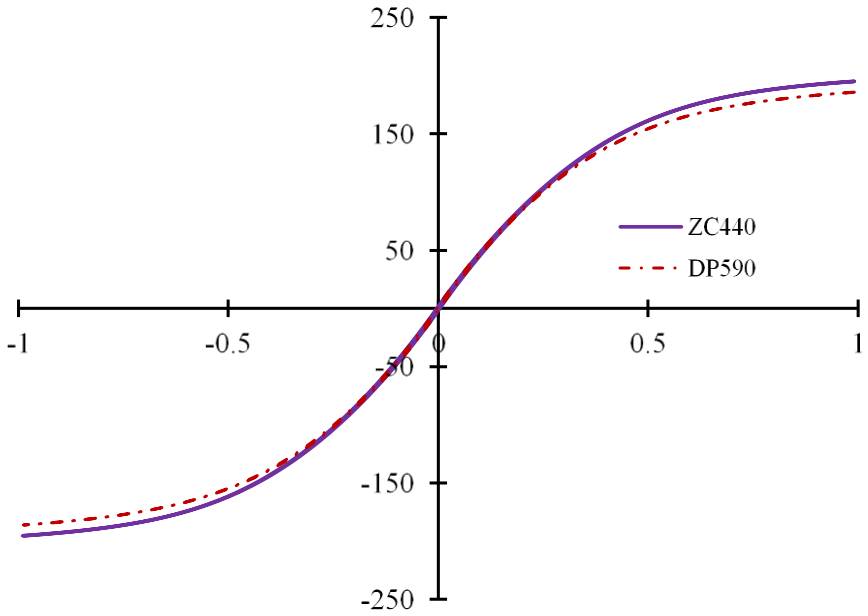

Figure 3.2 B-M curve of DP590 and ZC440 steel sheet.

A vacuum atmosphere was constructed around the model. The number of rotations per unit ampere was assigned to current density in the excitation for the specified tool. The model was set in its own environment. Excitation refers to current and current density in terms of the number of turns per unit ampere. The design of the electromagnet tool was carried out using these parameters. For FEA analysis of tensile specimen with the EMUTT tool, the magnetic flux density analysis was taken into study along the parallel length of the tensile specimen and the cross-sectional surfaces at ends of the parallel length along the width. The total number of five tool were assigned on the basis of turns per ampere for the evaluation of magnetostatics distribution of filed. The assigned tools can be stated in a variety of ways with regard to the current and copper coil gauge diameter; in essence, they match the current and coil gauge diameter combination. The optimal gauge wire for creating an electromagnet magnet is 20 gauge [97], as the gauge diameter grows and the coil's resistance drops. This study aims to measure the magnetic flux density within the specimen's gauge length to assist in tool development.

3.2.2 Magnetostatic finite element analysis

The Maxwell Ansoft V13 software was used to simulate the effect of electromagnetic field in the tensile specimen. In the magnetostatic simulation analyses, the magnetic flux density along the parallel length of the tensile specimen. A CAD model of a standard tensile specimen is used to simulate the magnetic performance of the EMUTT tools. A parallel length of a tensile specimen is a region where plastic deformation takes place and leads to the necking in the gauge length and therefore a uniform MF is applied in this region with the help of a EMUTT tool to produce a magnetic flux density. The tensile specimen behaves as an electromagnet core inside the EMUTT tool. The magnetic flux distribution contour plots in the tensile specimens are determined for five distinct tools, *tool-A* through *tool-E*, as illustrated in Figures 3.3 (a) to (e). These five electromagnet tools are developed with varying

outer diameters of winding coils, but the length of the coils is kept equal to the parallel length of the tensile specimen to focus the magnetic field in the desired region.

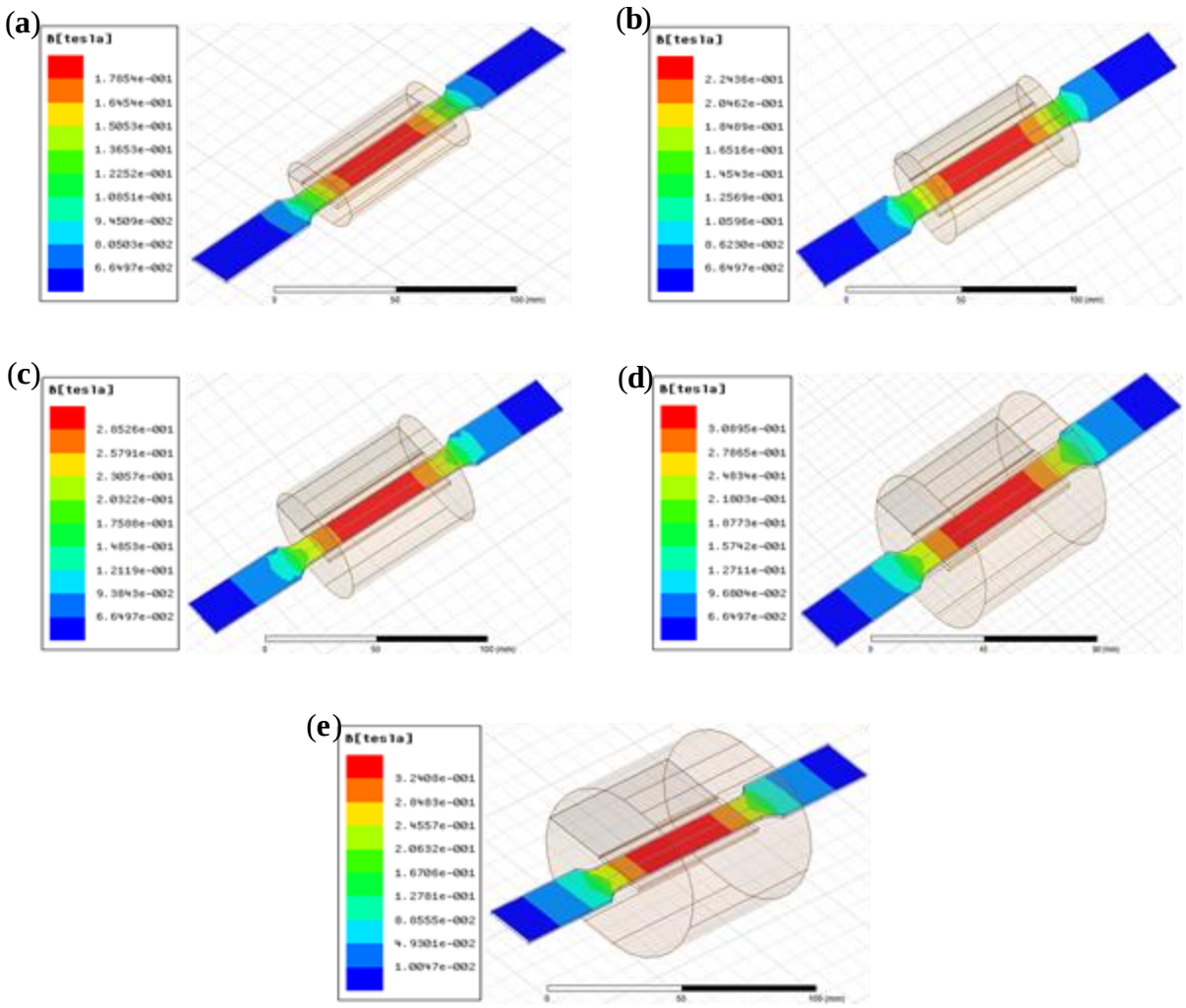

Figure 3.3 Magnetostatic simulations with (a) *tool-A*, (b) *tool-B*, (c) *tool-C*, (d) *tool-D* and (e) *tool-E*.

3.2.2.1 Magnetic flux density distribution with EMUTT tools on varying thicknesses of ZC440 and DP590 steel sheets

The results of magnetic flux distribution from *tool-A* to *tool-E* derived from simulations was then utilised to investigate the impact of the magnetic field on the tensile characteristics of DP590 and ZC440 steel with varying thicknesses as shown in Figure 3.4. From the variations of magnetic flux density plots, higher values are noticed at the center of the parallel length. The value of magnetic flux density decreases away from the center along the length. The

values of magnetic flux density increase from *tool-A* to *tool-C* and then slope get down with *tool-D* and *tool-E* at the center of the specimen in all the cases. This indicates that the difference between the values of the magnetic flux density will reduce further beyond a certain limit of *tool-E*, if the tools are designed with increase in the number of turns in coils more than that of *tool-E*. The simulation results facilitated in the design of EMUTT tools as per the requirement of the magnetic flux density at the parallel length in order to achieve the objectives.

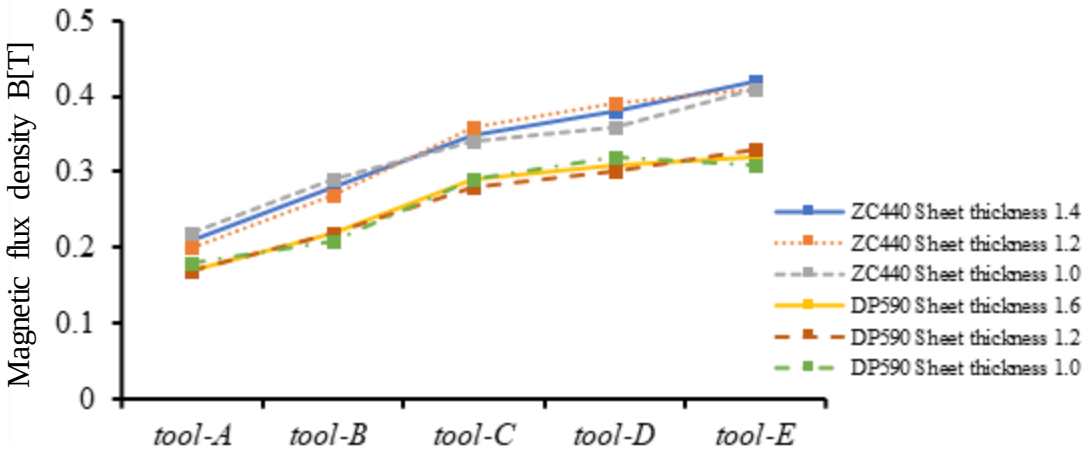

Figure 3.4 Results of magnetic flux density with EMUTT tools on different thicknesses of ZC440 and DP590 tensile specimens.

The result obtained from FEA concluded that the design of *tool-A* to *tool-E* has more effect in term magnetic flux density in ZC440 followed by DP590 specimens. It also says that the MF increased from *tool-A* to *tool-E* in both the cases but the slope gets flatten after *tool-C*. The highest magnetic flux density observed with *tool-E* is 0.42T in ZC440 and 0.33T in DP590.

3.2.3 Final CAD design of electromagnetic uniaxial tensile test (EMUTT) tool

On the basis of the FEA of EMUTT tools for the tensile specimen of different thicknesses of ZC440 and DP590, tool final design was created using the PTC Creo 5.0 design software. In

the designing of new set up for uniaxial testing with MF, one standard bobbin was designed for different thicknesses and five different tools were designed thickness tools by varying dimensions of the outer diameter and the bobbin length was kept constant for all the cases. The detailed design parameters for the five different EMUTT tools are given in Table 3.3.

Table 3.3 Detail of design parameters for tools

EMUTT tools	Coil length in *X*-axis (L_{cx}) in mm	Coil length in *Z*-axis (L_{cz}) in mm
tool-A	39	23
tool-B	48	36
tool-C	58	42
tool-D	62	47
tool-E	68	52

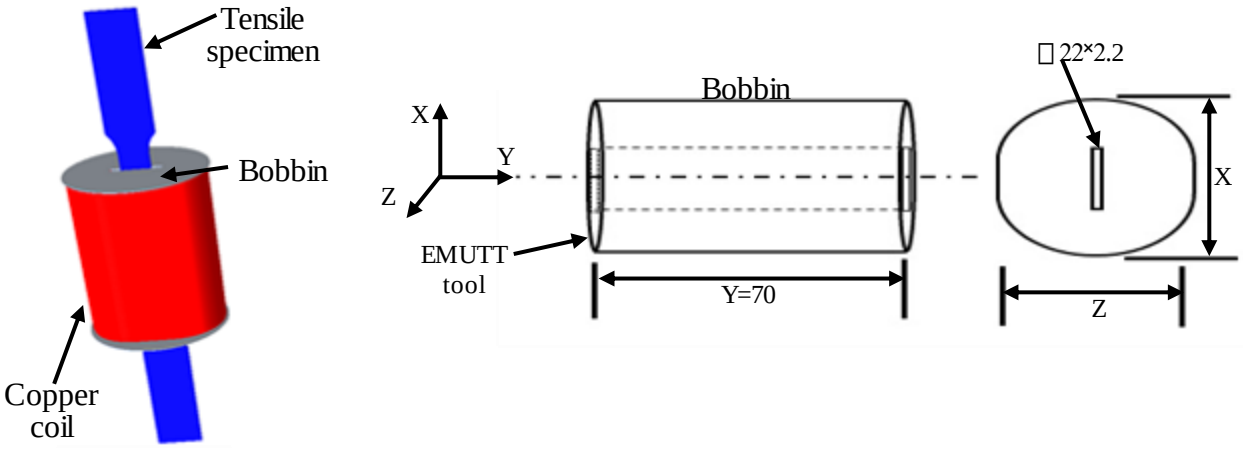

Figure 3.5 Final dimensions of bobbin design for EMUTT tools.

Bobbin was designed using the input from the FEA analysis. The final bobbin dimension is given in Figure 3.5. It was decided that the number of turns of copper coil is varying for *tool-A* to *tool-E*, for that using 20-gauge wire. Stainless steel material used for the bobbin is lighter in weight, easy to machine and that could restrict the MF it has non-ferrous material. The thickness of bobbin sheet was kept low to assist in heat transfer while heating of coils.

3.3 Analytical model of the electromagnetic tool

The final tool dimensions were found analytically, based on the output of simulations for the magnetic flux density distribution in the specimen's width and parallel length. Figure 3.6 (a) displays a schematic diagram with two perspectives of the tool with the specimen in situ.

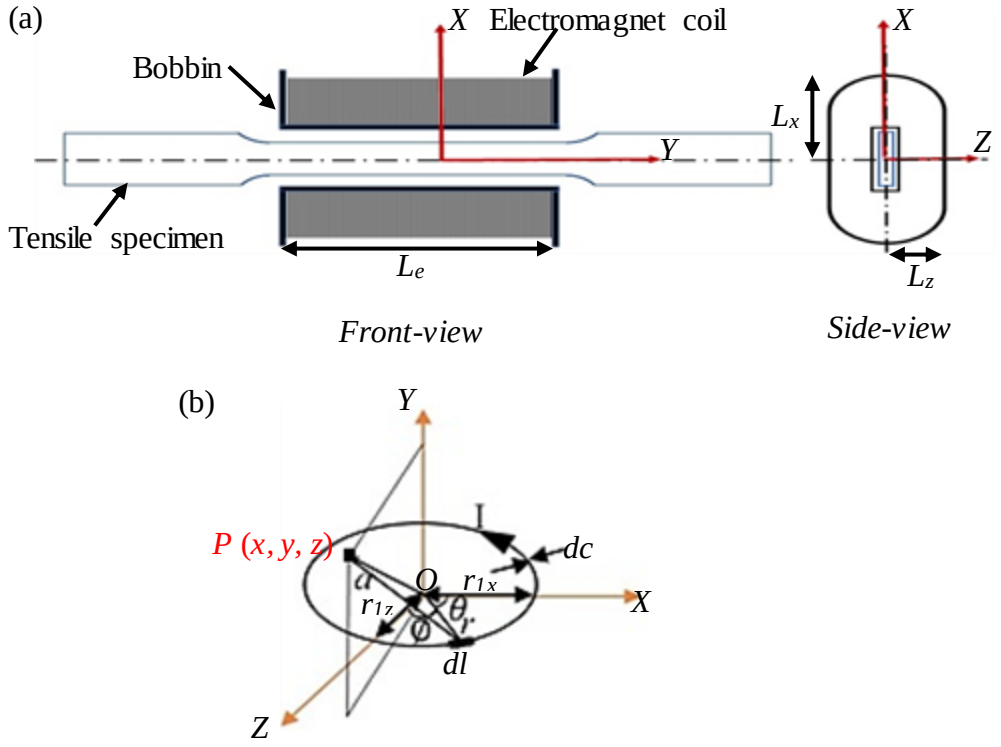

Figure 3.6 (a) Schematic of electromagnetic tool in 2D with front and side-view and (b) cartesian coordinate system for single turn of the coil.

A distinct set of input parameters, such as a fixed current, the relative permeability of copper wire, the B-M curve of the tensile specimen, and the number of turns per ampere, influence the analytical design. The lower resistance of the copper wire is correlated with the longer tool operating times. All tools have internal dimensions of 22mm in the X-axis and 2.2mm in the Z-axis, respectively. The length of the electromagnet coil (Le) was maintained at 70 mm along the Y-axis, and the diameter of the enabled copper wire (dc) was 0.914mm.

The Biot-Savart law defined magnetic field strength was calculated by using the electromagnetic field distribution and correlated to the magnetic flux density [98]. It is a basic law that derives the distribution of MF strength generated by the electromagnetic coils.

As shown in Figure 3.6 (b), a single turn of coil loop is placed in the *X-O-Z* plane. The radius of coil is denoted by *r*, current *I* flows in a current coil loop, and at any point *P* (*x*,*y*,*z*) a micro-element *Idl* is selected to determine the MF. The distance vector $\vec{S}$ that connects the micro-element to the point *P* and its position vector $\vec{P}$, the relationship [100] is given by:

$$\vec{S} = \vec{P} - I\vec{dl} \tag{3.1}$$

$$= (x - r.cos\,\emptyset)\vec{\imath} + (y - r.sin\,\emptyset)\vec{j} + z\vec{k} \tag{3.2}$$

where, $\vec{\imath}$, $\vec{j}$ and $\vec{k}$ represent a unit vector in *X*, *Y* and *Z* axis of the current coil loop.

$$S^3 = \left(\sqrt{(x - r.cos\,\emptyset)^2 + (y - r.sin\,\emptyset)^2 + z^2}\right)^3$$

$$= (x^2 + y^2 + z^2 + r^2 - 2rx\,cos\,\emptyset - 2ry\,sin\,\emptyset)^{\frac{3}{2}} \tag{3.3}$$

where, *S* is the magnitude of distance vector $\vec{S}$. Let $R' = \sqrt{x^2 + y^2 + z^2}$ where R' represents the distance between the center of the coil and the point *P* (*x*, *y*, *z*).

$$\vec{dl} \times \vec{S} = \begin{vmatrix} i & j & k \\ -r.sin\,\emptyset.d\emptyset & r.cos\,\emptyset.d\emptyset & 0 \\ x - r.cos\,\emptyset & y - r.sin\,\emptyset & z \end{vmatrix} \tag{3.4}$$

The electromagnetic field strength ($\vec{H}$) at point *P* (*x*, *y*, *z*) can be considered based on the Biot-Savart law, [99] and is given by

$$\vec{H}(x, y, z) = \frac{n}{4\pi} \oint \frac{I\vec{dl} \times \vec{S}}{S^3} \tag{3.5}$$

The total number of excitation coils are taken as *n*. The elliptical and polynomial integrations were solved by truncated series expansion to determine the value of $\frac{1}{S^3}$ in Equation (3.5) [100]. The value of $\frac{1}{S^3}$ is obtained as given below:

$$\frac{1}{S^3} = \left(R_p^2 + r^2\right)^{-3/2} \cdot \left(1 + \frac{3r(x\cos\emptyset + y\sin\emptyset)}{R_p^2 + r^2} + \frac{15r^2(x\cos\emptyset + y\sin\emptyset)^2}{2\left(R_p^2 + r^2\right)^2} + \frac{35r^3(x\cos\emptyset + y\sin\emptyset)^3}{2\left(R_p^2 + r^2\right)^3}\right) \quad (3.6)$$

Substituting the Equations (3.6) and (3.4) into the Equation (3.5) and then integrating, we can get the magnitude of MF strength in *X*, *Y*, and *Z* direction at any point *P* through point *O* of cartesian coordinates [101] can be calculated as given below:

$$H_{1x} = \frac{I{r_1}^2}{4(R_p^2 + {r_1}^2)^{\frac{3}{2}}}\left[\frac{3x\,y_i}{\left(R_p^2 + r_1^2\right)} + \frac{105r_1^2x^3y_i}{8\left(R_p^2 + r_1^2\right)^3} + \frac{105r_1^2zx^2y_i}{8\left(R_p^2 + r_1^2\right)^3}\right] \quad (3.7)$$

$$H_{1y} = \frac{I{r_1}^2}{4(R_p^2 + {r_1}^2)^{\frac{3}{2}}}\left[2 - \frac{3(z^2 + x^2)}{\left(R_p^2 + r_1^2\right)} + \frac{15r_1^2(z^2 + x)^2}{2\left(R_p^2 + r_1^2\right)^2} - \frac{105r_1^2(z^2 + x^2)^2}{8\left(R_p^2 + r_1^2\right)^3}\right] \quad (3.8)$$

$$H_{1z} = \frac{I{r_1}^2}{4(R_p^2 + {r_1}^2)^{\frac{3}{2}}}\left[\frac{3z\,y_i}{\left(R_p^2 + r_1^2\right)} + \frac{105r_1^2z^3y_i}{8\left(R_p^2 + r_1^2\right)^3} + \frac{105r_1^2yz^2y_i}{8\left(R_p^2 + r_1^2\right)^3}\right] \quad (3.9)$$

where, magnetic field strengths H_{1x}, H_{1y}, and H_{1z} are represented in *X*, *Y*, and *Z* directions, r_1 is coil radius in *X* and *Z* directions and longitudinal coil wound is represented by y_i. Here, R_p is the distance measured from a point *O* to a point *P* (Figure 3.6).

$$R_p = \sqrt{x^2 + y_i^2 + z^2} \quad (3.10)$$

For the design of the EMUTT tools, varying the parameters of electromagnetic coil in radial (r_1) and longitudinal (y_i) directions are as given below:

$$r_1 = \frac{r_{1x}r_{1z}}{\sqrt{r_{1x}^2\sin^2\theta + r_{1z}^2\cos^2\theta}} + jd_c\,, \quad 0 < j \le n \quad (3.11)$$

$$y_i = y + id_c\,, \quad 0 < i \le m \quad (3.12)$$

here, *j* represents the number of turns of coil (varying from 0 to *n*) radially along *X* and *Z* directions, *i* represents the number of turns of coil in the longitudinal *Y* direction and r_{1x}, r_{1z} and *y* are the initial points in Cartesian coordinates (Figure 3.6 b), where the value of r_{1x} is 11 mm, r_{1z} is 1.1 mm and the value of y is zero.

The different diameters of EMUTT tools from *tool-A* to *tool-E* depends upon the number of turns in the radial direction, and the length is fixed for all the tools. The total MF strength

(H_t) on the tensile specimen was calculated in the longitudinal and transverse directions by using the Equations (3.11) and (3.12) with the Equations (3.7), (3.8), and (3.9). The strength of MF is assumed to remain constant in thickness (*Z-axis*) direction and therefore, the MF strength H_{1z} is taken as zero. The determination of the total MF strength (H_t) at the tensile specimen is given as:

$$H_t = \sqrt{H_{1x}^2 + H_{1y}^2} \tag{3.13}$$

The magnetic flux density (*B*) is calculated[100] using total magnetic field strength (H_t) at any point in a free space as given by:

$$B = \mu_0 H_t \tag{3.14}$$

where, μ_0 is the permeability of air in free space equal to $4\pi \times 10^{-7}$ N/A^2.

The tensile specimen of a ferromagnetic material gets magnetized with the applied magnetics flux density (*B*). Therefore, the final magnetic flux density (B_f) applied to the tensile specimen is given below:

$$B_f = B + \mu_0(M_{TS}) \tag{3.15}$$

where, M_{TS} is the value of the magnetization taken from the B-M plot (shown in Figure 3.2) for the given specimen material.

The total calculated MFstrength (H_t) is determined along the gauge length by using the co-ordinates from the center of the specimen (Figure 3.6) taken as *X* = 6.25 mm to -6.25 mm, *Y* = -35 mm and *Z* = 0. The magnetic flux density was analytically calculated by using Equation (3.15) on the gauge length of the tensile specimen with the five different tools for *tool-A* to *tool-E* as given in Table 3.4.

The practical reading of magnetic flux density on the tensile specimen with the effects of EMUTT tools measured at the cross-sectional surfaces at ends of the parallel length along the width. The digital gaussmeter with the hall sensor thickness of 0.5mm were used for taking

the practical readings. The practical reading of magnetic flux density at the gauge length for the *tool-A, tool-B, tool-C, tool-D* and *tool-E*, are given in Table 3.4 for ZC440 and DP590 steel sheet thicknesses.

Table 3.4 Results of magnetic flux density along the gauge length of the tensile specimen

EMUTT tools	Results of Magnetic flux density at gauge length (T)	ZC440 (Sheet thickness) in mm			DP590 (Sheet thickness) in mm		
		1.0	1.2	1.4	1.0	1.2	1.6
tool-A	Simulation	0.20	0.20	0.21	0.18	0.17	0.17
	Analytical	0.15	0.18	0.18	0.15	0.15	0.16
	Practical	0.14	0.15	0.16	0.14	0.14	0.15
tool-B	Simulation	0.29	0.27	0.28	0.22	0.22	0.21
	Analytical	0.26	0.25	0.27	0.18	0.19	0.19
	Practical	0.24	0.26	0.28	0.19	0.18	0.20
tool-C	Simulation	0.34	0.36	0.35	0.29	0.28	0.29
	Analytical	0.30	0.32	0.33	0.25	0.25	0.26
	Practical	0.30	0.31	0.32	0.24	0.25	0.27
tool-D	Simulation	0.36	0.39	0.38	0.31	0.30	0.32
	Analytical	0.33	0.34	0.35	0.27	0.28	0.29
	Practical	0.32	0.31	0.33	0.27	0.27	0.29
tool-E	Simulation	0.41	0.41	0.42	0.32	0.33	0.31
	Analytical	0.39	0.38	0.39	0.28	0.29	0.30
	Practical	0.37	0.37	0.38	0.27	0.28	0.29

The results of distribution of magnetic flux density with five different *tool-A* to *tool-E*, obtained by practical, analytical and simulation methods are given in Table 3.4. The practical results of magnetic flux density obtained from the *tool-A* to *tool-E* when compared with the results obtained from numerical methods are observed to be marginally lower than the predicted values and follows the same trend in the case of ZC440 and DP590 steel sheet. The magnetic flux density at the gauge length on the tensile specimen indicates that the volume of the specimen along the length was fully magnetized with the electromagnetic tool. The results of magnetization of the tensile specimens with five different tools from *tool-A* to *tool-E* are expected to affect the tensile properties.

CHAPTER 4

EXPERIMENTAL PROCEDURE

The various techniques and methods employed for conducting the experiments to characterize the properties of ZC440 and DP590 steel sheet are discussed in this chapter. The electromagnetic tool set up was fabricated for conducting the tensile properties with and without MF. The anisotropy study was conducted for characterization sheet formability behaviour with and without MF at 20% of plastic strain. The microstructural characterization was conducted on the tested specimen for 20% of plastic strain with and without MF. On the basis of the results of anisotropy and tensile properties, an electromagnetic tool was developed for Erichsen cupping setup and sheet formability studied with and without MF.

4.1 Determination of tensile properties

The sheet metals tensile characteristics have a significant impact on how it deforms during forming processes. In order to define the behaviour of the material in FE simulations and anticipate the formability of sheet, the stress-strain curves and normal anisotropy are important.

To determine the tensile properties and anisotropy of ZC440 and DP590 steel sheet metals with and without MF, the tensile specimens prepared as per ASTM-E8M (full-size specification) (Figure 4.1 a) for uniaxial tension test were cut by CO_2 Laser (Figure 4.1 b) in such a way that its orientation is arranged at 0°, 45°, and 90° with respect to the rolling direction (RD) of the sheet as shown in Figure 4.1 (c). All the tensile tests were performed on a 50kN universal testing machine (UTM) with a crosshead speed of 5mm/min. Each tensile test was performed thrice to capture the reproducibility of the experimental data points.

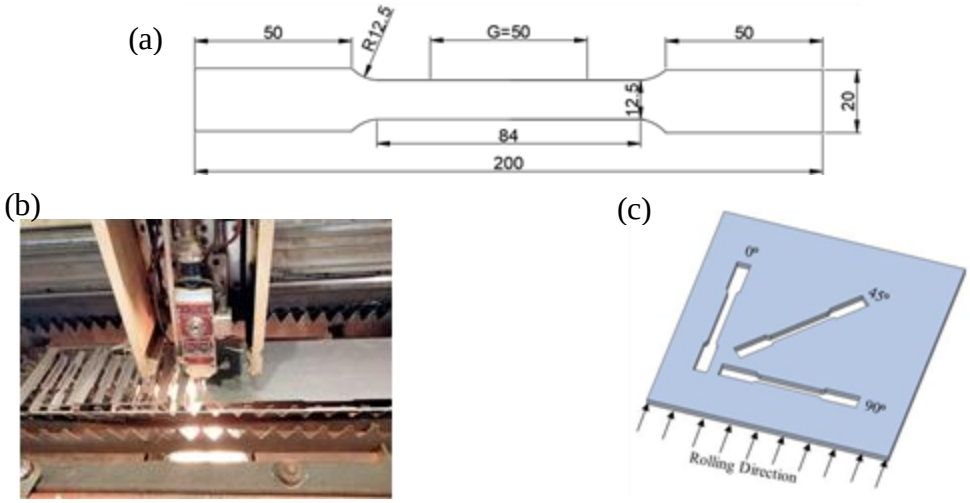

Figure 4.1 (a) Dimension of tensile specimen as per ASTM-E8M (full-size), (b) Laser cutting of full-size tensile test specimens and (c) Tensile specimen arrangement at 0°, 45°, and 90° with respect to the RD.

The engineering stress-strain data was transformed into plots of true stress-true strain data using the following equations:

$$\sigma = \sigma_e(1 + \varepsilon_s) \quad (4.1)$$

$$\varepsilon = ln(1 + \varepsilon_s) \quad (4.2)$$

where, σ = true stress, ε = true strain, σ_e = engineering stress and ε_s = engineering strain.

The log-log plots of true stress-true strain give the values of strain hardening exponent (n) and strength coefficient (K). From the general power law of strain hardening ($\sigma = K\varepsilon^n$), where σ and ε stand for true stress and strain, respectively, the values of the strength co-efficient (K) and strain hardening exponent (n) were calculated from true stress-true strain plots, taking into account the data from within the uniform plastic deformation range.

The normal anisotropy or average plastic strain ratio ($\bar{R}$) of the ZC440 and DP590 steel sheets with and without MF were obtained using the uni-axial stress test of specimens oriented at 0°, 45°, and 90° with respect to the rolling direction, as per ASTM-E517. Tensile specimens were plastically deformed to 20% of plastic strain and cross heads were halted in automatic mode

using the choices available in the machine's specific software, Tinius Olsen Horizon. The width and gauge length were measured before and after the test with a digital vernier calliper, and the plastic strain ratio (R) was computed in all three directions with respect to the RD using the following equations:

$$R = \frac{\varepsilon_w}{\varepsilon_t} = \frac{\varepsilon_w}{-(\varepsilon_w+\varepsilon_l)} = \left[\frac{ln\left(\frac{w_f}{w_0}\right)}{ln\left(\frac{l_0 w_0}{l_f w_f}\right)}\right] \quad (4.3)$$

where, ε_w is true width strain, ε_l is true longitudinal strain, ε_t is true thickness strain, w_0, l_0 are initial width and length, and w_f, l_f are final width and length.

The normal anisotropy ($\bar{R}$) was calculated using the plastic strain ratio (R) values obtained in three different orientations, using the standard formula as given below:

$$\bar{R} = \left(\frac{R_0+2R_{45}+R_{90}}{4}\right) \quad (4.4)$$

where, $R_{0,}$ R_{45} and R_{90} indicate the plastic strain ratio of the tensile specimens oriented at 0°, 45° and 90° with respect to RD.

The $\bar{R}$ value depends on the precision of the prepared edges' squareness and flatness and is highly susceptible to inaccuracy, particularly in width measurement. Therefore, in order to accurately determine the plastic strain ratio, all of the tensile specimens were made by laser cutting.

The error analysis of the plastic strain ratio was also calculated using the ASTM-E517 standard. The error analysis was conducted on the tested specimens with 20% of the plastic strain at 0°, 45° and 90° to the rolling direction with and without the magnetic field. The standard deviation of the value of plastic strain ratio was calculated as below [102]:

$$s(R) = \left\{s(\varepsilon_w)^2\left[\frac{\partial R}{\partial \varepsilon_w}\right]^2 + s(\varepsilon_l)^2\left[\frac{\partial R}{\partial \varepsilon_l}\right]^2\right\}^{1/2} \quad (4.5)$$

where, $s(R)$ is the standard deviation of the plastic strain ratio, $s(\varepsilon_w)$ and $s(\varepsilon_l)$ are the standard deviation in values of true strains in width and length, respectively. The coefficients of variation '$v(R)$', for a given plastic strain ratio were calculated using the following equation.

$$v(R) = \frac{s(R)^2}{R^2} = (1+R)\left[v(\varepsilon_w)^2 + v(\varepsilon_l)^2\right]^{1/2} \quad (4.6)$$

The coefficients of variation '$v(R)$' of the tested specimens with 20% of the plastic strain at 0°, 45° and 90° to the rolling direction with and without the magnetic field were calculated. It was noticed that the values of coefficient of variation '$v(R)$' lies within the acceptable range as per the standard.

4.2 EMUTT tool setup

An experimental setup comprising of five numbers of EMUTT tools wass designed for a universal testing machine (UTM) to carry out a set of uniaxial tensile tests and anisotropy tests as shown in Figure 4.2 (a). A table top UTM with 50kN capacity is controlled by a software HORIZON to run the machine. The tensile specimen as per ASTM-E8M standard was mounted inside the electromagnetic tool and the specimen was held in between the lower and the upper jaw of the machine. The upper jaw of the machine is movable and is connected with a load cell whereas the lower jaw is fixed. A DC regulated power supply was used to connect the electromagnetic tool to produce the magnetic field in the tensile specimens. The DC regulated supply control voltage and current during the test produced constant magnetic field in the tensile specimen. The magnitude of magnetic field was measured with the help of a digital gaussmeter. The probe of the gauss meter is 0.5mm that helps to measure the magnetic field on the tensile specimen. The five EMUTT tools are labeled as *tool-A* to *tool-E* are shown in Figure 4.2 (b), and were used to study the distribution of magnetic flux density in the tensile specimens and the resulting effects on the tensile properties of the ZC440 and DP590 steel.

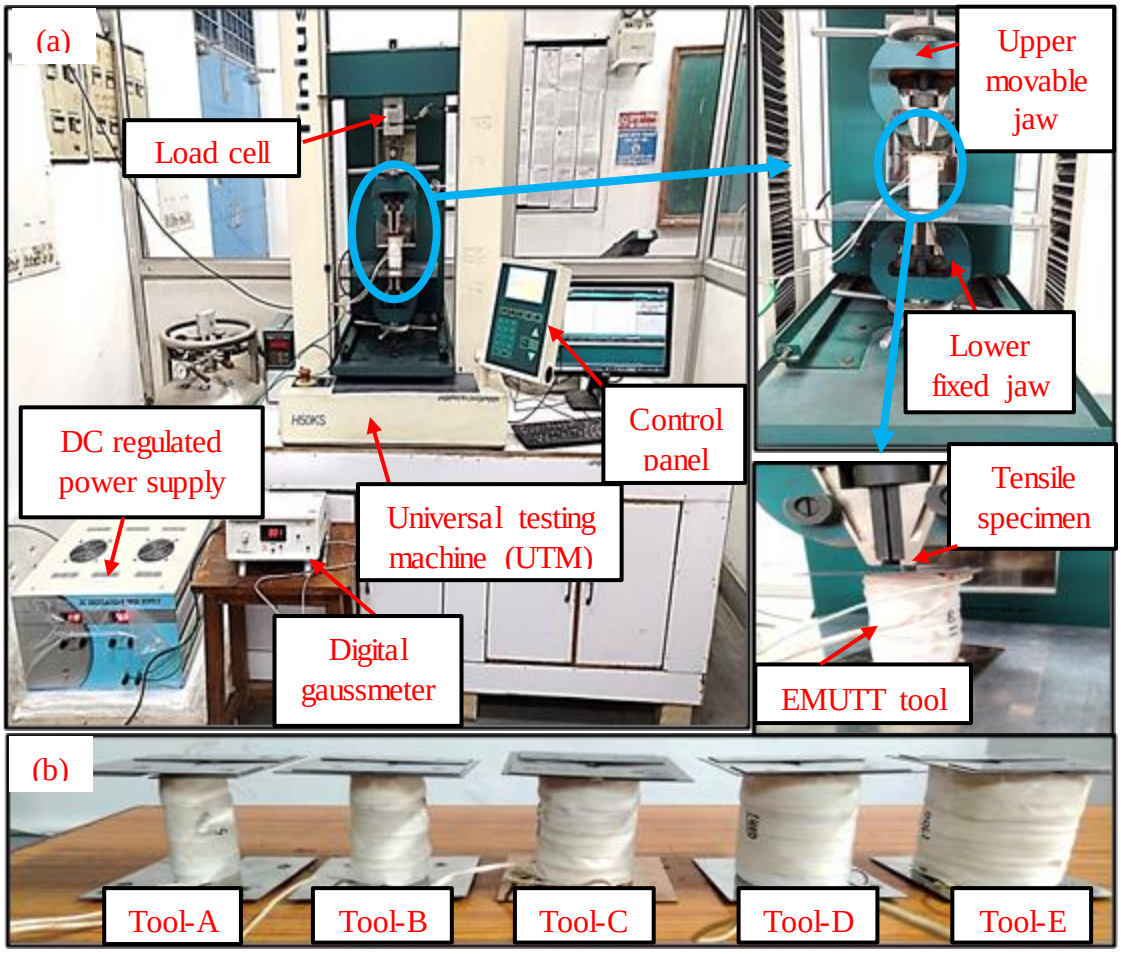

Figure 4.2 (a) Experimental setup showing EMUTT tool attached to the specimen on a UTM and (b) set of five EMUTT tools.

A set of three tensile samples in each direction were tested to capture the reproducibility of results. The tensile experiments were carried out with and without the use of EMUTT tools to observe the changes in the tensile properties of the sheet. The EMUTT tools were fabricated on the basis of the results obtained from magnetostatic simulation as explained in section 3.2. The tools consist of a winding coil of copper enabled wire of 20 gauge. The experiments were performed to validate the magnetostatic results obtained from simulations of EMUTT tools with different parameters and conditions as given in Table 4.1.

Table 4.1 Experimental parameters for EMUTT tools

DC power supply	Parameters
tool-A	7V, 5A
tool-B	9V, 5A
tool-C	13V, 5A
tool-D	20V, 5A
tool-E	33V, 5A

4.3 Microstructural characterization

The microstructural characterization was conducted on the specimens taken from the tensile testing at 20% of plastic strain with and without MF oriented at 0°, 45°, and 90° with respect to the rolling direction of the ZC440 and DP590 steel sheet for different thickness.

4.3.1 Sectioning

Common shearing and sawing procedures cause plastic deformation that seriously damages the specimen cross-section and leaves a bevelled surface that complicates microstructural analysis. Because of this, specimen from the parent materials and tensile tested specimen at 20% of plastic strain, were meticulously cut using a diamond abrasive wheel and a coolant in order to achieve a flat cross-sectional surface and eliminate undesired surface characteristics.

4.3.2 Grinding and electropolishing

Generally, silicon carbide (SiC) grit sizes large enough are used to create an initially smooth surface. Using emery papers with grades (grit sizes) of 220, 400, 600, 800, 1000, 1200, 1500, and 2000 the fine grinding sequence was carried out in progressive order of fineness. The specimens underwent a final process of fine polishing using electropolishing (Struers^{TM} Lectropol-5) as shown in Figure 4.3, resulting in a scratch free surface for electron backscatter diffraction (EBSD).

Figure 4.3 Electropolishing set up.

The ZC440 and DP590 steel specimens were dipped in electrolyte solution of 80% methanol and 20% of perchloric acid. The electropolishing was conducted at 14 V DC and 253K for 16 seconds. In metallographic investigations, this kind of surface is required to view the EBSD microstructure.

4.3.3 Electron backscatter diffraction

To study the deformation behaviour of the tested specimens with and without the use of EMUTT tools, electron backscattered diffraction (EBSD) technique was used for microstructural characterization. For EBSD studies, a TSL-EDAX OIM system mounted on an FEI Quanta-3D field emission gun (FEG) scanning electron microscope (SEM) was used (Figure 4.4).

In all the cases, tensile tested specimens deformed to 20% of plastic strain was considered for microstructural investigations using EBSD and the required samples were taken from the center of the gauge length of the tested specimens as shown in Figure 4.5. In the results obtained by EBSD measurement, grain orientation is represented in three orthogonal axes of the specimen as normal direction (ND), longitudinal direction (LD) and transverse direction (TD). The changes in the grains due to plastic deformation with the effect of magnetic field is also correlated with the changes in tensile properties. The results of EBSD are described in the terms of inverse pole figure, grain boundary map, misorientation angle distribution, pole

figures, kernel average misorientation, geometrically necessary dislocations, and twin boundary map.

Figure 4.4 Field emission gun (FEG) scanning electron microscope (SEM) for electron backscattered diffraction (EBSD) analysis.

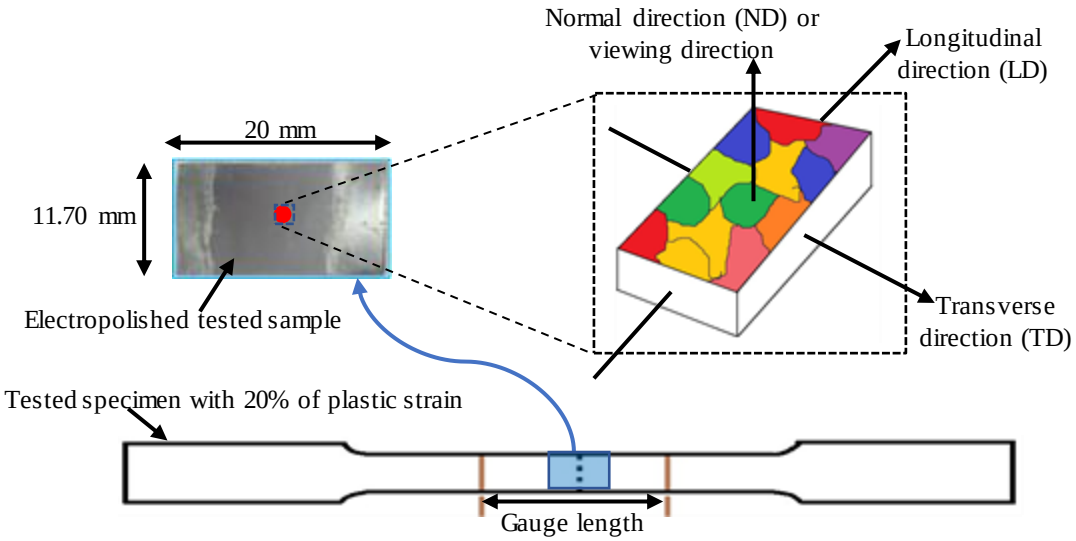

Figure 4.5 Magnified view of tested specimen at the center of the gauge length for EBSD analysis.

4.4 Erichsen cupping test set up with electromagnetic tool

The Erichsen cupping test was performed appropriately according to the ASTM-E643 international standard. This standard test method explains the plastic deformation that can occur during stretch forming in metallic sheets and strips with a thickness of 0.1mm to 2mm and a width of 90mm or more.

4.4.1 Design of electromagnetic tool for Erichsen cupping

Tensile properties and anisotropy obtained with the MF *tool-A* to *tool-E*, confirmed that the results of *tool-C* have greater impact on the material properties of both the material and hence MF results were further used for formability analysis. A modified electromagnetic tool was designed for the Erichsen cupping test samples. An FEA model was prepared and simulated for the sheet sample (300 mm of length × 90 mm of Width × 1.6 mm of thickness) with the same parameters as assigned to the tool. The simulation results of the contour plot of magnetic flux density on the sheet with two electromagnetic tools of the same dimensions were used for achieving approximately 0.29T at the focus area of the sheet are shown in Figure 4.6 (a). A square box shows the focus area during deformation. The magnetic flux density in the center area of the sheet was observed to be 0.29T. The distribution of the magnetic flux density plot in the functional area of the length and width of the sheet is shown in Figure 4.6 (b). It was observed that the tool developed for the Erichsen cupping confirm with the results obtained with EMUTT *tool-C*. The bobbin for electromagnetic tool was made up for 0.5 mm thickness stainless steel sheet which is same as for EMUTT tool bobbin and final dimensions of the bobbin are given in Figure 4.7.

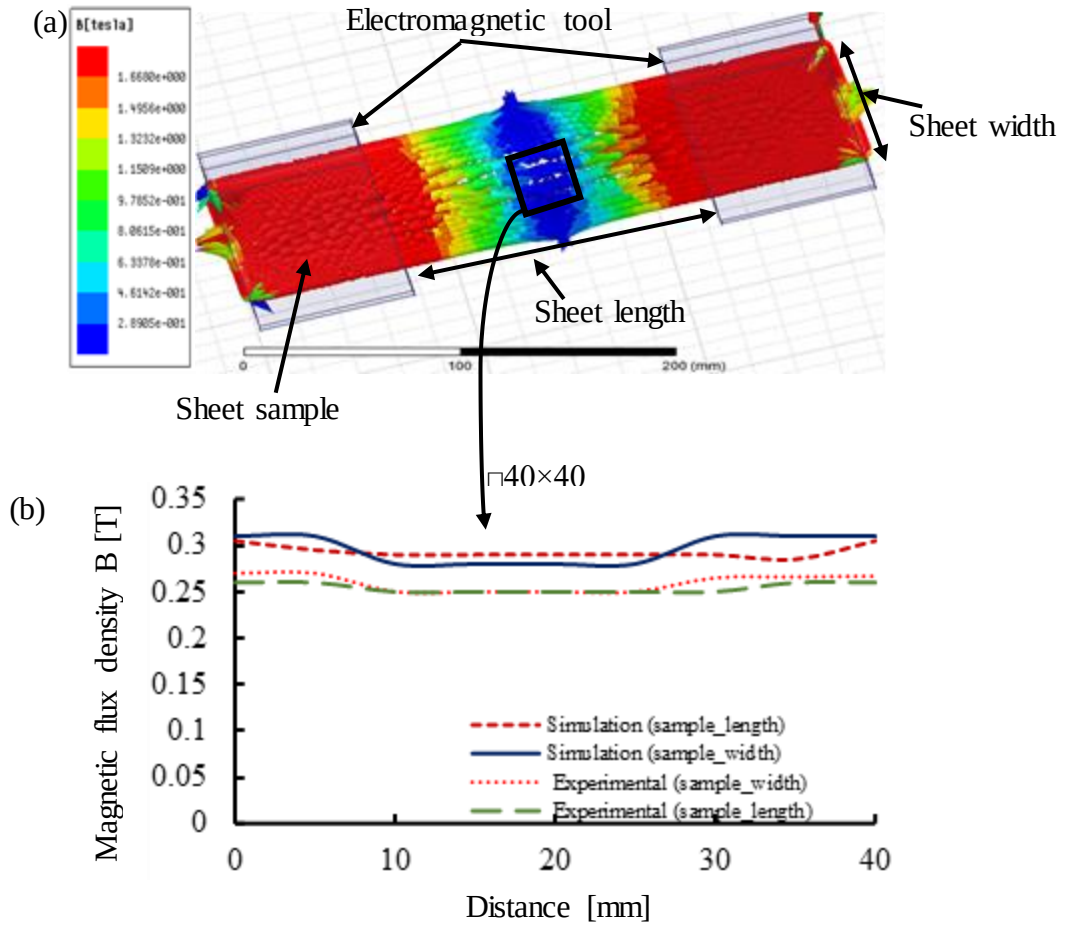

Figure 4.6 (a) Magnetic flux distribution contour plot for Erichsen cupping experiment, (b) Comparison of Experimental and the simulation results of the magnetic flux density at the center of the sheet along the width and length.

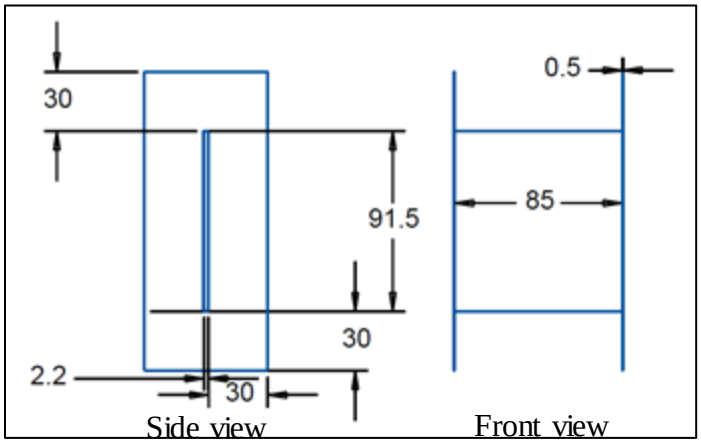

Figure 4.7 Bobbin final dimensions for the Erichsen cupping experiment.

4.4.2 Sheet metal blank preparations

For characterization of the sheet formability in the stretch forming with and without MF, the blanks were prepared as per the ASTM-E643 standard. The blanks were cut through the CO_2

laser cutting machine for sample tested without magnetic field (90mm of length × 90mm of Width and thickness of the samples is 1.0, 1.2 and 1.6mm) for DP590 sheet and 1.0, 1.2 and 1.4mm for ZC440 sheet. On the other the blanks were taken for MF tests on Erichsen cupping measured 300mm of length × 90mm of width and thickness varied as per ZC440 and DP590 material. The blanks were cleaned with acetone after laser cutting.

4.4.3 Electromagnetic tool setup on Erichsen cupping

The formability of the steel sheet was evaluated with Erichsen index (IE) number in which a spherical punch with Ø20 mm was used to deform the sheet by stretching it (with and without the MF) into a die with a clearance so that the punch displacement corresponds to the IE at which necking occurs a tool setup a shown in Figure 4.8 (a). The blanks were placed at the center of the punch and fixed in between the die and holder. A thick layer of petroleum grease was applied on the punch surface to avoid the friction in between the sheet and punch.

The experiments were conducted on the manually operated Erichsen cupping machine as shown in Figure 4.8 (a). An electromagnet was switched on before proceeding the test. Both the tools were connected in series with the DC regulated power supply and with help of digital gauss meter the magnetic field was measured at the surface of blank. To avoid the losses of magnetic field a thin sheet of stainless steel was tighten on the holder and die surface. A 14 A current and 30 V voltage DC supplied was needed for producing the 0.29T at the center of the blank which is in front of the profile of the punch. A manually continually load was applied on the wheel till the crack line is seen on the mirror. The dial indicator shows the depth of the cup or Erichsen index. After the cup was drawn then Erichsen index was again verified by the height gauge as shown in Figure 4.8 (b).

Figure 4.8 (a) Erichsen cupping experiment setup with MF, (b) vernier height gauge for IE value measurement, (C) BECT-100 Erichsen tester (IIT Roorkee) for force measurement.

For the measurement of the punch force the Erichsen cupping test was performed on the computer controlled Erichsen cupping tester BECT-100 as shown in Figure 4.8 (c). The necking is sensed by a sudden drop in the punch force and the test was stopped. It was observed that the percentage thinning is higher with MF in comparison to the results obtained without MF. The value of IE was determined for deformed sheet tested with and without MF. The same process was followed as the manually operated machine in case of with and without MF. The force graph confirmed the effect of magnetic field on the ZC440 and DP590 steel sheet. The percentage of error observed in the value of IE between the manually and the computer controlled was negligible. The deformed sheet thicknesses with and without MF of ZC440 and DP590 material is shown in Figure 4.9 (a) and (b), respectively.

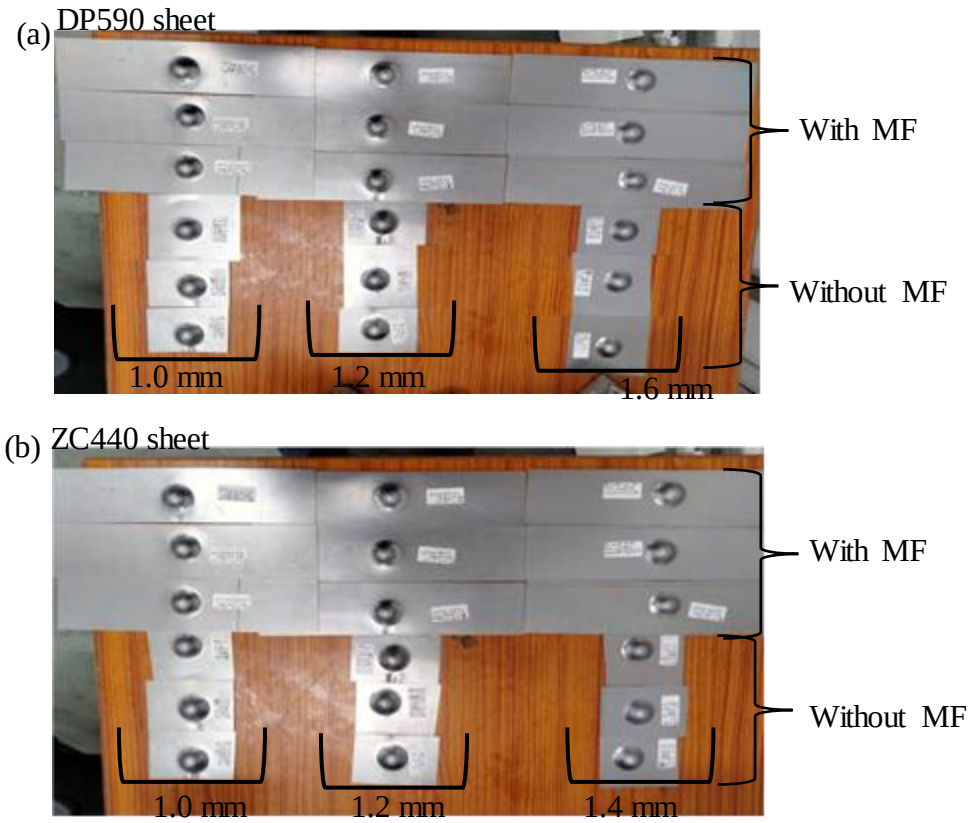

Figure 4.9 (a) Deformed sheet thicknesses with and without MF of DP590, (b) Deformed sheet thicknesses with and without MF of ZC440.

A relation between the height and the radius of the dome was determined at transverse-section view of the dome profile (images captured with 70X inverted microscope and processed in the Creo software). The dome height was obtained using the Erichsen cupping experiments. The formability of the steel sheet was evaluated with Erichsen Index (IE) number in which a spherical punch with Ø20 mm is used to deform the sheet by stretching it (with and without the MF) into a die with a clearance so that the punch displacement corresponds to the IE at which necking occurs.

CHAPTER 5

FINITE ELEMENT SIMULATION OF ERICHSEN CUPPING INDEX

The researchers have used a range of analytical and numerical techniques to study and assess the deformation behaviour of sheet metal during forming. Typical methods for figuring out forming loads and restricting deformation, like the slab method, upper and lower bound approaches, and slip line field theory. Unfortunately, these methods have a low degree of accuracy because they simplify the problem by making a lot of assumptions. However, because of developments in computer technology, the Finite Element Method (FEM) may now be used to study sheet metal forming operations in an efficient manner. Finite Element Analysis, or FEA, is currently the most popular mathematical method used to assist design engineers in moving past time-consuming, experience-based trial and error approaches to achieve desired outcomes. The division of the body into finite elements connected by nodes is the fundamental concept of FEM. To derive an approximate solution, a set of algebric equations are generated using the discretized form of virtual work expression in space and time [103]. The nodal displacements of the element are obtained by solving these FE equations, and these nodal displacements are then fed into the element operator matrices to calculate the stress and strain tensors at element integration sites. After using a FE method to model a typical sheet metal forming process, the resulting FE equations are strongly non-linear due to the large deformations (material and geometric non-linearities) involved in the metal forming as well as the change in boundary conditions (boundary non-linearity) brought on by friction at the interfaces between the sheet metal and the forming tools. Because of this, the numerical solution of these FE equations requires the use of incremental processes based on explicit time integration schemes or implicit time schemes. The computation of the time-

history of nodal displacements and element stresses and strains in FE simulations requires a significant amount of computer resources because of the nature of the forming processes.

Since the Erichsen cupping test was used to evaluate sheet metal quality, it was usually utilised to determine the sheet metal's formability and the point at which through-thickness failure occurred [104,105]. For structural components, the impact of stretch formability on the metal's crystalline structure has also been thoroughly studied because any flaws that are introduced into the sheet during forming could be harmful [106,107]. Because employing sheet metal and lowering component weights has numerous financial benefits, research has mostly focused on behaviour of the metal [108] and evaluating the formability of the sheet [104]. The surface strain to failure has not been completely defined by deep drawing changes or simulations of the Erichsen cupping test [109].

In this work, Erichsen cupping test simulation was performed as per ASTM-E643 for the ZC440 (1.0 1.2 and 1.4mm) and DP590 (1.0 1.2 and 1.6mm) steel in various sheet thicknesses. The commercial software ABAQUS was used to run the simulations. Using MF plastic strain data as the failure criterion in the postprocessor, these simulations have predicted the Erichsen index (IE) both with and without the data. The simulations have employed the IE values inferred from the established correlations to increase the precision of failure prediction. The following explains the crucial steps in the simulation technique.

5.1 About the software

The current study used ABAQUS (version 6.10.1) software to simulate sheet formability by using stretch the sheet with and without MF plastic strain data of the ZC440 and DP590 sheet. For stretching simulations, ABAQUS's explicit solution process is utilised because it can quickly and easily handle complex contact problems; however, the implicit method is employed. Formability simulations typically give lower non-linearity and remove the die and

punch constraints (non-contact problem). Formability problems are typically solved more quickly by ABAQUS-standard (Implicit) than by Explicit. As a result, it is recommended to use Explicit for the bending simulation and export the finished model to ABAQUS- Standard afterward.

5.2 Modelling and simulations of sheet stretching process

The current work treats the stretching process of sheet as a non-linear issue. In general, nonlinearity in the bending issue can originate from three sources: nonlinearity in the material, nonlinearity in the boundary, and nonlinearity in the geometry. The reason for material nonlinearity is the anisotropic sheet metals' plastic behaviour, which follows the strain hardening power law in the true-strain and true-stress curve region.

As with the stretching process, boundary nonlinearity results from changes in the boundary conditions. The sheet metal is first put on the die shoulder during the stretching operation, allowing just the bottom surface of the sheet metal to come into contact with the die shoulder. The top surface of the sheet metal comes into contact with the holder bottom surface and locked the sheet. Punch makes touch with the upper surface of the sheet metal to stretch it; the material then undergoes plastic deformation until it eventually makes punch force goes drop down and sheet thickness get cracked. Contact boundary conditions cause a significant and instantaneous change in the model's response when a contact happens during a simulation, leading to non-linearity. The third cause of nonlinearity has to do with how a model's geometry evolves as it is being analysed. When a sheet of metal is stretched, it deforms significantly and the punch force is not parallel to the bent sheet. As the displacements and velocities at the start of the increment determine the state at the end of the increment, this is known as "explicit" behaviour. When it comes to simulations, a lot of increments are needed. However, the cost of an explicit method is substantially lower per increment than an implicit

approach because no global set of equations are solved in each increment. For these reasons, non-linear analysis is a good fit for ABAQUS-Explicit.

In order to understand the plastic deformation during stretching and its effect on formability phenomenon, simulations for stretching were carried out for ZC440 and DP590 parent sheets with variation in of sheet thicknesses and their results are compared with MF data of plastic strain. The stretching simulations were carried out for parent materials during which the dimension of specimens for stretching taken as quarter diameter of the original sheet blank diameter that is 90mm considered for the modelling as shown in Figure 5.1. The deformable surfaces defining the surface of the blank as a homogeneous continuum shell and the thickness of the shell was assigned as thickness of the sheet.

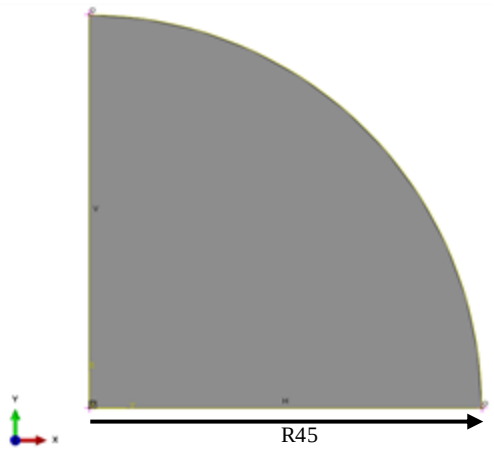

Figure 5.1 Sheet blank surface modelled in FEA (dimensions in mm)

In ABAQUS, the default value for thickness integration by Simpson rule with five points integration was used for both the materials specimens. Three types of integration schemes like the Gauss, Simpson, and Lobatto integration schemes are suggested for use in Finite Element simulations. The integration scheme and integration sites across sheet thickness determine the prediction of formability [110]. Many scholars have demonstrated in their investigations that the accuracy of formability prediction is unaffected by more integration points than 5 to 7

[111,112]. Because formability is a function of stretching moment, which is a function of stress distribution in sheet thickness, shell elements necessitate numerical integration of stress and strain through thickness in order to calculate force and bending moment [113]. The Simpson rule with five integration points method was chosen since the number of integration points directly impacts the simulation time.

The focus of simulation was not to study the stress variation in the die, holder and punch. So, these were modelled as discrete rigid surfaces as shown in Figure 5.2 (a), (b) and (c), respectively. Moreover, discrete rigid surfaces assigned coarse meshing and quarter dimension of model considered for less time consuming to simulate. The punches were modelled to have profile radii of 10mm, die with radius of 13.5mm, and holder with radius of 15mm. All the tools were modelled using ABAQUS CAE interface and were assembled as shown in Figure 5.3.

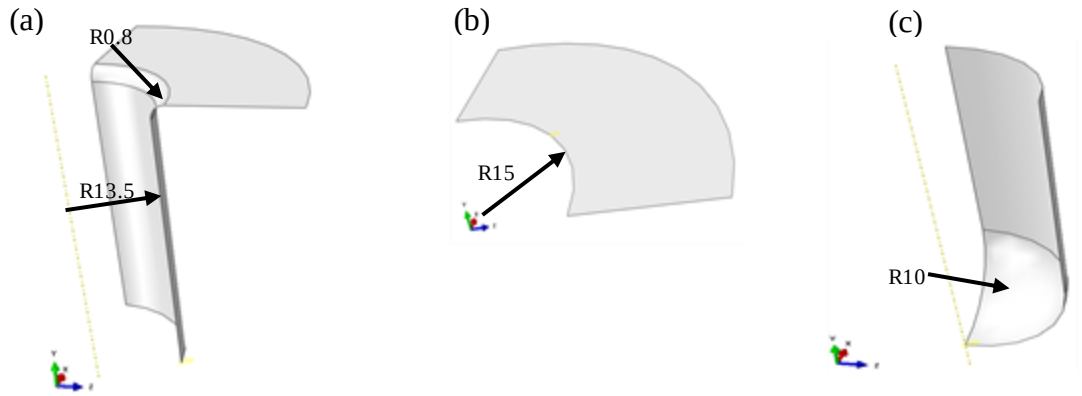

Figure 5.2 Shell quarter model (a) die surface, (b) holder surface, and (c) punch surface are discrete rigid parts (all dimensions in mm).

The die, holder and punch were modelled as discrete rigid shell with R3D4 shell elements. The R3D4 shell element is a 4-node 3-D bilinear rigid quadrilateral. On the other hand, the sheet blank has S4R shell elements and is a deformable shell planar. With four nodes, reduced

integration, hourglass control, and finite member stresses, the S4R shell element is a thin shell element.

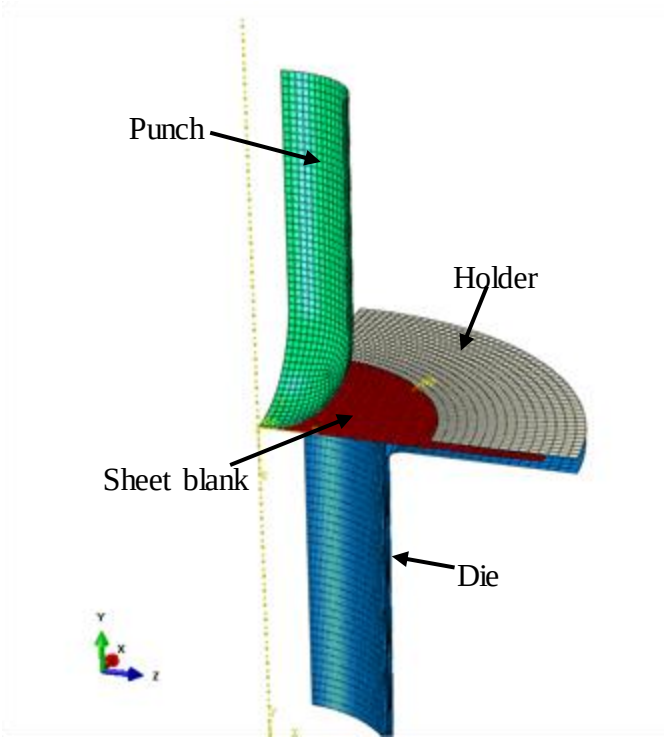

Figure 5.3 Assembly of shell quarter model parts for stretching simulation of sheet metal.

The number of elements, nodes and variables used in the FE simulation model for simulation were found by the trial simulations and converging the mesh elements with punch force graph. In the stretching of conventional blank given by the velocity to the punch, at a certain point where the punch force goes drop down and the element get stretched to indicate the necking occurs. The punch force with the mesh elements size graph is shown in Figure 5.4 (a). It is seen that the punch force higher in coarse mesh size (element size 3) as compared to the finer mesh size (element size 0.3). In the element size of 0.5 and 0.3 give almost same graph of force with displacement. On the basis of the punch force graph with displacement, elements size was again compared with the mesh elements numbers as shown in Figure 5.4 (b). It shows that at the mesh element increased punch force get decreased, but at mesh element size 0.5 and 0.3 very less change in force values was observed. It is also observed that at the coarse

mesh size taking less time but is gives inaccuracy and at very fine mesh gives the accuracy but increased the simulation time.

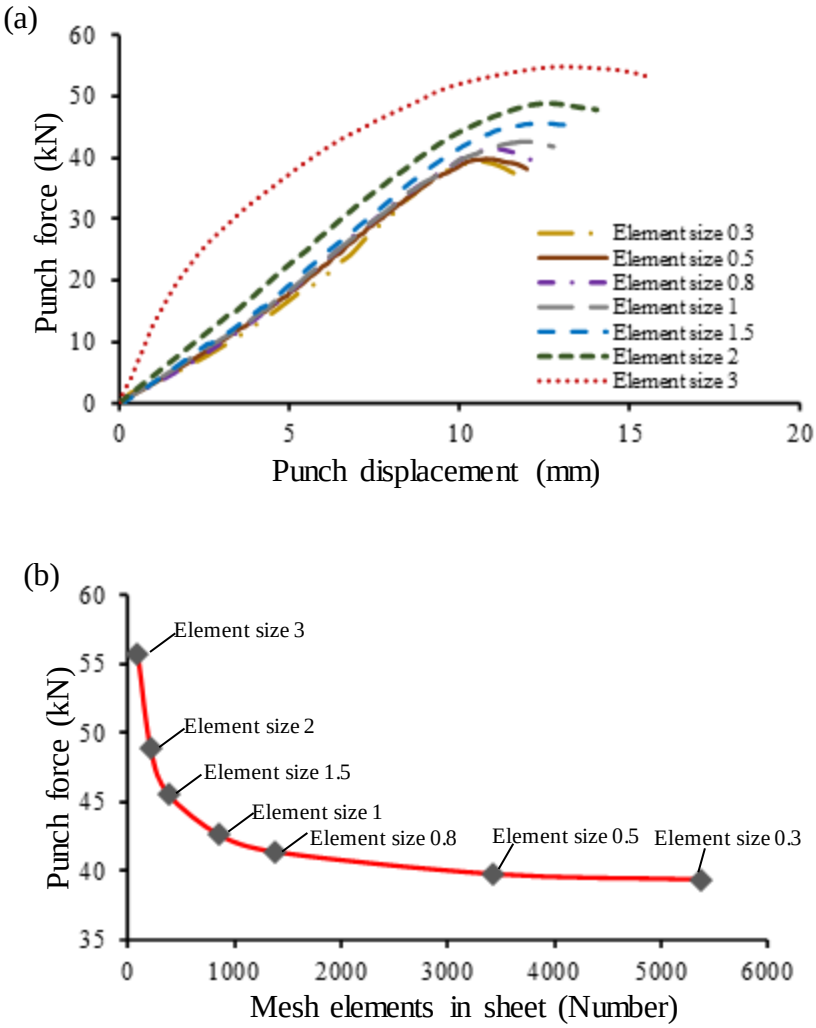

Figure 5.4 Erichsen cupping FEA analysis for mesh convergence plots (a) punch force vs. punch displacement in different elements size, and (b) punch force vs. mesh elements number of different elements size.

In order to calculate the dynamic response of the discrete rigid holder a point mass has to be assigned to the reference point on these rigid bodies. In quasi-static analysis, the punch load must be applied as smoothly as possible to maximise efficiency and accuracy; jerky and abrupt load application creates stress waves in the blank, leading to a noisy and imprecise solution; gradual load application calls for tiny acceleration changes between increments, resulting in a gradual change in displacement and velocity; and the explicit method, with its integrated

amplitude curve, generates a smooth loading amplitude that was assigned to the punch's reference point. An example of application of punch load during stretching simulation is shown in Figure 5.5.

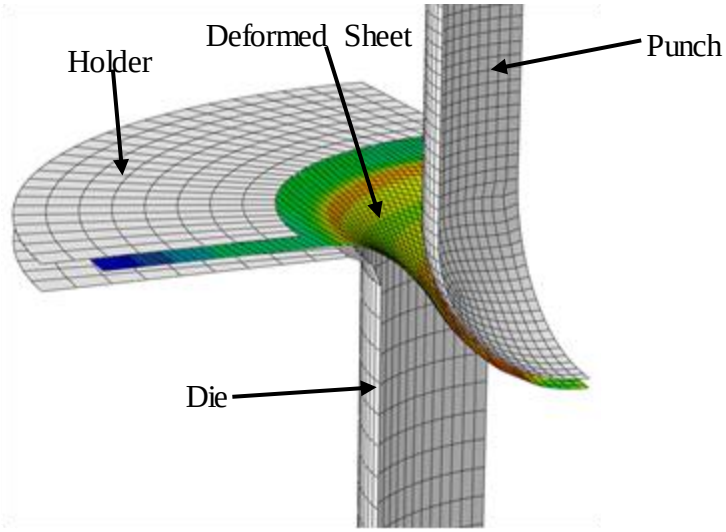

Figure 5.5 Simulation of stretch forming on Erichsen cupping test setup of ZC440 and DP590 steel sheet.

5.3 Material model

A material's post-yield hardening and yield point provide information about its nonlinear plastic behaviour. Elastic strains are strains connected to elastic deformation, whereas plastic strains are strains connected to fixed deformation. The true stress-true strain plot obtained from the uniaxial tension test makes it clear that the sheet material experiences uniform plastic strains between the yield point and the UTS. The strain hardening continues according to the power law of strain hardening ($\sigma = K\varepsilon^n$), where n is the strain hardening exponent and K is the strength coefficient. The majority of sheet materials are anisotropic in nature, which is measured by the plastic strain ratio, in addition to obeying the power law of strain hardening. It has been used in FE modelling to incorporate anisotropy of sheets [114]. Hill's plasticity model, also known as Hill's 1948 yield potential, is an extension of the Mises yield function

for anisotropic materials. It is expressed in terms of rectangular cartesian stress components as given below:

$$f(\sigma) = \sqrt{F(\sigma_{22} - \sigma_{33})^2 + G(\sigma_{33} - \sigma_{11})^2 + H(\sigma_{11} - \sigma_{22})^2 + 2L\sigma_{23}^2 + 2M\sigma_{31}^2 + 2N\sigma_{12}^2} \quad (5.1)$$

where L, M, and N are found from shear tests on the material in various orientations, while F, G, and H are constants derived through uniaxial tension testing. They are described as

$$F = \frac{(\sigma_0)^2}{2}\left(\frac{1}{\bar{\sigma}_{22}^2} + \frac{1}{\bar{\sigma}_{33}^2} - \frac{1}{\bar{\sigma}_{11}^2}\right) = \frac{1}{2}\left(\frac{1}{R_{22}^2} + \frac{1}{R_{33}^2} - \frac{1}{R_{11}^2}\right) \quad (5.2)$$

$$G = \frac{(\sigma_0)^2}{2}\left(\frac{1}{\bar{\sigma}_{33}^2} + \frac{1}{\bar{\sigma}_{11}^2} - \frac{1}{\bar{\sigma}_{22}^2}\right) = \frac{1}{2}\left(\frac{1}{R_{33}^2} + \frac{1}{R_{11}^2} - \frac{1}{R_{22}^2}\right) \quad (5.3)$$

$$H = \frac{(\sigma_0)^2}{2}\left(\frac{1}{\bar{\sigma}_{11}^2} + \frac{1}{\bar{\sigma}_{22}^2} - \frac{1}{\bar{\sigma}_{33}^2}\right) = \frac{1}{2}\left(\frac{1}{R_{11}^2} + \frac{1}{R_{22}^2} - \frac{1}{R_{33}^2}\right) \quad (5.4)$$

$$L = \frac{3}{2}\left(\frac{\tau_0}{\bar{\sigma}_{23}}\right)^2 = \frac{3}{2}\left(\frac{1}{R_{23}^2}\right) \quad (5.5)$$

$$M = \frac{3}{2}\left(\frac{\tau_0}{\bar{\sigma}_{13}}\right)^2 = \frac{3}{2}\left(\frac{1}{R_{13}^2}\right) \quad (5.6)$$

$$N = \frac{3}{2}\left(\frac{\tau_0}{\bar{\sigma}_{12}}\right)^2 = \frac{3}{2}\left(\frac{1}{R_{12}^2}\right) \quad (5.7)$$

where, $\tau_0 = \sigma_0/\sqrt{3}$, σ_{ij} is non zero stress component and $\bar{\sigma}_{ij}$ is the measured value of yield stress, σ_0 is yield stress by user defined.

The anisotropic yield stress ratios are R_{11}, R_{22}, R_{33}, R_{12}, R_{13} and R_{23}.

The six yield stress ratios are given by $\frac{\bar{\sigma}_{11}}{\sigma_0}, \frac{\bar{\sigma}_{22}}{\sigma_0}, \frac{\bar{\sigma}_{33}}{\sigma_0}, \frac{\bar{\sigma}_{12}}{\tau_0}, \frac{\bar{\sigma}_{13}}{\tau_0}$ and $\frac{\bar{\sigma}_{23}}{\tau_0}$

where the material's yield stresses along the rolling, transverse, thickness, and diagonal directions are, in order, where $\bar{\sigma}_{11}$, $\bar{\sigma}_{22}$, $\bar{\sigma}_{33}$, and $\bar{\sigma}_{13}$.

The yield stress in the thickness direction is hard to determine. Therefore, using the following formulas, the anisotropy yield stress ratios are calculated using equation below:

$$R_{11} = R_{12} = R_{23} = 1 \quad (5.8)$$

$$R_{22} = \sqrt{\frac{R_{90}(R_0+1)}{(R_0+R_{90})}} \quad (5.9)$$

$$R_{33} = \sqrt{\frac{R_{90}(R_0+1)}{R_0(R_{90}+1)}} \quad (5.10)$$

$$R_{13} = \sqrt{\frac{3(R_0+1)R_{90}}{(R_{90}+R_0)(2R_{45}+1)}} \quad (5.11)$$

where, R_0, R_{45} *and* R_{90} are the experimentally obtained plastic strain ratios for the specimens orientated with respect to the RD at 0°, 45°, and 90°. The experimentally obtained values of anisotropy yield stress ratios for the ZC440 (varies thickness 1.0, 1.2 and 1.4mm) and DP590 (varies thickness 1.0, 1.2 and 1.6mm) materials with and without MF are presented in Tables 5.1 and 5.2, respectively. The different yield stress ratios were employed in FE simulations to account for anisotropy in the cases of ZC440 and DP590 steels with and without MF. Since the yield stress ratio values with the MF for both the materials (ZC440 and DP590) in all the thicknesses are higher than the case of values obtained without MF. The explicit approach of stretching simulations has allocated a density of steel (7850 kg/m^3) to deformable sheet metal because of the dynamic character of the problem. All of the simulations in ABAQUS have used experimental engineering stress and engineering strain data of parent sheets tested with and without MF.

Table 5.1 Yield stress ratios used in FEA to incorporate anisotropy of ZC440 steels with and without MF

Sheet thickness (mm)	Testing conditions	R_{11}	R_{22}	R_{33}	R_{12}	R_{13}	R_{23}
1.0	Without MF	1.0	1.018	1.026	1.0	1.047	1.0
	With MF	1.0	1.072	1.012	1.0	1.048	1.0
1.2	Without MF	1.0	1.050	1.031	1.0	1.068	1.0
	With MF	1.0	1.117	1.026	1.0	1.088	1.0
1.4	Without MF	1.0	1.068	1.040	1.0	1.057	1.0
	With MF	1.0	1.154	1.029	1.0	1.090	1.0

Table 5.2 Yield stress ratios used in FEA to incorporate anisotropy of DP590 steels with and without MF

Sheet thickness (mm)	Testing conditions	R_{11}	R_{22}	R_{33}	R_{12}	R_{13}	R_{23}
1.0	Without MF	1.0	1.011	1.025	1.0	1.070	1.0
	With MF	1.0	1.065	1.028	1.0	1.073	1.0
1.2	Without MF	1.0	1.015	1.047	1.0	1.074	1.0
	With MF	1.0	1.088	1.053	1.0	1.107	1.0
1.6	Without MF	1.0	1.055	1.039	1.0	1.142	1.0
	With MF	1.0	1.125	1.040	1.0	1.152	1.0

5.4 Contact and boundary conditions in stretching simulations

The blank was defined as the master and the tool were considered as slave surfaces. The surface between the blank and tool was defined by using forming one way surface to surface card. The tool was positioned along the working direction (z-axis). Before running the simulation for analysis, a gap equal to blank thickness (as per given materials thickness of ZC440 and DP590 steels) was provided between the holder and die where middle surface of the shell was considered. To avoid the penetration of the tool, the middle surface of the blank shell interacts with the tool center before proceeding simulations in all the cases. The punch travel in the negative Y direction with a velocity of 0.42mm/s as shown in Figure 5.6 (a). To avoid wrinkling and allow material flow into the die, an optimum blank holding force 10N was applied on the blank by holder surface as shown in Figure 5.6 (b). To run the simulations successfully, a step time was taken as 1.2 and get the optimum results to avoid simulation run time.

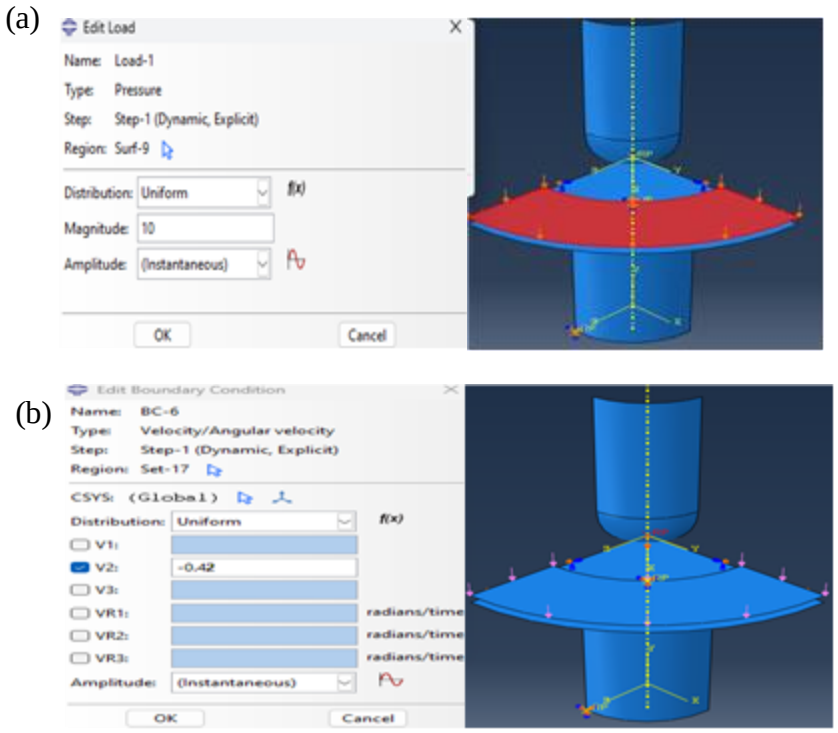

Figure 5.6 FE simulation boundary conditions for (a) holder pressure, and (b) punch velocity.

A wide range of engineering issues necessitate defining contact between two or more components. Shear forces that prevent the components in contact from sliding are produced by friction between the two surfaces. Determining the surfaces in touch is the goal of contact definition in order to assess the contact pressures that are produced. In FEA, contact definitions are a unique kind of discontinuous constraint that only becomes active when two surfaces come into contact, allowing forces to transfer between components. Coulomb's law of friction ($\tau = \mu p$) is a widely used method to define the interaction between surfaces at room temperature. The contacting surfaces won't slide until the shear stress across the interface reaches the limiting frictional shear stress (τ), which is given by this equation. In order to establish contact properties with automatic controls, friction formulation was used to describe penalty contact. At the blank-punch interfaces, the coefficient of friction was assigned as 0.05, respectively [115-117]. Punch velocity in the Y-direction was

predetermined, and the die was given a boundary condition of 'Encastre' (zero displacement and rotation about x, y, and z).

5.5 Erichsen cupping simulation and measurement

The original output file from the simulated stretching process of sheet blank history, all constraints in the Erichsen cupping tester model are removed before evaluating and capturing the outcomes of the stretch forming simulations. The Erichsen cupping index or the punch displacement contour images after sheet deformed till the necking with and with MF plastic strain data of the ZC440 and DP590 steels are shown in Figure 5.7 and 5.8, respectively. For the section sheet thickness, nodes displacement was captured at the edges of deformed sheet blank by creating a path.

In order to examine the variability in punch force regarding punch displacement, a set was defined on the punch's reference point to record anticipated data for punch force and displacement in simulations. For the specified sets, a historical output request was assigned for the punch force and displacement. A built-in digital filter called "smooth2" that may eliminate unwanted frequency content from a discrete time-domain single smoothened the acquired data points for punch force and displacement [118].

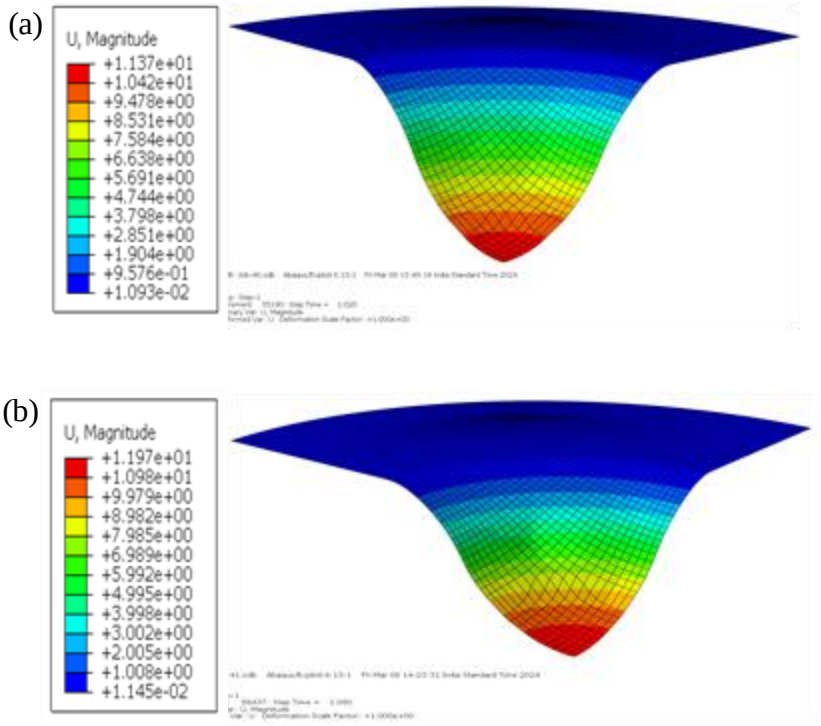

Figure 5.7 FE simulation of Erichsen cupping depth contour plots of the ZC440 sheet (a) without MF and (b) with MF.

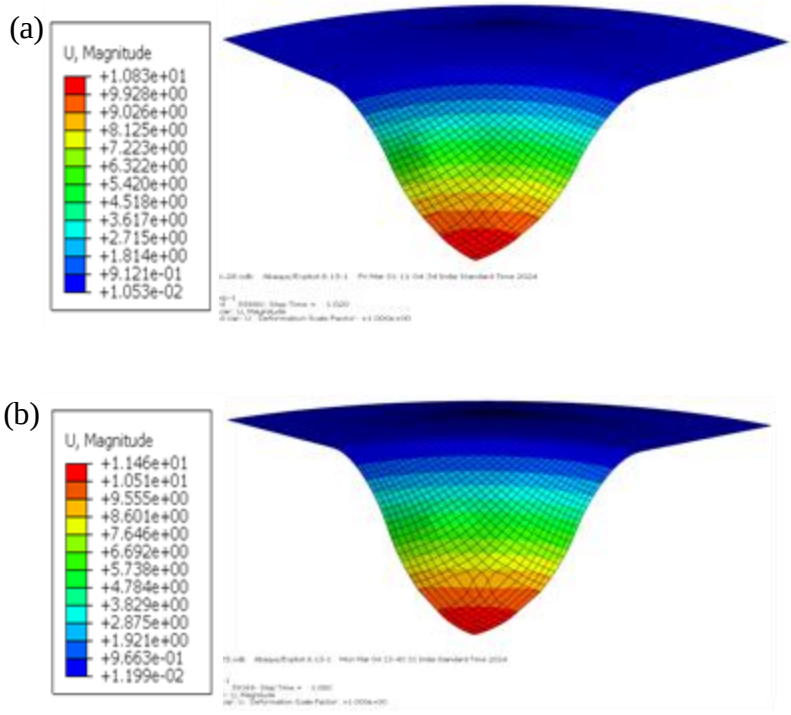

Figure 5.8 FE simulation of Erichsen cupping depth contour plots of the DP590 sheet (a) without MF and (b) with MF.

CHAPTER 6

RESULTS AND DISCUSSION: FORMABILITY CHARACTERIZATION

The experiments were performed to observe the changes in the tensile properties and behaviour of the material during plastic deformation under the effect of five different magnitudes of magnetic field. Based on the degree of improvement in the results of tensile properties, the best one among the five tools is chosen. In order to understand the variation in tensile properties due to MF, the results are further explained on the basis of the microstructural features obtained from the center of the gauge length of the tested tensile specimens with 20% of plastic strain of the specimens.

6.1 Tensile properties of DP590 steel

The results obtained from uniaxial tension tests in three different orientations with and without MF are summarized in Table 6.1. The values of yield strength (YS) and ultimate tensile strengths (UTS) without MF are observed to be the maximum in the specimens with an orientation of 45° to the RD, followed by the specimen oriented at 0° and 90°. The values of strain hardening exponent (*n*) which exhibits the stretchability are found to have a small variation w.r.t. the RD. The value of normal anisotropy is approximately 0.97 which indicates an average formability of the sheet.

The tensile properties of the specimens oriented at 0°, 45°, and 90° to the RD obtained with the use of EMUTT *tool-A* to *tool-E* are also obtained by experiments as given in Table 1. It is observed that the YS and UTS increases initially with the increase in the magnitude of the MF from *tool-A* to *tool-C* and then decreases with *tool-D* to *tool-E* although the MF increases. The decrease in these properties could be attributed to the deviation of MF away from the tensile specimen being tested resulting in a non-uniform MF. The values of YS of the sheet

material tested with orientations of 0°, 45°, and 90° to the RD are observed to increase to 448 MPa, 467 MPa, and 459 MPa, respectively, as a result of the MF utilizing *tool-C*. A similar trend of increase in the values of UTS is also seen with MF.

Table 6.1 Tensile properties of DP 590 steel sheet (1.6 mm) with and without MF.

Experimental conditions	Orientation w.r.t. the RD	YS (%0.2) (MPa)	UTS (MPa)	% Elongation	*n*	*R*	$\bar{R}$	$v(R)$
Without MF	0°	419±1.1	572±1.3	25.0	0.189	1.06	0.97	~3.2%
	45°	442±1.5	594±1.4	22.6	0.181	0.78		~2.9%
	90°	421±1.6	581±1.2	23.1	0.186	1.25		~4.1%
EMUTT tools (MF applied longitudinal to load direction)								
tool-A (0.17 T)	0°	431±1.6	576±1.6	23.4	0.174	1.10	1.03	~2.5%
	45°	451±2.1	599±1.5	22.1	0.169	0.83		~3.2%
	90°	438±1.9	587±1.7	22.2	0.176	1.30		~3.9%
tool-B (0.22 T)	0°	434±1.7	581±1.7	23.0	0.177	1.16	1.07	~4.5%
	45°	455±1.8	602±1.8	21.8	0.171	0.88		~2.7%
	90°	441±1.5	594±1.5	22.0	0.177	1.39		~3.5%
tool-C (0.29 T)	0°	448±1.5	601±2.0	24.1	0.179	1.31	1.19	~2.8%
	45°	467±1.9	619±1.7	21.8	0.175	0.93		~2.6%
	90°	459±1.7	613±1.6	22.2	0.178	1.59		~3.7%
tool-D (0.31 T)	0°	436±2.1	582±2.0	23.1	0.176	1.24	1.10	~3.4%
	45°	457±2.1	604±2.0	22.0	0.173	0.86		~4.6%
	90°	449±2.0	596±2.0	22.0	0.173	1.45		~4.1%
tool-E (0.32 T)	0°	432±2.0	579±2.0	23.5	0.177	1.26	1.07	~4.2%
	45°	454±2.0	603±2.0	22.5	0.176	0.88		~3.5%
	90°	453±2.0	592±2.0	22.3	0.177	1.35		~2.8%

The increase in YS and UTS may be attributed to the alignment of the spin direction under the effect of MF which is applied parallel to the loading direction along the length of the specimen. In the case of the results obtained without MF, the spin orientation w.r.t. the loading direction are at random. It is assumed that the spins are completely aligned and forms a good spin to spin coupling due to MF. The MF results in spin-to-spin coupling (bond interaction of

spins) with electron clouds as a result of which the molecular bonds become stronger [119,120]. The values of strain hardening exponent vary marginally due to the effect of MF with the *tool-A* to *tool-E* in all the cases. The percentage elongation obtained for the tested specimens reduces marginally with *tool-A* to *tool-C* but increases slightly with *tool-D* and *tool-E*. The slight reduction in the ductility of the material could be attributed to the interaction of spins with the dislocations due to the effect of MF [17].

Among all the EMUTT tools, best tensile strength and anisotropy are found in the specimens tested with MF using *tool-C* and hence it is adopted for further investigations. The results of engineering stress- engineering strain and true stress-true strain obtained by uniaxial tensile testing of specimens with an orientation of 0°, 45° and 90° to the RD with and without the MF for DP590 1.6mm sheet thickness are shown in Figure 6.1. Due to the MF, the tensile strength in the specimens tested with an orientation of 0°, 45° and 90° is observed to increase by 4.2%, 3.5% and 5.2%, respectively which can be attributed to the hindrance offered to the movement of dislocations.

The tensile properties of the specimens oriented at 0°, 45°, and 90° to the RD of DP590 steel sheet with 1.0mm and 1.2mm of thickness obtained with the use of EMUTT *tool-C* obtained by experiments are given in Table 6.2. The values of YS of the DP590 1.0mm sheet material tested with orientations of 0°, 45°, and 90° to the RD are observed to increase to 503 MPa, 517 MPa, and 489 MPa, respectively, as a result of the MF. A similar trend of increase in the values of UTS is also seen with MF. Due to the MF, the tensile strength in the specimens tested with an orientation of 0°, 45° and 90° is observed to increase by 5.6%, 3.0% and 4.3%, respectively.

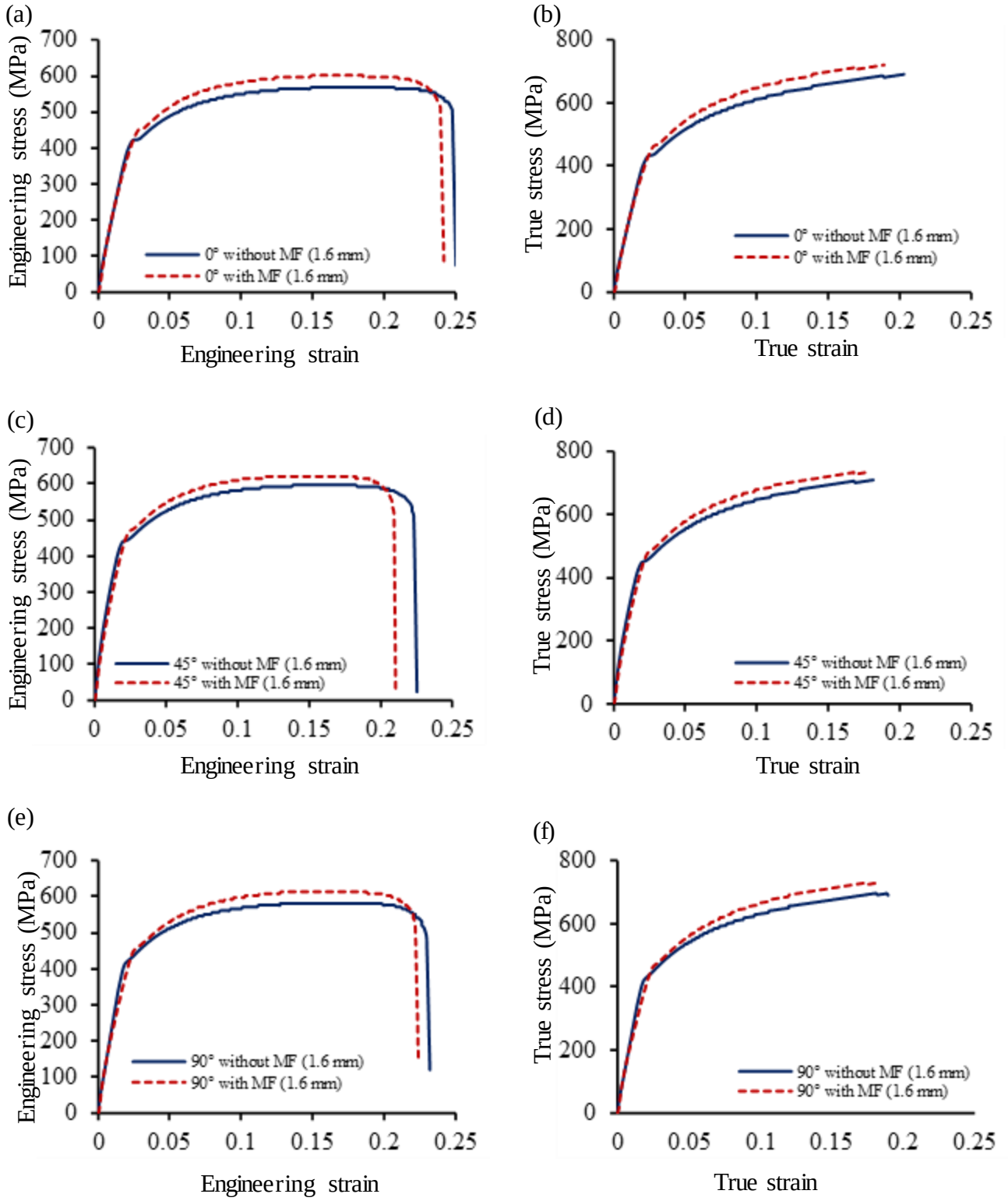

Figure 6.1 Engineering stress-strain plots and true stress-true strain plots with respect to the RD of DP590 sheet thickness 1.6 mm, (a)-(b) 0°, (c)-(d) 45° and (e)-(f) 90°, respectively.

The values of YS of the DP590 1.2mm sheet material tested with orientations of 0°, 45°, and 90° to the RD are observed to increase to 497 MPa, 515 MPa, and 505 MPa, respectively, as a result of the MF. A similar trend of increase in the values of UTS is also seen with MF. Due to the MF, the tensile strength in the specimens tested with an orientation of 0°, 45° and 90° is observed to increase by 4.2%, 3.8% and 5.4%, respectively.

Table 6.2 Tensile properties of DP590 steel sheet (1.0 and 1.2 mm) with and without MF

Experimental conditions	Orientation w.r.t. the RD	YS (%0.2) (MPa)	UTS (MPa)	% Elongation	n	R	$\bar{R}$	$v(R)$
Without MF (1.0 mm)	0°	476±1.8	619±1.6	22.1	0.180	0.90	0.89	~4.5%
	45°	504±1.3	654±1.7	20.4	0.177	0.87		~3.8%
	90°	469±1.7	637±2.0	19.1	0.176	0.94		~2.9%
With MF (1.0 mm)	0°	503±1.9	648±1.7	20.9	0.174	1.08	1.10	~3.1%
	45°	517±2.0	683±1.9	19.7	0.173	0.96		~3.6%
	90°	489±1.8	670±1.9	18.6	0.170	1.4		~3.9%
Without MF (1.2 mm)	0°	477±1.5	631±1.8	21.7	0.179	0.89	0.91	~3.1%
	45°	496±1.6	657±1.6	21.5	0.15	0.84		~3.7%
	90°	479±1.4	628±1.5	19.1	0.171	1.07		~2.5%
With MF (1.2 mm)	0°	497±1.8	661±2.1	21.0	0.171	1.12	1.11	~2.7%
	45°	515±1.7	685±1.8	21.1	0.170	0.95		~3.7%
	90°	505±2.1	662±1.8	18.7	0.165	1.42		~2.4%

The results of engineering stress- engineering strain and true stress-true strain for DP590 1.2 mm sheet thickness obtained by uniaxial tensile testing of specimens with an orientation of 0°, 45° and 90° to the RD with and without the MF are shown in Figure 6.2. The results of engineering stress- engineering strain and true stress-true strain for DP590 1.0 mm sheet thickness obtained by uniaxial tensile testing of specimens with an orientation of 0°, 45° and 90° to the RD with and without the MF are shown in Figure 6.3.

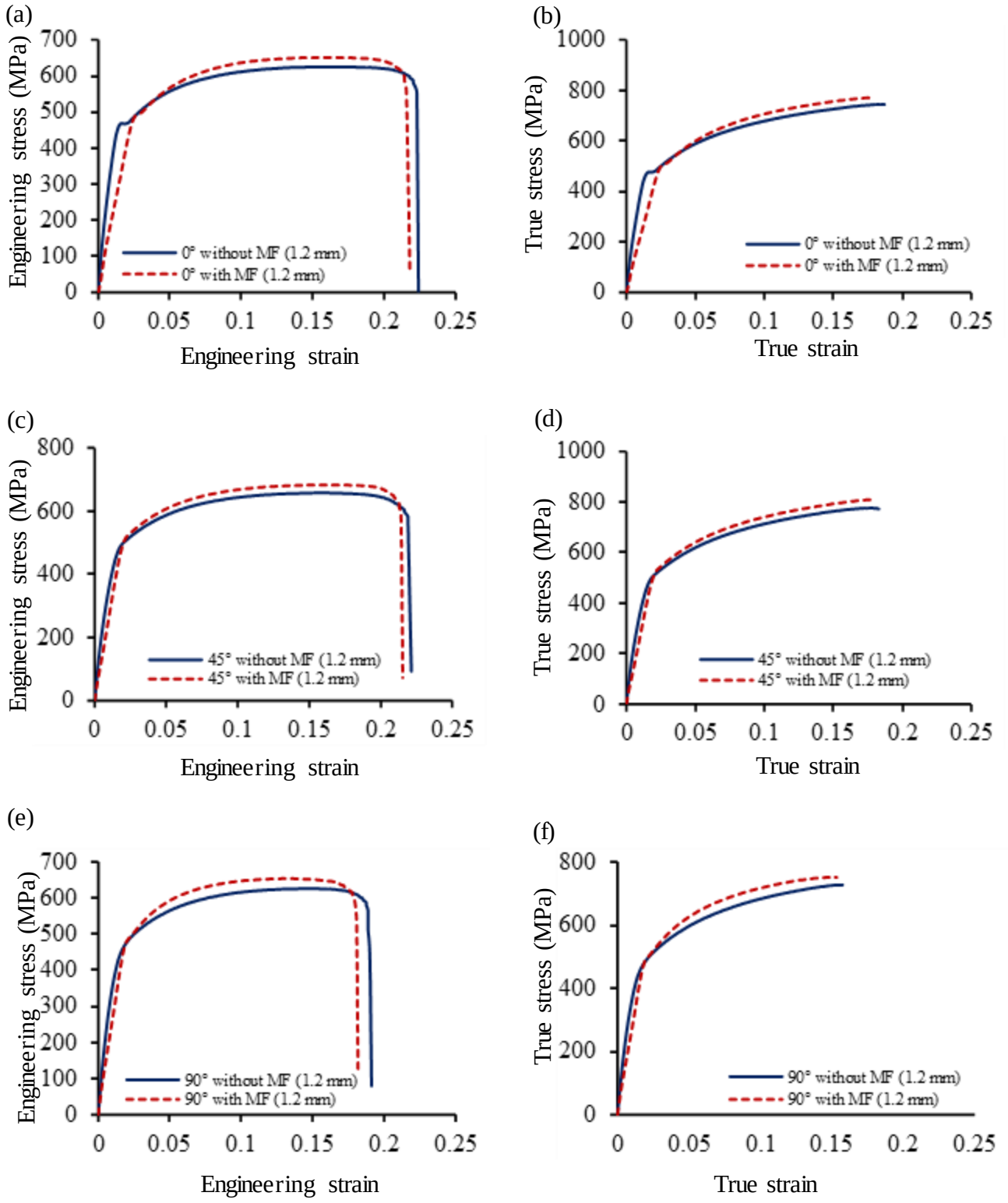

Figure 6.2 Engineering stress-strain plots and true stress-true strain plots with respect to the RD of DP590 sheet thickness 1.2 mm, (a)-(b) 0°, (c)-(d) 45° and (e)-(f) 90°, respectively.

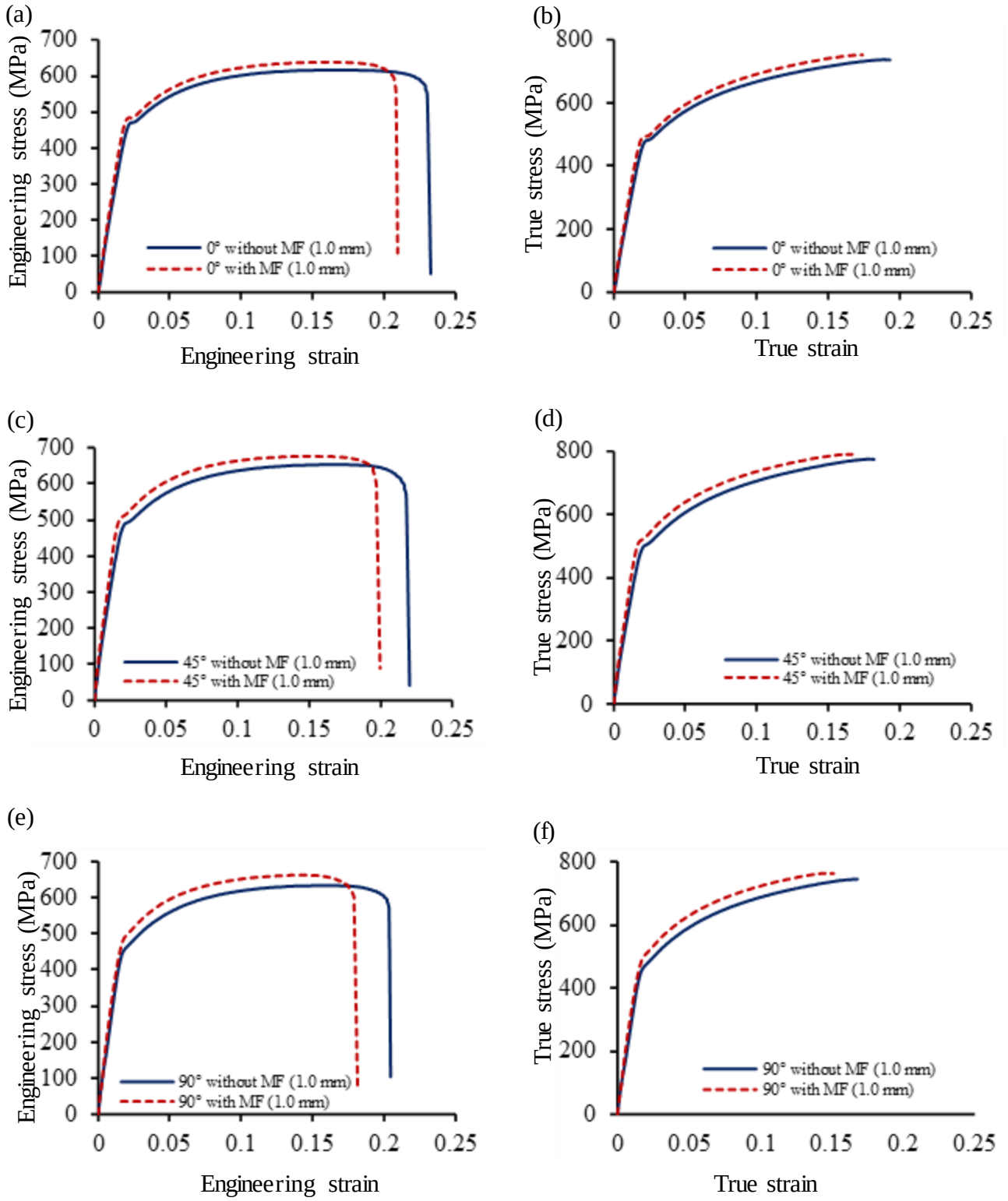

Figure 6.3 Engineering stress-strain plots and true stress-true strain plots with respect to the RD of DP590 sheet thickness 1.0 mm, (a)-(b) 0°, (c)-(d) 45° and (e)-(f) 90°, respectively.

An average reduction in percentage elongation of about 3% was obtained for the samples tested with a magnetic field compared to the results obtained for the samples tested without a magnetic field in all the cases of the DP590 sheet thickness. It is observed that the MF produced by the EMUTT tool has affected the tensile properties due to variation in thicknesses. The sheet thickness 1.6mm tensile properties get higher changes followed by the 1.2mm and 1.0mm sheet thickness of DP590.

The change in the anisotropy of the DP590 steel sheet with 1.6, 1.2 and 1.0mm thickness is observed in terms of plastic strain ratio (R) when tested to 20% of plastic strain with and without the MF as shown in Figure 6.4 (a), (b) and (c), respectively. The average values of plastic strain ratio of the DP590 1.6 mm specimens tested in three different orientations that is 0°, 45° and 90° without the magnetic field are evaluated as 1.06, 0.78 and 1.25, respectively and the values of normal anisotropy ($\bar{R}$) is approximately 0.97. The average value of plastic strain in three different orientations i.e., 0°, 45° and 90° with the magnetic field are evaluated as 1.31, 0.93 and 1.59, respectively. The value of normal anisotropy of the sheet with the magnetic field is approximately 1.19 which is approximately 23.4% higher than that of the results obtained without the magnetic field and a comparison is also shown in Figure 6.4 (a).

The average values of plastic strain ratio of the DP590 1.2 mm specimens tested in three different orientations that is 0°, 45° and 90° without the magnetic field are evaluated as 0.89, 0.84 and 1.07, respectively and the values of normal anisotropy ($\bar{R}$) is approximately 0.91. The average value of plastic strain in three different orientations i.e., 0°, 45° and 90° with the magnetic field are evaluated as 1.12, 0.95 and 1.42, respectively. The value of normal anisotropy of the sheet with the magnetic field is approximately 1.11 which is approximately 22.0% higher than that of the results obtained without the magnetic field and a comparison is also shown in Figure 6.4 (b).

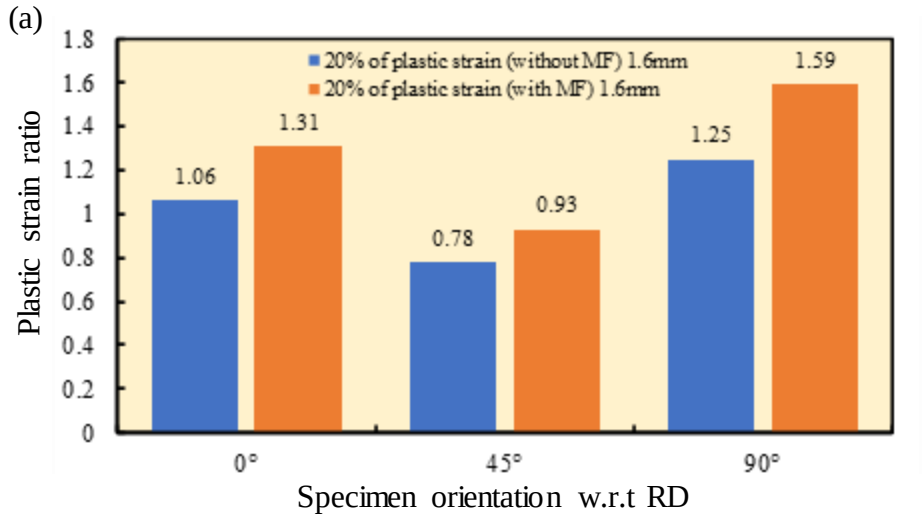

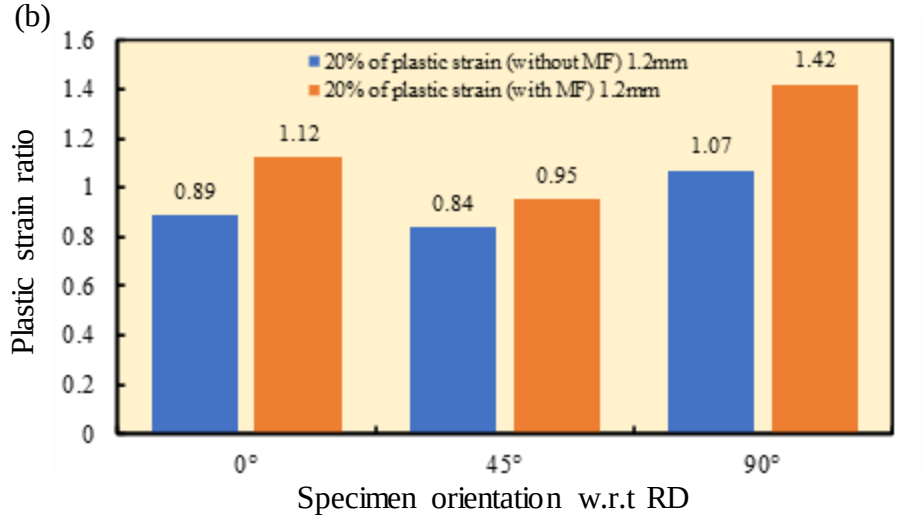

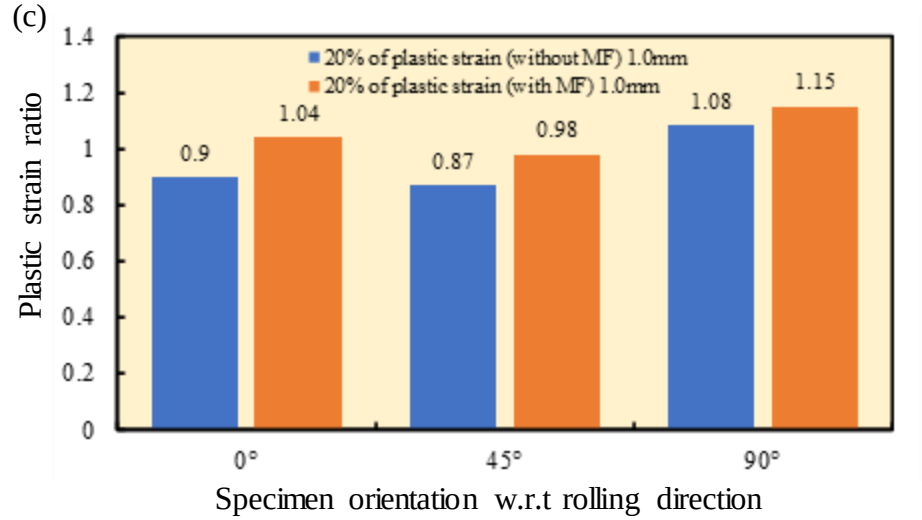

Figure 6.4 Variation of plastic strain ratio with respected to RD of DP590 sheet thickness as (a) 1.6 mm (b) 1.2 mm and (c) 1.0 mm.

The average values of plastic strain ratio of the DP590 1.0 mm specimens tested in three different orientations that is 0°, 45° and 90° without the magnetic field are evaluated as 0.90, 0.87 and 1.08, respectively and the values of normal anisotropy ($\bar{R}$) is approximately 0.93. The average value of plastic strain in three different orientations i.e., 0°, 45° and 90° with the magnetic field are evaluated as 1.04, 0.98 and 1.15, respectively. The value of normal anisotropy of the sheet with the magnetic field is approximately 1.04 which is approximately 11.5% higher than that of the results obtained without the magnetic field and a comparison is also shown in Figure 6.4 (c).

Based on the analysis of the variation of plastic strain ratio with respect to the rolling direction under the effect of magnetic field, highest plastic strain ratio is observed in tensile specimen oriented at 90º to the RD followed by the tensile specimen oriented at 0º and 45º to the rolling direction in all three directions. Moreover, a higher value of plastic strain ratio is observed when tested with the magnetic field for the specimens oriented at 0º and 90º to the RD as compared to that of the value obtained with specimens tested without the magnetic field. It is concluded that the effect of MF on the normal anisotropy of 1.6 mm followed by the 1.2 and 1.0 mm of DP590 steel sheet. The coefficients of variation '$v(R)$' of the tested specimens with 20% of the plastic strain at 0°, 45° and 90° to the rolling direction with and without the magnetic field for DP590 steel sheet in all three thicknesses are reported in Table 6.1 and Table 6.2. It is noticed that the values of coefficient of variation '$v(R)$' lies within the acceptable range as per the standard.

6.2 Tensile properties of ZC440 steel

The tensile properties of the specimens oriented at 0°, 45°, and 90° to the RD of ZC440 steel sheet with 1.4mm, 1.0mm and 1.2mm of thickness obtained with the use of MF obtained by experiments are given in Table 6.3. The values of YS of the ZC440 1.4 mm sheet material tested with orientations of 0°, 45°, and 90° to the RD are observed to increase to 336 MPa,

347 MPa, and 322 MPa, respectively, as a result of the MF. A similar trend of increase in the values of UTS is also seen with MF. Due to the MF, the tensile strength in the specimens tested with an orientation of 0°, 45° and 90° is observed to increase by 7.9%, 7.0% and 8.7%, respectively.

Table 6.3 Tensile properties of ZC440 steel sheet (1.0,1.2, and 1.4 mm) with and without MF

Experimental conditions	Orientation w.r.t. the RD	YS (%0.2) (MPa)	UTS (MPa)	% Elongation	n	R	$\bar{R}$	$v(R)$
Without MF (1.4 mm)	0°	304±2.1	443±2.0	30.1	0.228	1.10	1.11	~3.5%
	45°	318±1.8	454±2.1	27.0	0.212	1.03		~4.7%
	90°	294±1.9	444±2.5	29.2	0.220	1.31		~5.1%
With MF (1.4 mm)	0°	336±2.7	476±1.5	27.9	0.218	1.48	1.39	~5.5%
	45°	347±2.3	486±2.2	24.8	0.206	1.18		~6.2%
	90°	322±2.1	482±1.9	26.6	0.211	1.72		~3.9%
Without MF (1.2 mm)	0°	335±1.9	434±1.9	27.7	0.213	1.07	1.04	~3.1%
	45°	368±1.9	456±1.7	26.3	0.211	0.95		~3.7%
	90°	364±2.0	447±1.5	24.5	0.205	1.22		~2.5%
With MF (1.2 mm)	0°	369±1.3	468±1.9	26.6	0.207	1.35	1.26	~2.7%
	45°	398±1.8	486±1.9	25.7	0.203	1.08		~3.7%
	90°	400±1.5	485±1.6	23.4	0.199	1.53		~2.4%
Without MF (1.0 mm)	0°	350±1.7	438±1.8	28.4	0.214	0.97	0.97	~2.8%
	45°	374±1.6	442±2.1	26.5	0.209	0.92		~2.7%
	90°	363±18	435±1.8	23.3	0.197	1.08		~2.6%
With MF (1.0 mm)	0°	385±1.9	473±1.8	26.7	0.207	1.24	1.17	~2.9%
	45°	402±1.8	470±2.0	25.1	0.199	1.07		~3.1%
	90°	399±1.9	471±1.7	22.6	0.191	1.31		~2.7%

The values of YS of the ZC440 1.2mm sheet material tested with orientations of 0°, 45°, and 90° to the RD are observed to increase to 369 MPa, 398 MPa, and 400 MPa, respectively, as a result of the MF. A similar trend of increase in the values of UTS is also seen with MF. Due

to the MF, the tensile strength in the specimens tested with an orientation of 0°, 45° and 90° is observed to increase by 7.8%, 6.6% and 8.0%, respectively. The values of YS of the ZC440 1.0 mm sheet material tested with orientations of 0°, 45°, and 90° to the RD are observed to increase to 385 MPa, 402 MPa, and 399 MPa, respectively, as a result of the MF. A similar trend of increase in the values of UTS is also seen with MF. Due to the MF, the tensile strength in the specimens tested with an orientation of 0°, 45° and 90° is observed to increase by 5.0%, 4.5% and 6.8%, respectively.

Higher values of YS and UTS are observed in the specimens tested with the effect of MF, than that of the specimens tested without the effect of MF. The values of YS and UTS are observed to be higher in the specimens tested with orientation of 45° to the rolling direction followed by the specimens oriented at 0° and 90°. The values of strain hardening exponent are observed to vary marginally due to the effect of MF in all the cases of tested specimens.

The results of engineering stress- engineering strain and true stress-true strain for ZC440 1.4 mm sheet thickness obtained by uniaxial tensile testing of specimens with an orientation of 0°, 45° and 90° to the RD with and without the MF are shown in Figure 6.5. It is observed that the MF increased the tensile strength in case of 90° to the RD followed by the 0° and 45° to the RD. It is observed that the MF increases the yield and tensile strengths of the material but slightly decreases the percentage elongation. The change in the tensile properties may be ascribed to the hindrance of movement of dislocations due to the MF. This indicates that the magnetic domains are properly aligned in the direction of the applied MF that causes the spin directions of the electrons to align to the loading direction along the length of the specimen in all the cases tested with MF. Whereas, in the case of tested specimen without the MF, the spin orientations are assumed to be distributed in a random manner with respect to the loading direction.

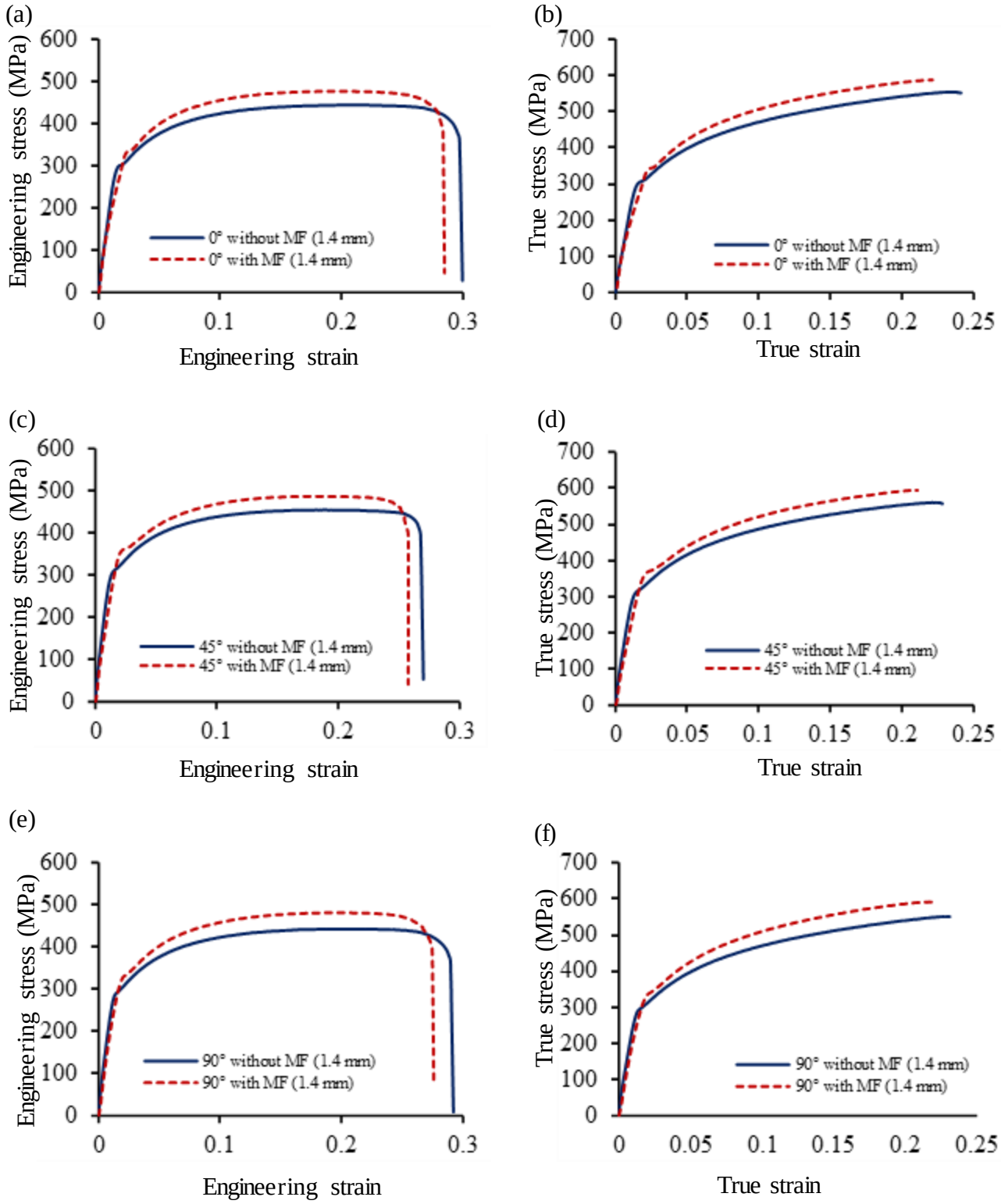

Figure 6.5 Engineering stress-strain plots and true stress-true strain plots with respect to the RD of ZC440 sheet thickness 1.4 mm, (a)-(b) 0°, (c)-(d) 45° and (e)-(f) 90°, respectively.

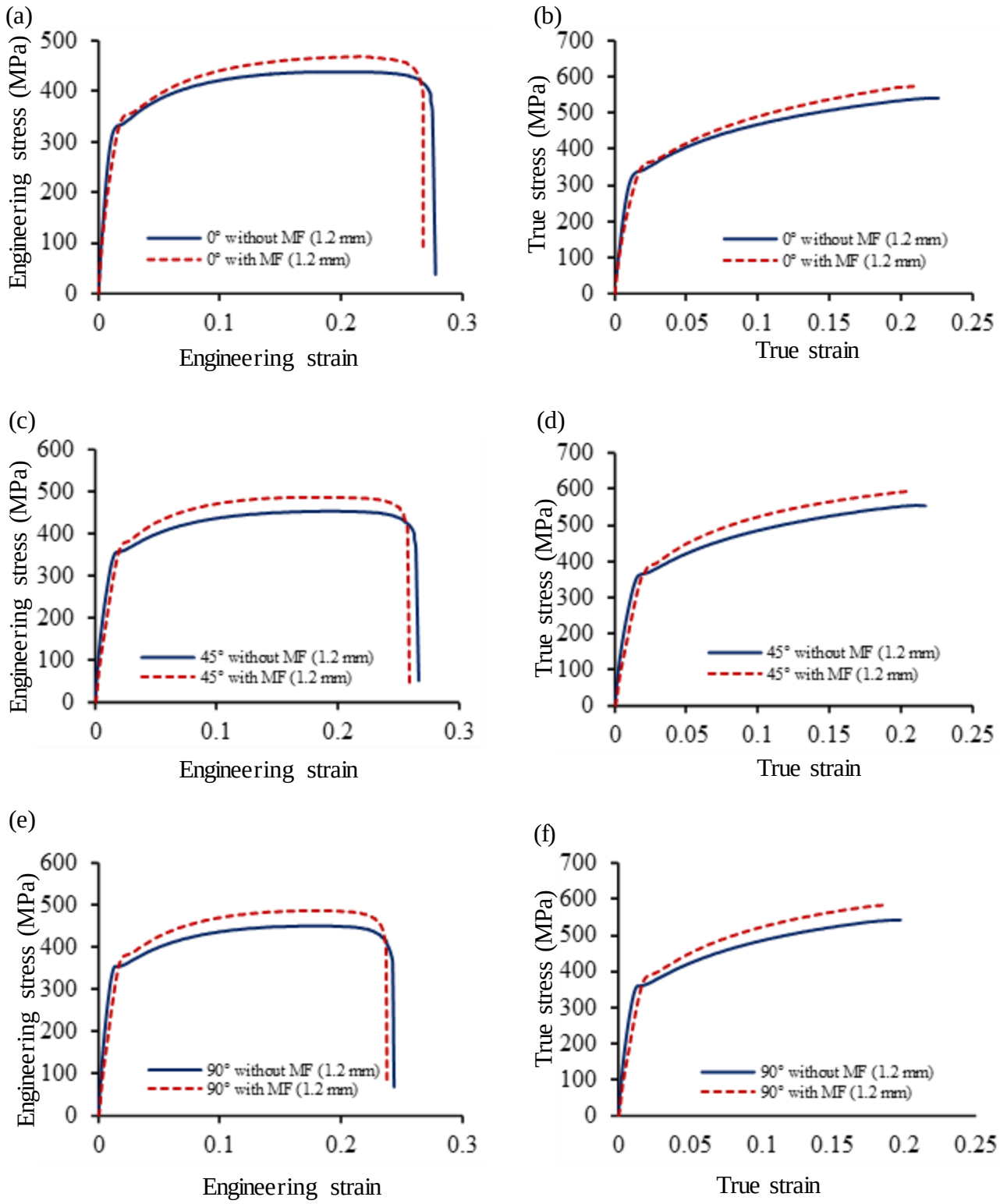

Figure 6.6 Engineering stress-strain plots and true stress-true strain plots with respect to the RD of ZC440 sheet thickness 1.2 mm, (a)-(b) 0°, (c)-(d) 45° and (e)-(f) 90°, respectively.

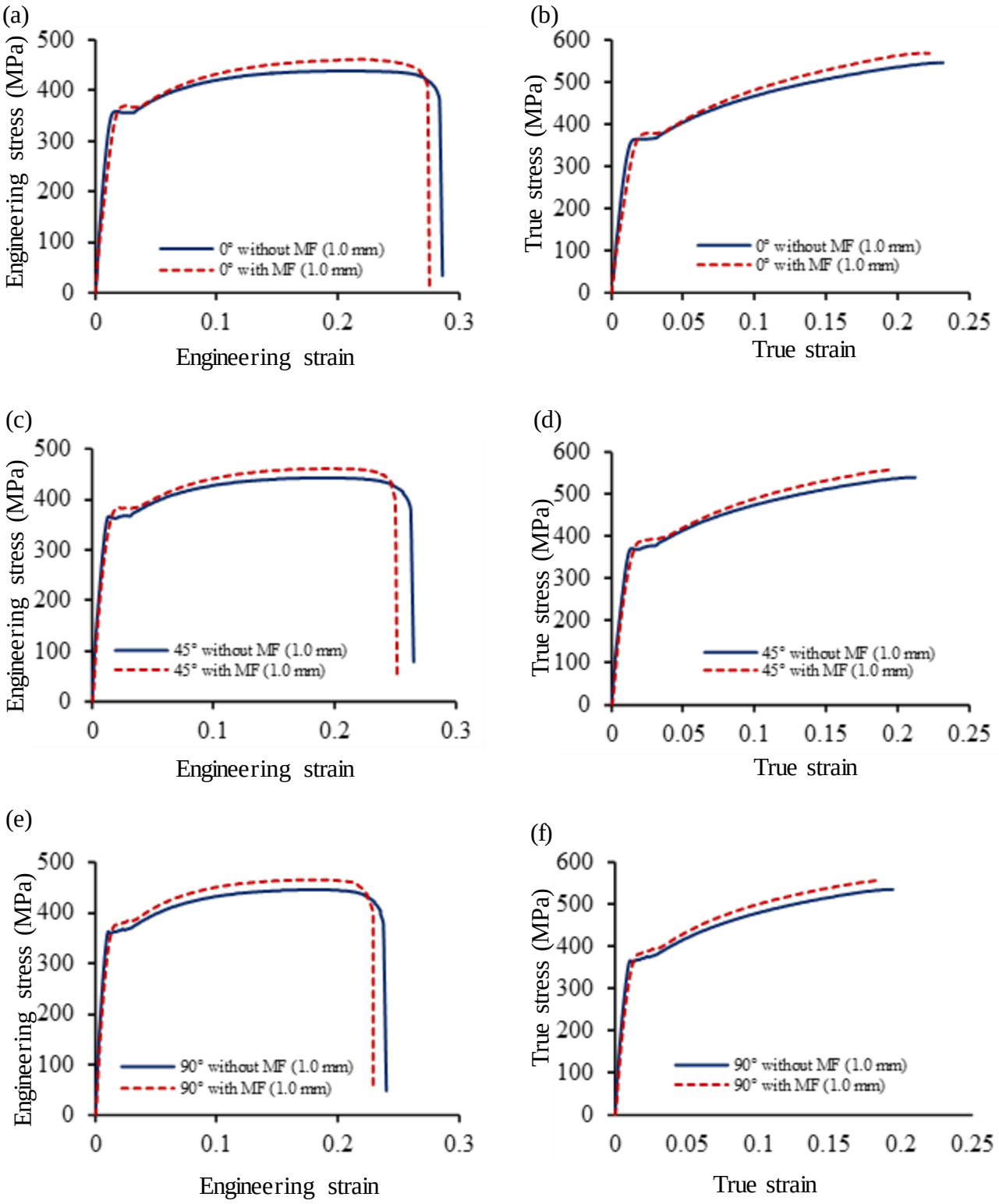

Figure 6.7 Engineering stress-strain plots and true stress-true strain plots with respect to the RD of ZC440 sheet thickness 1.0 mm, (a)-(b) 0°, (c)-(d) 45° and (e)-(f) 90°, respectively.

The results of engineering stress- engineering strain and true stress-true strain for ZC440 1.2 mm sheet thickness obtained by uniaxial tensile testing of specimens with an orientation of 0°, 45° and 90° to the RD with and without the MF are shown in Figure 6.6. It is observed that the MF increased the tensile strength in case of 90° to the RD followed by the 0° and 45° to the RD. The results of engineering stress- engineering strain and true stress-true strain for ZC440 1.0 mm sheet thickness obtained by uniaxial tensile testing of specimens with an orientation of 0°, 45° and 90° to the RD with and without the MF are shown in Figure 6.7. It is observed that the MF increased the tensile strength in case of 90° to the RD followed by the 0° and 45° to the RD.

The change in the anisotropy of the ZC440 steel sheet with 1.4, 1.2 and 1.0mm thickness is observed in terms of plastic strain ratio (R) when tested to 20% of plastic strain with and without the MF as shown in Figure 6.8 (a), (b) and (c), respectively. The average values of plastic strain ratio of the ZC440 1.4 mm specimens tested in three different orientations that is 0°, 45° and 90° without the magnetic field are evaluated as 1.1, 1.03 and 1.31, respectively and the values of normal anisotropy ($\bar{R}$) is approximately 1.11. The average value of plastic strain in three different orientations i.e., 0°, 45° and 90° with the magnetic field are evaluated as 1.48, 1.18 and 1.72, respectively. The value of normal anisotropy of the sheet with the magnetic field is approximately 1.39 which is approximately 25.1% higher than that of the results obtained without the magnetic field and a comparison is also shown in Figure 6.8 (a).

The average values of plastic strain ratio of the ZC440 1.2 mm specimens tested in three different orientations that is 0°, 45° and 90° without the magnetic field are evaluated as 1.07, 0.95 and 1.22, respectively and the values of normal anisotropy ($\bar{R}$) is approximately 1.04.

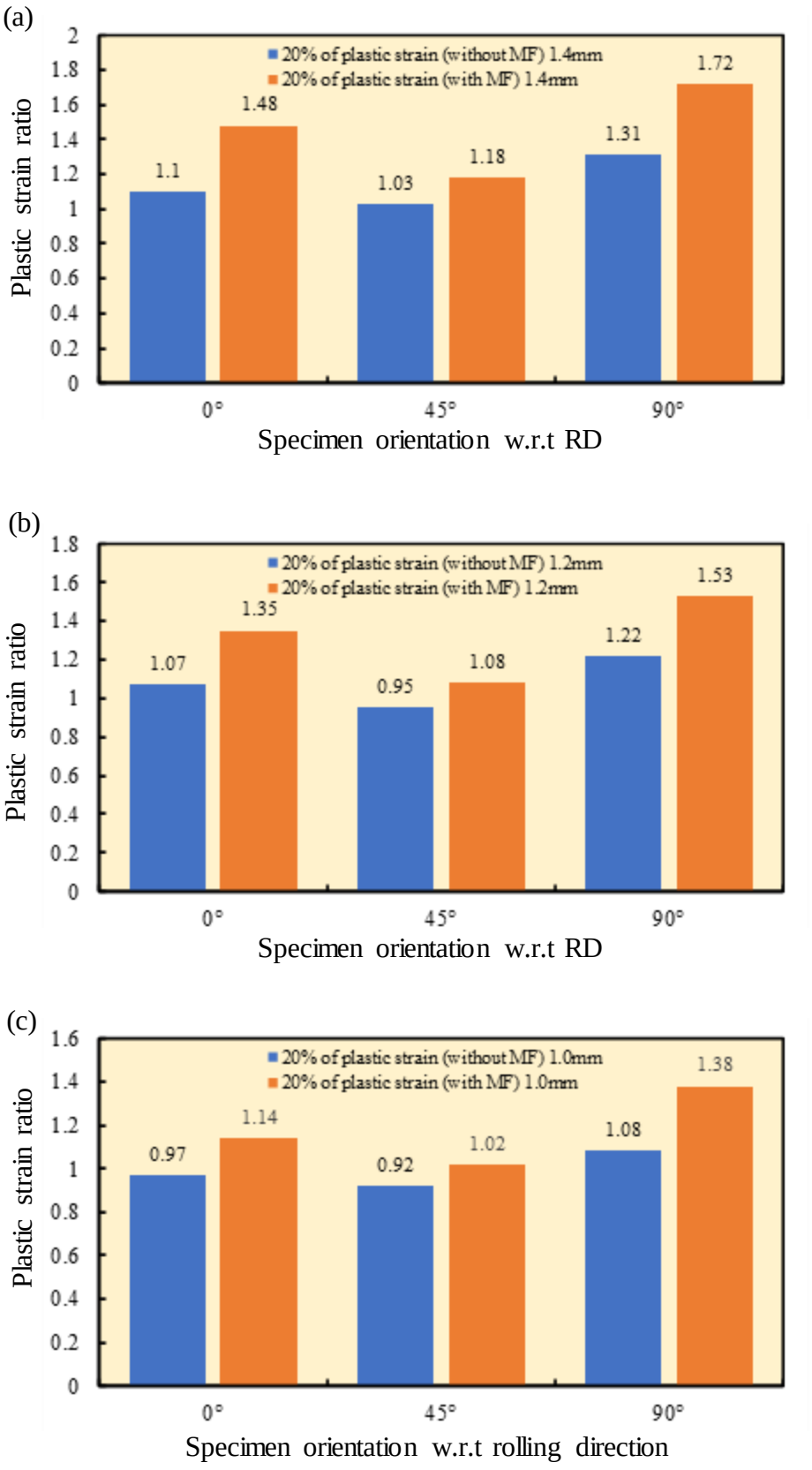

Figure 6.8 Variation of plastic strain ratio with respected to RD of ZC440 sheet thickness as (a) 1.4 mm (b) 1.2 mm and (c) 1.0 mm.

The average value of plastic strain in three different orientations i.e., 0°, 45° and 90° with the magnetic field are evaluated as 1.35, 1.08 and 1.53, respectively. The value of normal anisotropy of the sheet with the magnetic field is approximately 1.26 which is approximately 21.2% higher than that of the results obtained without the magnetic field and a comparison is also shown in Figure 6.8 (b). The average values of plastic strain ratio of the ZC440 1.0 mm specimens tested in three different orientations that is 0°, 45° and 90° without the magnetic field are evaluated as 0.97, 0.92 and 1.08, respectively and the values of normal anisotropy ($\bar{R}$) is approximately 0.97. The average value of plastic strain in three different orientations i.e., 0°, 45° and 90° with the magnetic field are evaluated as 1.14, 1.02 and 1.38, respectively. The value of normal anisotropy of the sheet with the magnetic field is approximately 1.14 which is approximately 17.5% higher than that of the results obtained without the magnetic field and a comparison is also shown in Figure 6.8 (c).

Based on the analysis of the variation of plastic strain ratio with respect to the rolling direction under the effect of magnetic field, highest plastic strain ratio is observed in tensile specimen oriented at 90º to the RD followed by the tensile specimen oriented at 0º and 45º to the rolling direction in all three directions. Moreover, a higher value of plastic strain ratio is observed when tested with the magnetic field for the specimens oriented at 0º and 90º to the RD as compared to that of the value obtained with specimens tested without the magnetic field. It is concluded that the effect of MF on the normal anisotropy of 1.4 mm followed by the 1.2 and 1.0 mm of DP590 steel sheet. The coefficients of variation '$v(R)$' of the tested specimens with 20% of the plastic strain at 0°, 45° and 90° to the rolling direction with and without the magnetic field for DP590 steel sheet in all three thicknesses are reported in Table 6.3. It is noticed that the values of coefficient of variation '$v(R)$' lies within the acceptable range as per the standard.

It is concluded that the effectiveness of MF on the tensile properties and normal anisotropy of ZC440 steel sheet is followed by the DP590 steel sheet. It means the EMUTT tool work based on the magnetization of the steel sheet because ZC440 higher magnetization compared to the DP590 steel sheet. This work also concludes that the EMUTT higher effect on tensile properties with thicker material as compared to thinner sheet. The magnetic field affected more on the 90º to the RD of the tensile specimen as compared to the 0º and 45º to the RD.

6.3 Erichsen index

The formability of the steel sheet is evaluated with Erichsen Index (IE) number in which a spherical punch with Ø20 mm is used to deform the sheet by stretching it (with and without the MF) into a die with a clearance so that the punch displacement corresponds to the IE at which necking occurs. The necking is sensed by a sudden drop in the punch force and the test is stopped. The value of IE for deformed DP590 sheet tested with and without MF are displayed in a transverse-section view as shown in Figure 6.9.

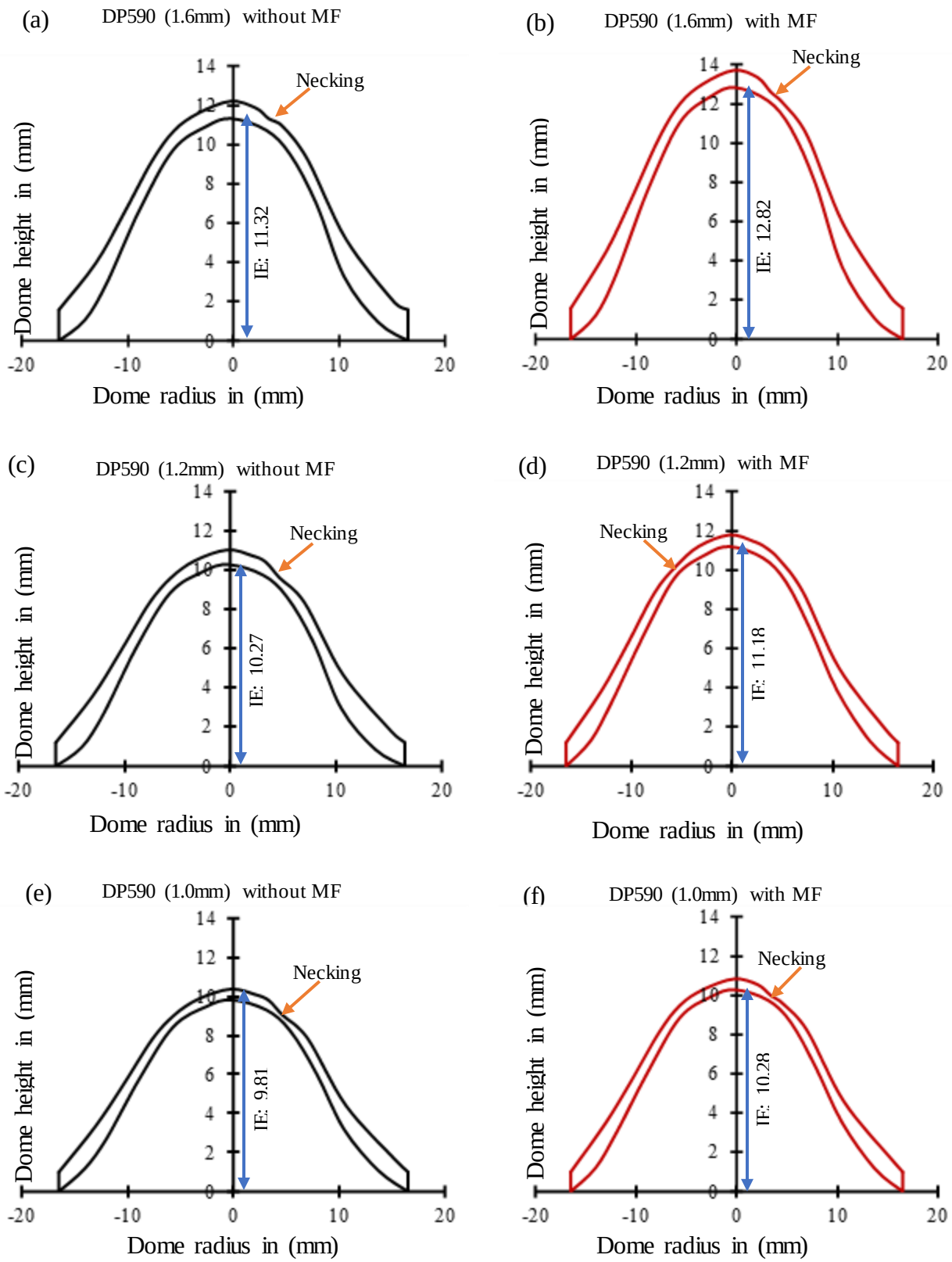

Figure 6.9 Experimental measured value of Erichsen Index dome height vs dome radius with and without MF for DP590 (a)-(b) 1.6mm, (c)-(d) 1.2mm, and (e)-(f) 1.0mm.

The value of IE for deformed DP590 1.6mm sheet tested without MF is 11.32 is shown in Figure 6.9 (a). At the necking the thickness of wall is observed to be 0.60mm where the test

was stopped. The value of IE for deformed DP590 1.6mm sheet tested with MF is 12.82 which is approximately 13.25% higher than the case of without magnetic field in same thickness as shown in Figure 6.9 (b). At the necking the thickness of wall is observed to be 0.48mm where the test was stopped. It was observed that the MF reduces the cup wall thickness and it is thinner as compared to specimen tested without MF. The value of IE for deformed DP590 1.2mm sheet tested without MF is 10.27 is shown in Figure 6.9 (c). At the necking, the thickness of wall is observed to be 0.46mm where the test was stopped. The value of IE for deformed DP590 1.2mm sheet tested with MF is 11.18 which is approximately 8.8% higher than that the case of without magnetic field in same thickness as shown in Figure 6.9 (d). At the necking, the thickness of wall is observed to be 0.40mm where the test was stopped. It was observed that the MF reduces the cup wall thickness and it is thinner as compared to specimen tested without MF. The value of IE for deformed DP590 1.0mm sheet tested without MF is 9.81 is shown in Figure 6.9 (e). At the necking, the thickness of wall is observed to be 0.41mm where the test was stopped. The value of IE for deformed DP590 1.0mm sheet tested with MF is 10.28 which is approximately 4.8% higher than that the case of without magnetic field in same thickness as shown in Figure 6.9 (f). At the necking, the thickness of wall is observed to be 0.37mm where the test was stopped. It was observed that the MF reduce the cup wall thickness and it is thinner as compared to specimen tested without MF.

Due to MF the specimen is stretched considerably and necks exhibiting a higher height of cup and value of IE increased. The increase in the value of IE may be attributed to the higher normal anisotropy of the sheet due to MF. It was observed that the value of IE increased with the MF and it is more affected for the sheet thickness of 1.6mm followed by the 1.2mm and 1.0mm sheet thickness of DP590.

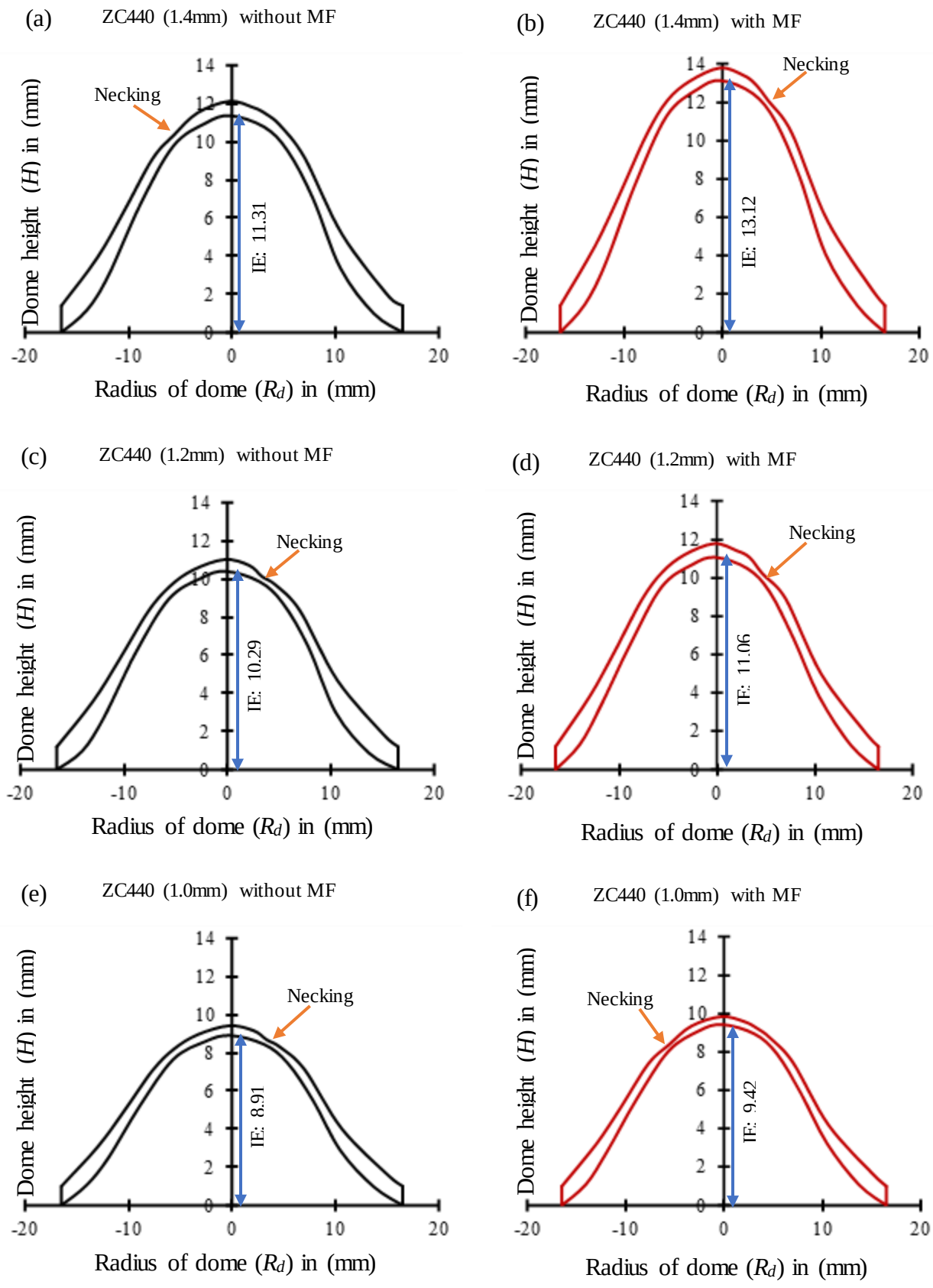

Figure 6.10 Experimental measured value of Erichsen Index dome height vs dome radius with and without MF for ZC440 (a)-(b) 1.4mm, (c)-(d) 1.2mm, and (e)-(f) 1.0mm.

The formability of the steel sheet was evaluated with Erichsen Index (IE) number in which a spherical punch with Ø20 mm is used to deform the sheet by stretching it (with and without the MF) into a die with a clearance so that the punch displacement corresponds to the IE at which necking occurs. The necking is sensed by a sudden drop in the punch force and the test is stopped. The value of IE for deformed ZC440 sheet tested with and without MF are displayed in a transverse-section view as shown in Figure 6.10.

The value of IE for deformed ZC440 1.4mm sheet tested without MF is 11.31 is shown in Figure 6.10 (a). At the necking, the thickness of wall is observed to be 0.51mm where the test was stopped. The value of IE for deformed ZC440 1.4mm sheet tested with MF is 13.12 which is approximately 16.0% higher than that without magnetic field in same thickness as shown in Figure 6.10 (b). At the necking, the thickness of wall is observed to be 0.49mm where the test was stopped. It was observed that the MF reduces the cup wall thickness and it is slight thinner as compared to specimen tested without MF. The value of IE for deformed ZC440 1.2mm sheet tested without MF is 10.29 is shown in Figure 6.10 (c). At the necking, the thickness of wall is observed to be 0.50mm where the test was stopped. The value of IE for deformed ZC440 1.2mm sheet tested with MF is 11.36 which is approximately 10.4% higher than that the case of without magnetic field in same thickness as shown in Figure 6.10 (d). At the necking, the thickness of wall is observed to be 0.45mm where the test was stopped. It was observed that the MF reduce the cup wall thickness and it is thinner as compared to specimen tested without MF. The value of IE for deformed ZC440 1.0mm sheet tested without MF is 8.91 is shown in Figure 6.10 (e). At the necking the thickness of wall is observed to be 0.42mm where the test was stopped. The value of IE for deformed ZC440 1.0mm sheet tested with MF is 9.42 which is approximately 5.8% higher than that without magnetic field in same thickness as shown in Figure 6.10 (f). At the necking the thickness of wall is observed to be

0.38mm where the test was stopped. It was observed that the MF reduce the cup wall thickness and it is thinner as compared to specimen tested without MF.

Due to MF the specimen is stretched considerably and necks exhibiting a higher height of cup and value of IE increased. The increase in the value of IE may be attributed to the higher normal anisotropy of the sheet due to MF. It was observed that the value of IE increased with the MF and its more affected on the sheet thickness of 1.4mm and followed by the 1.2mm and 1.0mm sheet thickness of ZC440. It is concluded that the value of IE is higher in the case of ZC440 as compared to DP590 steel sheet. The value of IE depends on the anisotropy of the material and the higher anisotropy change was observed in the 1.4mm sheet thickness of the ZC440 and followed by the DP590 1.6mm sheet.

6.4 Punch force-displacement curves

The punch force with relative displacement graph of DP590 tested with and without MF are shown in Figure 6.11. The punch force vs punch displacement plot for deformed DP590 1.6mm sheet tested with and without MF as shown in Figure 6.11 (a). The value of highest punch force is observed to be 41.30kN for DP590 1.6mm sheet tested without MF. The value of highest punch force is observed to be 46.30kN for DP590 1.6mm sheet tested with MF. Due to MF, the punch force required to deform the sheet is also observed to increase by 12.2%. The punch force vs punch displacement plot for deformed DP590 1.2mm sheet tested with and without MF is shown in Figure 6.11 (b). The value of highest punch force is observed to be 31.31kN for DP590 1.2mm sheet tested without MF. The value of highest punch force is observed to be 35.25kN for DP590 1.2mm sheet tested with MF. Due to MF, the punch force required to deform the sheet is also observed to increase by 12.5%. The punch force vs punch displacement plot for deformed DP590 1.0mm sheet tested with and without MF is shown in Figure 6.11 (c). The value of highest punch force is observed to be 25.27kN for DP590 1.0mm sheet tested without MF. The value of highest punch force is observed to be 28.53kN for

DP590 1.0mm sheet tested with MF. Due to MF, the punch force required to deform the sheet is also observed to increase by 12.8%. It is observed that the MF increased the punch force of the material during stretch forming of the material if magnetic field is applied perpendicular to punch central axis. In case of DP590 steel, in all the thicknesses of the material approximately 12% of punch is increased due to MF as compared to the sheet deformed without application of MF.

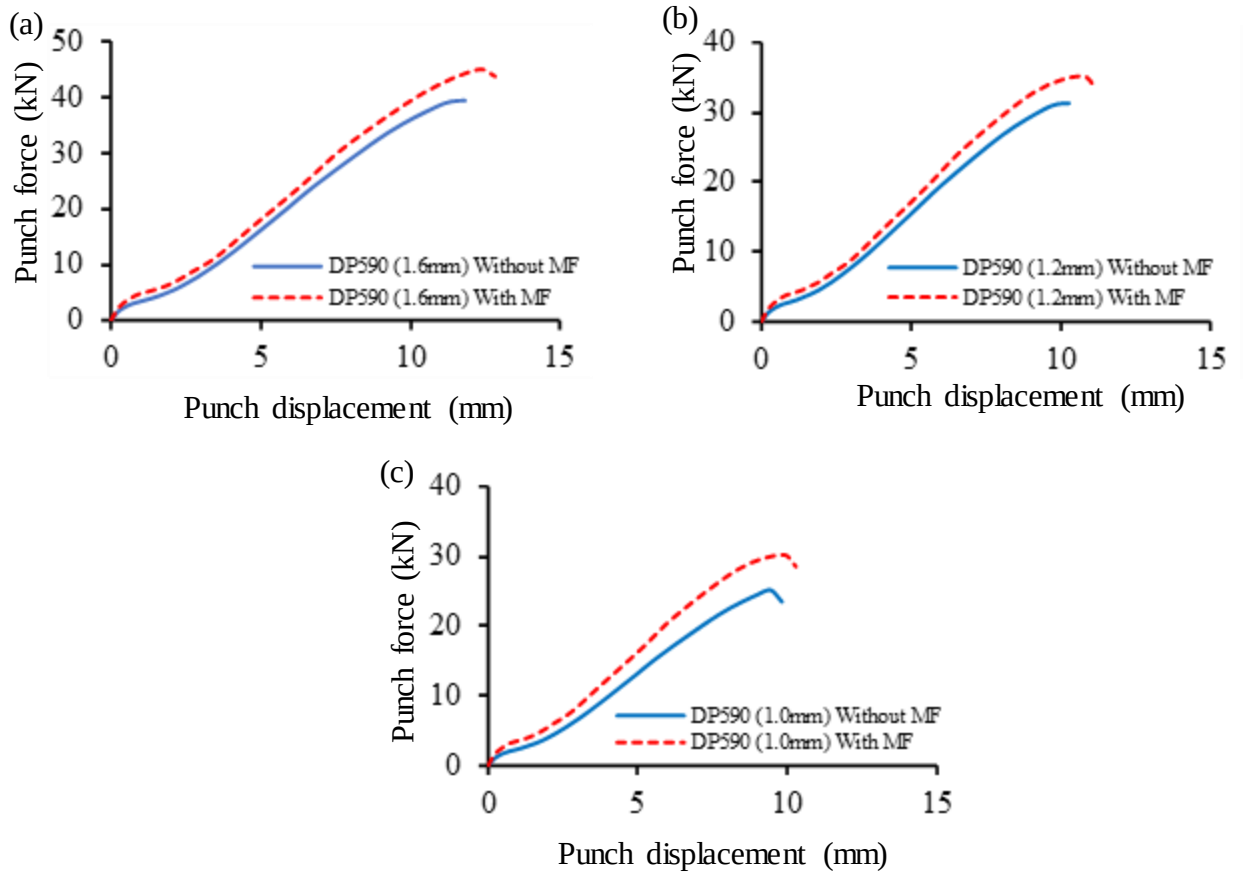

Figure 6.11 Experimental measured punch force vs punch displacement with and without MF for DP590 (a)-(b) 1.6mm, (c)-(d) 1.2mm, and (e)-(f) 1.0mm.

The punch force with relative displacement graphs of ZC440 tested with and without MF are shown in Figure 6.12. The punch force vs punch displacement plot for deformed ZC440 1.4mm sheet tested with and without MF is shown in Figure 6.12 (a). The value of highest

punch force is observed to be 31.72kN for ZC440 1.4mm sheet tested without MF. The value of highest punch force is observed to be 36.61kN for ZC440 1.4mm sheet tested with MF. Due to MF, the punch force required to deform the sheet is also observed to increase by 15.4%. The punch force vs punch displacement plot for deformed ZC440 1.2mm sheet tested with and without MF is shown in Figure 6.12 (b).

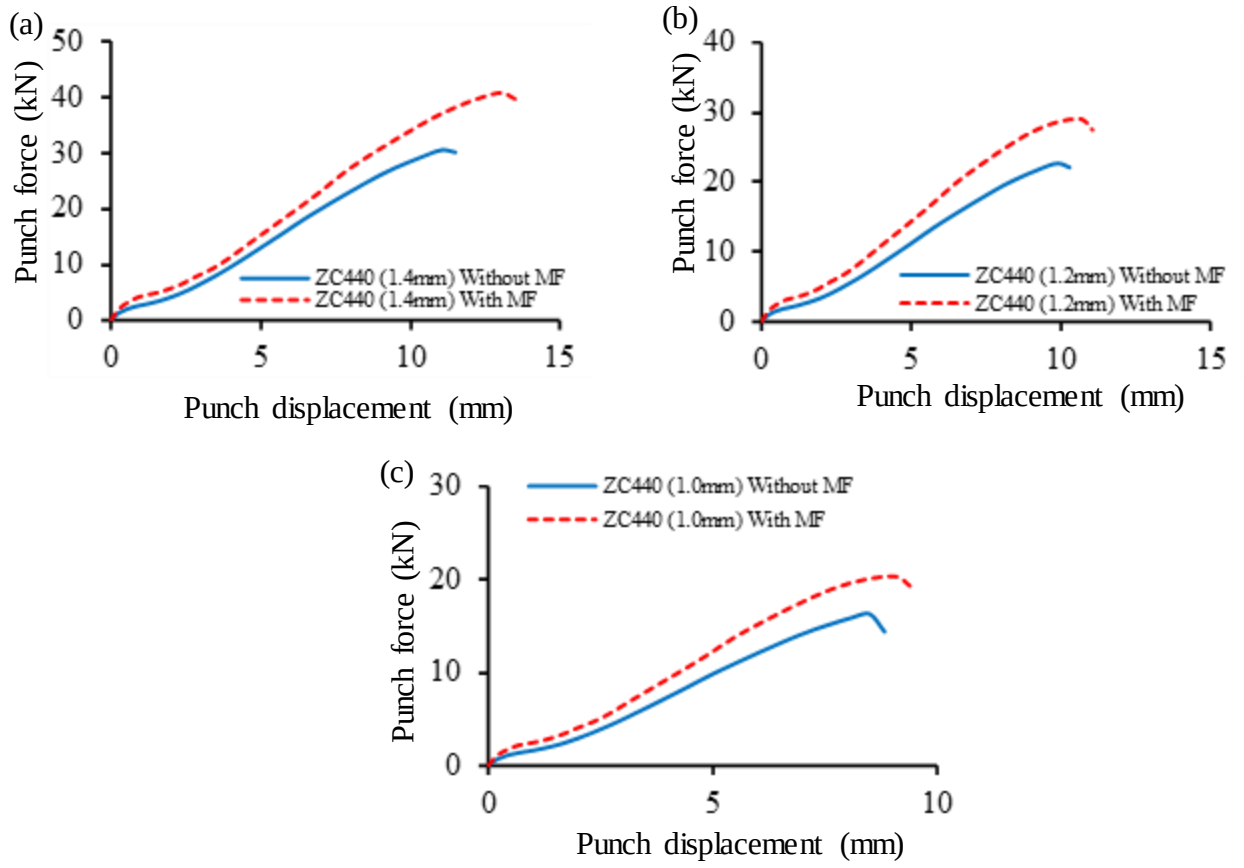

Figure 6.12 Experimental measured punch force vs punch displacement with and without MF for ZC440 (a)-(b) 1.4mm, (c)-(d) 1.2mm, and (e)-(f) 1.0mm.

The value of highest punch force is observed to be 23.79kN for ZC440 1.2mm sheet tested without MF. The value of highest punch force is observed to be 27.33kN for ZC440 1.2mm sheet tested with MF. Due to MF, the punch force required to deform the sheet is also observed to increase by 14.8%. The punch force vs punch displacement plot for deformed ZC440

1.0mm sheet tested with and without MF is shown in Figure 6.12 (c). The value of highest punch force is observed to be 16.69kN for ZC440 1.0mm sheet tested without MF. The value of highest punch force is observed to be 19.24kN for ZC440 1.0mm sheet tested with MF. Due to MF, the punch force required to deform the sheet is also observed to increase by 15.2%.

6.5 Summary

On the basis of the results and discussion presented in this chapter, the effect of MF observed in term of tensile properties and formability of the three thicknesses of DP590 and ZC440 is established. The performance of the EMUTT tools is observed with the DP590 steel of 1.6mm thickness and it is observed that the *tool-C* has higher effect on the tensile properties of the material. It was observed that the MF increased the tensile properties of DP590 steel approximately 4.5% and the slight change in the ductility of the material in all three thicknesses. The major changes of tensile properties are observed in the thickness of 1.6mm followed by the 1.2mm and 1.0mm. The normal anisotropy of the DP590 sheet increased by 23.4%, 22.0% and 11.5% in the sheet thickness of 1.6mm, 1.2mm and 1.0mm, respectively due to MF. In the case of the ZC440 steel sheet, the MF increased the tensile properties approximately 8.0% and the slight change in the ductility of the material in all three thicknesses. The major changes of tensile properties are observed in the thickness of 1.4mm followed by the 1.2mm and 1.0mm. The normal anisotropy of the ZC440 sheet increased by 25.1%, 21.2% and 17.5% in the sheet thickness of 1.4mm, 1.2mm and 1.0mm, respectively due to MF. The formability test of the sheets was conducted on the Erichsen cupping tester with and without the MF. The results of Erichsen index (IE) were observed in all the three thicknesses of the sheet of DP590 and ZC440 steels. It was noticed that the value of IE is increased in case of DP590 steel by 13.25%, 8.8% and 4.8% in the thickness of 1.6mm, 1.2mm and 1.0mm, respectively due to MF. In case of ZC440 steel sheet, the value of IE increased by 16.0%, 10.4% and 5.8% in the thicknesses of 1.4mm, 1.2mm and 1.0mm, respectively. It

is concluded that the magnetic field applied on the ZC440 and DP590 steel sheet in Erichsen cupping test increased the punch force by approximately 15% and 12%, respectively. It can also be concluded that ZC440 steel reported better under MF when compared to DP590 steel and takes more load during formability.

CHAPTER 7

RESULTS AND DISCUSSION: MICROSTRUCTURAL EXAMINATION

The microstructural features in the samples taken from the specimens tested to a plastic strain of 20% with three different orientations w.r.t. the RD with and without the effect of MF of DP590 (1.6mm) and ZC440 (1.4mm) steel are discussed in this chapter. The changes in the microstructure due to plastic deformation as a result of MF is also correlated with the changes in tensile properties. In all the cases, tensile tested specimens deformed to a value of plastic strain of 20% is considered for microstructural investigations using EBSD and the required samples were taken from the center of the gauge length of the tested specimens.

7.1 Microstructural examination of DP590 steel

7.1.1 Untested material DP590 steel

The microstructure obtained by electron backscattered diffraction (EBSD) technique of the untested parent material is shown in Figure 7.1. As shown in Figure 7.1 (a), the IPF with colour distribution triangle in the microstructure of the samples taken from an untested sheet obtained from EBSD shows that the percentage distribution of the plane (111) is 51%, followed by (101) and (001) as 16% and 33%, respectively. It is observed that the grains are equiaxed with a fraction value of 0.583 of the total grains having high angle grain boundary (HAGB) and rest of the low angle grain boundary (LAGB), an average grain size of approximately 4.5 µm indicating very fine grains is shown in Figure 7.1 (b). The microstructure also shows small islands of martensite uniformly distributed at the grain boundaries of equiaxed ferrite grains, being a typical DP steel. The Kernel Average Misorientation (KAM) map shows homogeneous recrystallized strain free grains (KAM <1°) with few scattered dislocations at the grain boundaries (Figure 7.1 (c)). The pole figures

corresponding to Figure 7.1 (a) in the distribution of planes {001}, {110} and {111} shows a higher intensity of peaks (6.043) in terms of multiples of random distribution (MRD) indicating a strong texture as shown in Figure 7.1 (d).

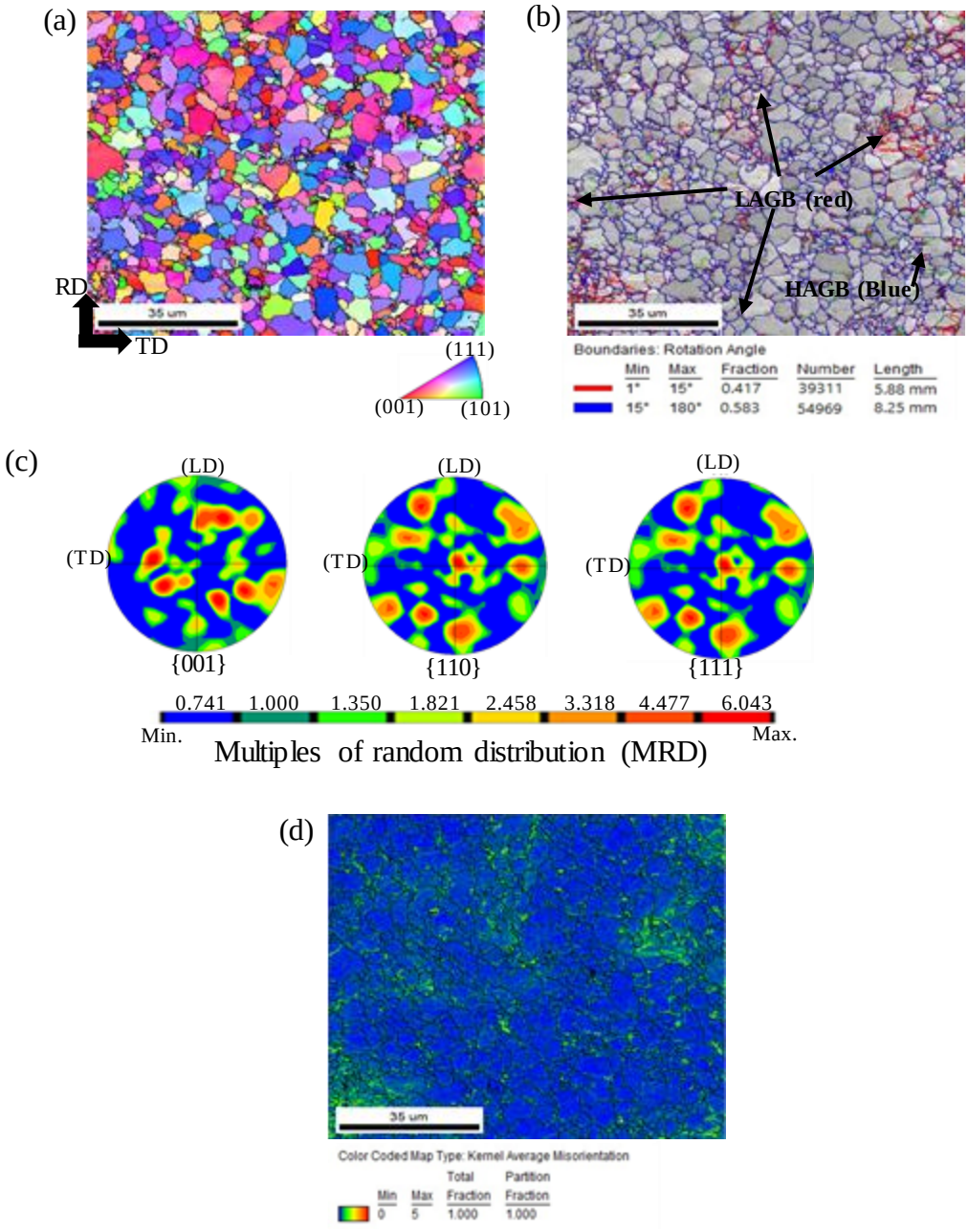

Figure 7.1 EBSD image of untested material of DP590: (a) inverse pole figure map and key, (b) grain boundary map (c) kernel average misorientation map (d) misorientation angle distribution and (e) pole figures.

7.1.2 Tested specimens of DP590 steel without magnetic field

The microstructures obtained by EBSD technique from the 20% plastic strain tested specimens at the 0°, 45°, and 90° w.r.t the RD are shown in Figure 7.2. Based on the inverse pole figure (IPF) maps and colour distribution in the microstructure of tested specimen oriented at 0° to the RD, it was observed that the distribution of plane (111) within microstructure is estimated to be 49% and followed by (001) and (101) plane estimated as 31% and 20%, respectively is shown in Figure 7.2 (a). It was also observed that the average grain size of approximately 6.3 μm. In Figure 7.2 (b), the grain boundary map confirms that the LAGB (0.656 number fraction) are much higher than the HAGB (0.344 number fraction). It shows that the dislocations density is higher with the increasing plastic strain of the specimen oriented at 0° to the RD. From the inverse pole figure (IPF) maps and colour distribution in the microstructure of tested specimen oriented at 45° to the RD, it was observed that the distribution of plane (111) within microstructure is estimated to be 47% and followed by (001) and (101) plane estimated as 44% and 9%, (see Figure 7.2 (c)). The average grain size of approximately 6.7 μm in the samples. The grain boundary map of the tested specimen oriented at 45° to the RD confirms that the LAGB (0.517 number fraction) are slightly higher than the HAGB (0.483 number fraction) as shown in Figure 7.2 (d).

The inverse pole figure (IPF) maps and colour distribution in the microstructure of tested specimen oriented at 90° to the RD is shown in Figure 7.2 (e). It is observed that the distribution of plane (111) within microstructure is estimated to be 53% and followed by (101) and (001) plane estimated as 27% and 20%, respectively with the average grain size of approximately 7.2 μm. The grain boundary map of the tested specimen oriented at 90° to the RD confirms that the LAGB (0.649 number fraction) are slightly higher than the HAGB (0.351 number fraction) as shown in Figure 7.2 (f).

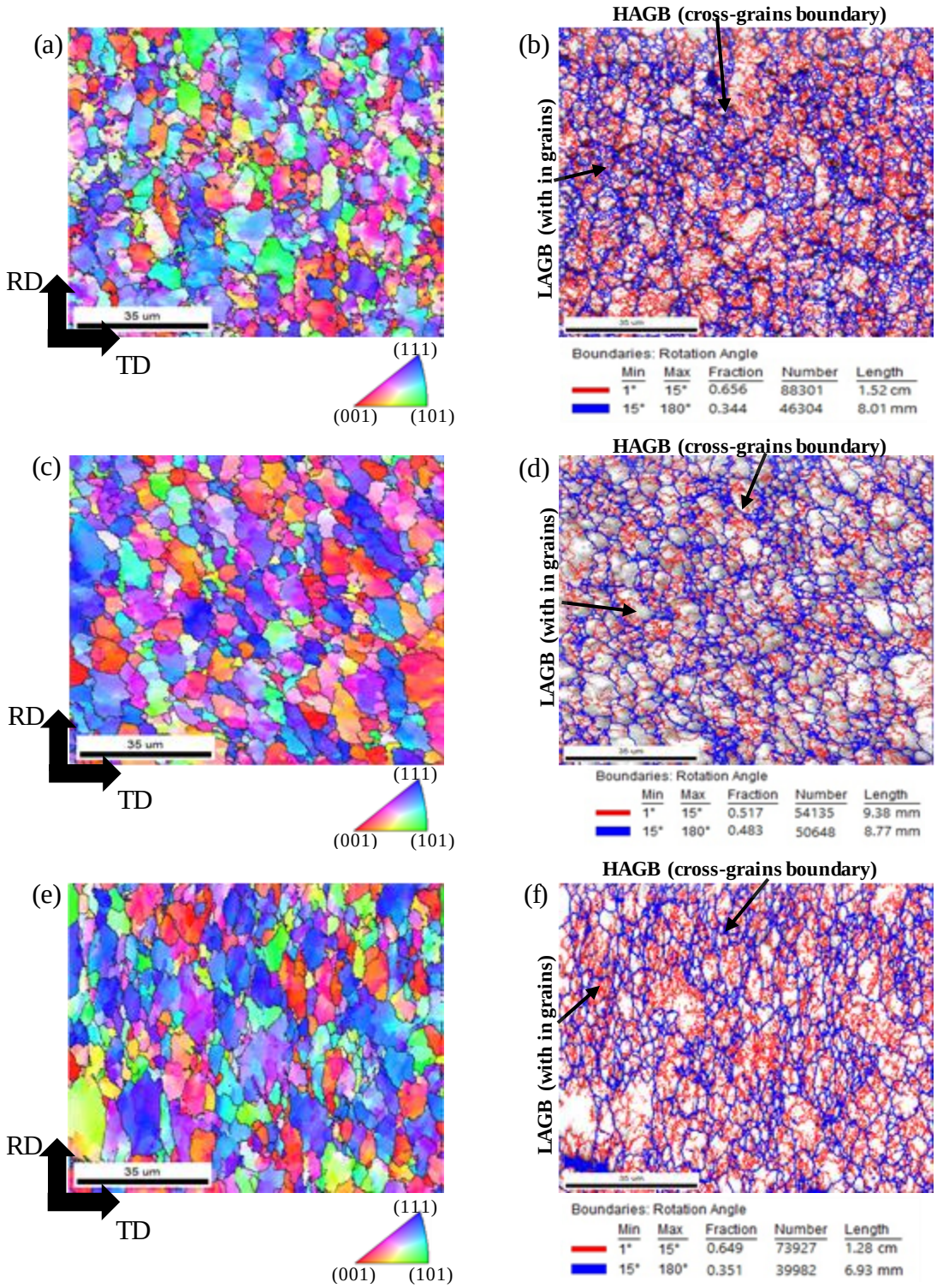

Figure 7.2 IPF maps and grain boundary maps without MF of DP590 1.6mm sheet at (a)-(a) 0°, (c)-(d) 45°, and (e)-(f) 90°.

The KAM distribution of sample taken from tested specimens oriented at the 0° to the RD of the sheet is shown in Figure 7.3 (a). The KAM map of the same sample shows the distribution of green colour within the grains due to local strain distribution and dislocation density. It was also observed that the less blue colour spot seen in the microstructure represent less change in dislocation density. KAM map at 0° to the RD shows majority of grains in green colour indicate higher dislocation density but larger grains are also observed with blue colour patches indicate a lower dislocation density.

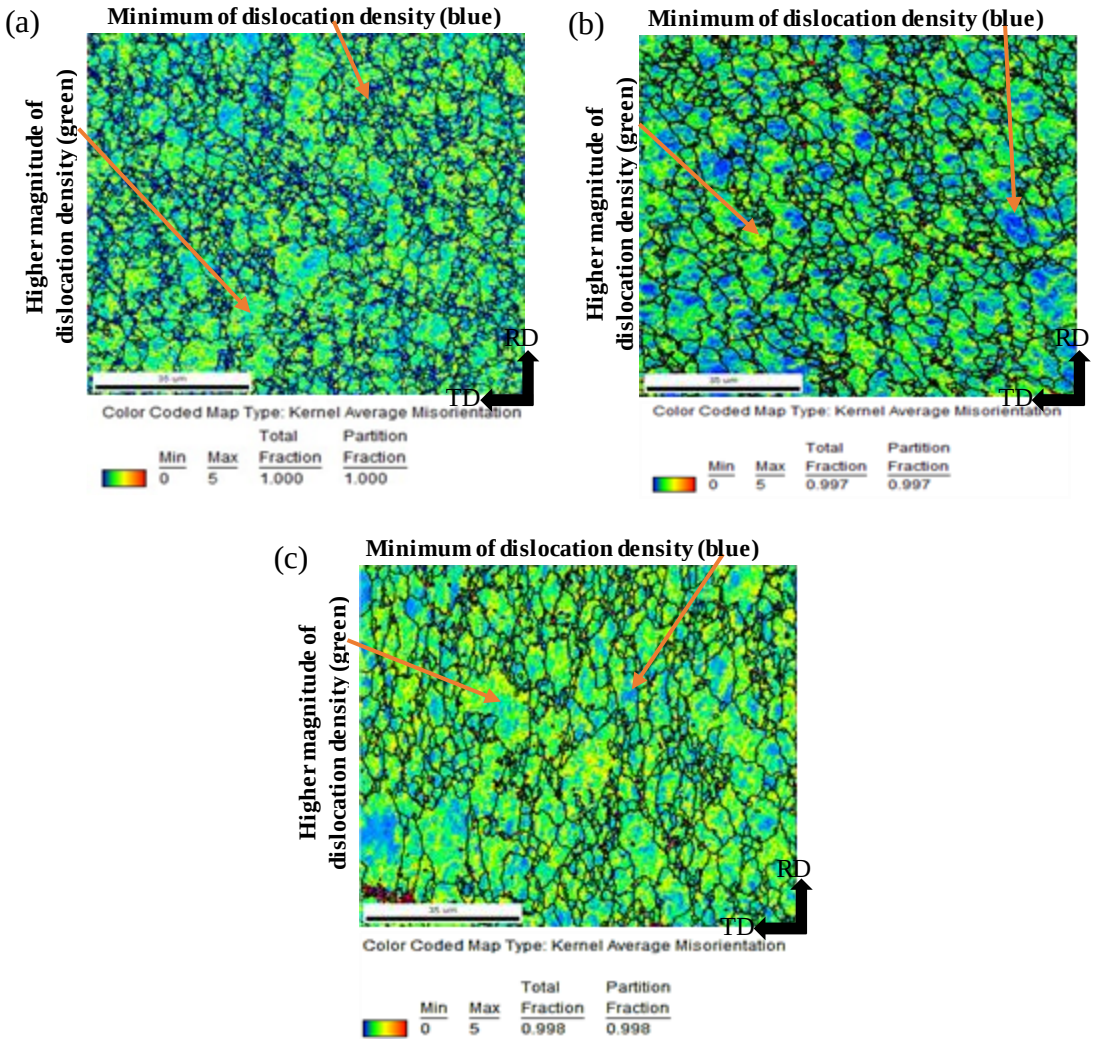

Figure 7.3 Distributions of KAM maps without MF for DP590 1.6mm at (a) 0°, (b) 45°, and (c) 90°.

The KAM distribution of sample taken from tested specimens oriented at the 45° to the RD of the sheet is shown in Figure 7.3 (b). The KAM map of the same sample shows that the maximum grains are not converted in the smaller grains within the bigger grain due to local strain distribution. It is representing in blue colour in the microstructure and LAGB occur near to the grain boundaries in of green. KAM map for 45° to the RD shows an almost equal distribution of area in green and blue colour within the microstructure. The KAM distribution of sample taken from tested specimens oriented at the 0° to the RD of the sheet is shown in Figure 7.3 (c). The KAM map of the same sample shows that the local strain distribution and dislocation density are seen in the maximum of grains and bigger grains are converted into smaller grains as seen by green and yellow colour distribution. KAM map at 90° to the RD shows majority of grains in green colour but larger grains are also observed with a higher area in blue colour patches when compared with results for 0° to RD.

7.1.3 Specimens tested of DP590 steel with magnetic field

The microstructures of the samples taken from the center of the 20% plastic strain tested specimens with three different orientations to the RD with the effect of applied MF using *tool-C* are shown in Figure 7.4. The IPF image with colour distribution triangle of the samples taken from tested specimens oriented at 0° to the RD is shown in Figure 7.4 (a). It is observed that the distribution of plane (111) within the grains is estimated to be only 34% which is lower than the specimens tested without the application of a MF (49%). It is also noticed that the distribution of plane (001) is 47% increased by approximately 16% with the applied MF on the tensile tested specimen as compared without MF Figure 7.2 (a). Moreover, the distribution of (110) plane is almost the same as seen in both the microstructures of specimens tested with and without the application of a MF and is estimated to be 19%.

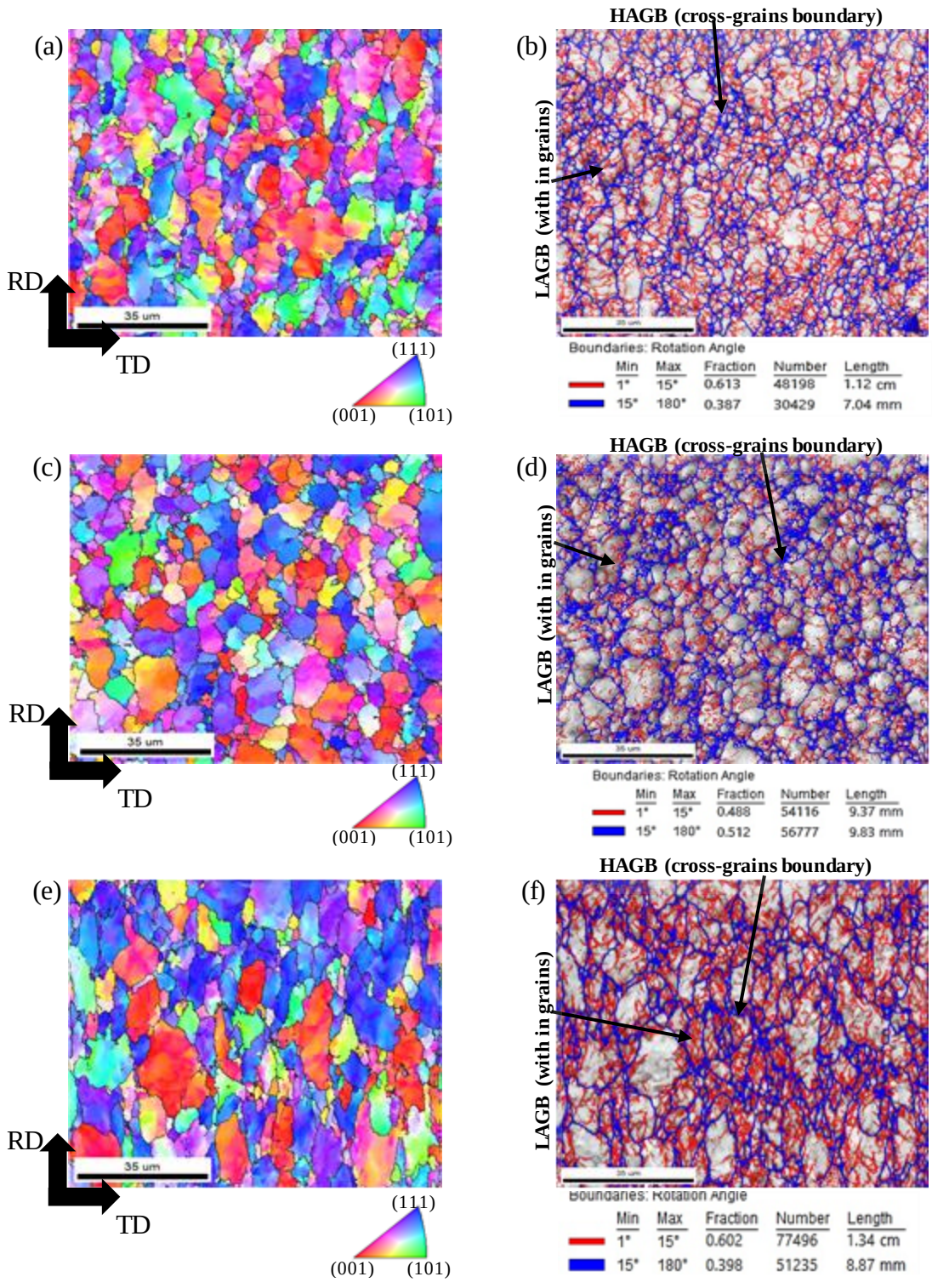

Figure 7.4 IPF maps and grain boundary maps with MF of DP590 1.6mm sheet at (a)- (a) 0°, (c)-(d) 45°, and (e)-(f) 90°.

The interplanar distance of (110) plane was determined by X-Ray Diffraction technique using a Rigaku-XRD (Wilcox-132) for the samples taken from the specimens oriented at 0° to the RD with and without the MF. The interplanar spacing of atoms in the {110} is observed to be 1.9129 A° at 2θ angle of 47.49° for the samples without MF. The interplanar distance is increased to 2.165 A° at 2θ angle of 41.68° for the samples tested with the effect of the MF. The increase in the interplanar spacing for a given plane indicates the higher degree of interaction of the dislocations with the spin orientations [121]. The plastic deformation in the metals is governed by the collective motion and interaction of dislocations on a slip plane which is affected by the interplanar spacing [122]. In the case of BCC metals, owing to the complex nature of the slip phenomenon, slip occurs on (110) plane in the closed packed direction <111> during plastic deformation [123]. This phenomenon might have resulted in the development of elongated grains with a size of approximately 9.2 μm as evident in the microstructure of the tested samples with the MF. The grain size obtained with the MF is increased almost 46% of the grain size obtained for the tested samples without MF for the same orientation w.r.t. the RD. Figure 7.4 (b) shows the grain boundary map depicting a distribution of grains with LAGB having a fraction of 0.613 of the whole microstructure which is lower than the value of fraction shown in Figure 7.2 (b). It may be concluded that the specimens tested with the MF offer higher strength and lower ductility as a smaller reduction in slip system indicates higher resistance to deformation and higher strength with reduced percentage elongation. Thus, at first glance, it appears that the MF orients the spin in the direction of applied load along the length of the specimen and interacts with the slip directions and planes [124].

The IPF image with colour distribution triangle of the samples taken from tested specimens oriented at 45° to the RD is shown in Figure 7.4 (c). It is observed that distribution of the plane (111) within the grains is estimated to be 41% which is lower than the specimens tested

without the application of the MF (47%). It is also noticed that the distribution of plane (001) is 48% which is slightly increased than the tensile tested specimen as compared without MF Figure 7.2 (c). Moreover, distribution of the plane (110) is almost the same as seen in both the microstructures of specimens tested with and without the application of a MF. In this case, the interplanar spacing of atoms in the {110} is observed to be 2.0213 A° at 2θ angle of 44.18° for the samples without MF. The interplanar distance is increased to 2.156 A° at 2θ angle of 41.85° for the samples tested with the effect of the MF. The average grain size obtained with the MF is 8.3 µm which is increased almost 24% of the grain size obtained for the tested samples without MF for the same orientation w.r.t. the RD. On the other hand, in the grain boundary map shown in Figure 7.4 (d), it was observed that the LAGB (0.488 number fraction) and HAGB (0.512 number fraction) is changed as compared with the sample tested without the MF (Figure 7.2 (d)). The majority of the grain's boundaries covered with HAGB and major part of LAGB of deformed grains are seen near to the grain's boundaries.

The IPF image with colour distribution triangle in the microstructure of the tested specimens with orientation at 90° to the RD is shown in Figure 7.4 (e). It shows that the percentage distribution of the plane (111) is 48% which is slight less than the cases of specimens tested without the application of MF (Figure 7.2 (e)). It was also noticed that the distribution of plane (001) is 36% which is 16% increased than the tensile tested specimen as compared to without MF samples. Moreover, the percentage distribution of the plane (110) within the grains is estimated to be 16% which is decreased almost 35% of the value obtained with that of the specimens tested without the MF (27%). In this case also, the interplanar spacing of atoms in the plane {110} is observed to increase due to the effect of the MF. The average grain size obtained with the MF is 10.3µm which is increased almost 43% of the grain size obtained for the tested samples without MF for the same orientation w.r.t. the RD. In Figure 7.4 (f), the grain boundary map shows that the LAGB (0.602 number fraction) is decreased and HAGB

(0.398 number fraction) is increased as compared with the sample tested without the MF (Figure 7.2 (f).

The KAM map of the samples taken from tested specimens oriented at 0° to the RD with MF is shown in Figure 7.5 (a). It is noticed that the few of grains are not deformed uniformly as compared with the samples tested without MF (Figure 7.3 (a)) for the same orientation. It concluded that the dislocations density of the microstructure is affected due to MF and change of the spin of the electrons along the direction of MF.

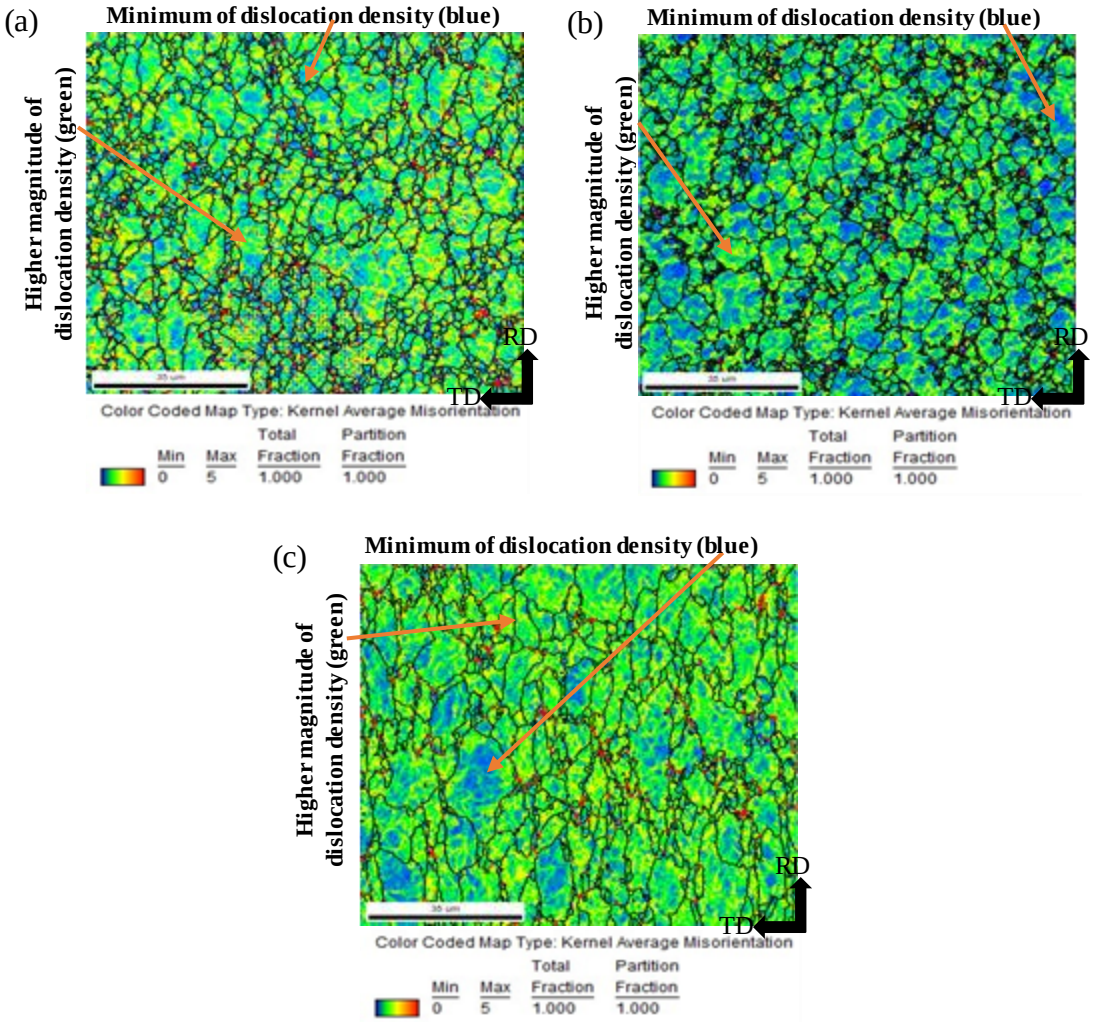

Figure 7.5 Distributions of KAM maps with MF for DP590 1.6mm at (a) 0°, (b) 45°, and (c) 90°.

The KAM map of the samples taken from tested specimens oriented at 45° to the RD with MF is shown in Figure 7.5 (b). It is observed that few grains are not deformed uniformly as compared with the samples tested without MF (Figure 7.3 (b)) for the same orientation. It can be concluded that the dislocations density decreased with the effect of the MF, but it gets less effect as compared with the specimen tested at 0° to the RD with MF. The KAM map of the samples taken from tested specimens oriented at 90° to the RD with MF is shown in Figure 7.5 (c). It is observed that the effect of MF restricted the motion of the dislocation density within grain which is seen as less local strain distribution with blue colour. It can be concluded that the dislocations density decreased with the effect of the MF. It was also noticed that the effect of MF is more in the case of 90° to the RD as compared to the other two directions when specimens were tested with MF.

7.1.4 Texture Evaluations of DP590 steel with and without magnetic field

The pole figures of the samples tested without MF are shown in Figures 7.6 (a), (b) and (c) show the comparison of the pole figures for the planes {001}, {110} and {111} corresponding to the EBSD maps shown in Figures 7.2 (a), (c) and (e), respectively. Similarly, the pole figures of the samples tested with MF are shown in Figure 7.6 (d), (e) and (f) show the comparison of the pole figures for the planes {001}, {110} and {111} corresponding to the EBSD maps shown in Figures 7.4 (a), (c) and (e), respectively. The study of texture is based on the EBSD analysis in term of pole figures for the planes {001}, {110} and {111} for the specimens tested with and without the MF is shown in Figure 7.6. The pole figures of specimen tested at 0° to the RD without and with MF are shown in Figure 7.6 (a) and (d), respectively shows the weak textures. It is also noticed that the effect of magnetic increased the texture strength of the material. The value of MRD increased from 2.090 to 3.514 which means the material exhibit strong texture as compared without MF. The pole figures of specimen tested at 45° to the RD without and with MF are shown in Figure 7.6 (b) and (e),

respectively shows the weak textures. It is observed that the effect of MF is very less on texture and the value of MRD sight change from 2.370 to 2.937 which means the material shows weak texture. If the texture does not change more with MF than that effect of change in anisotropy of the material is less.

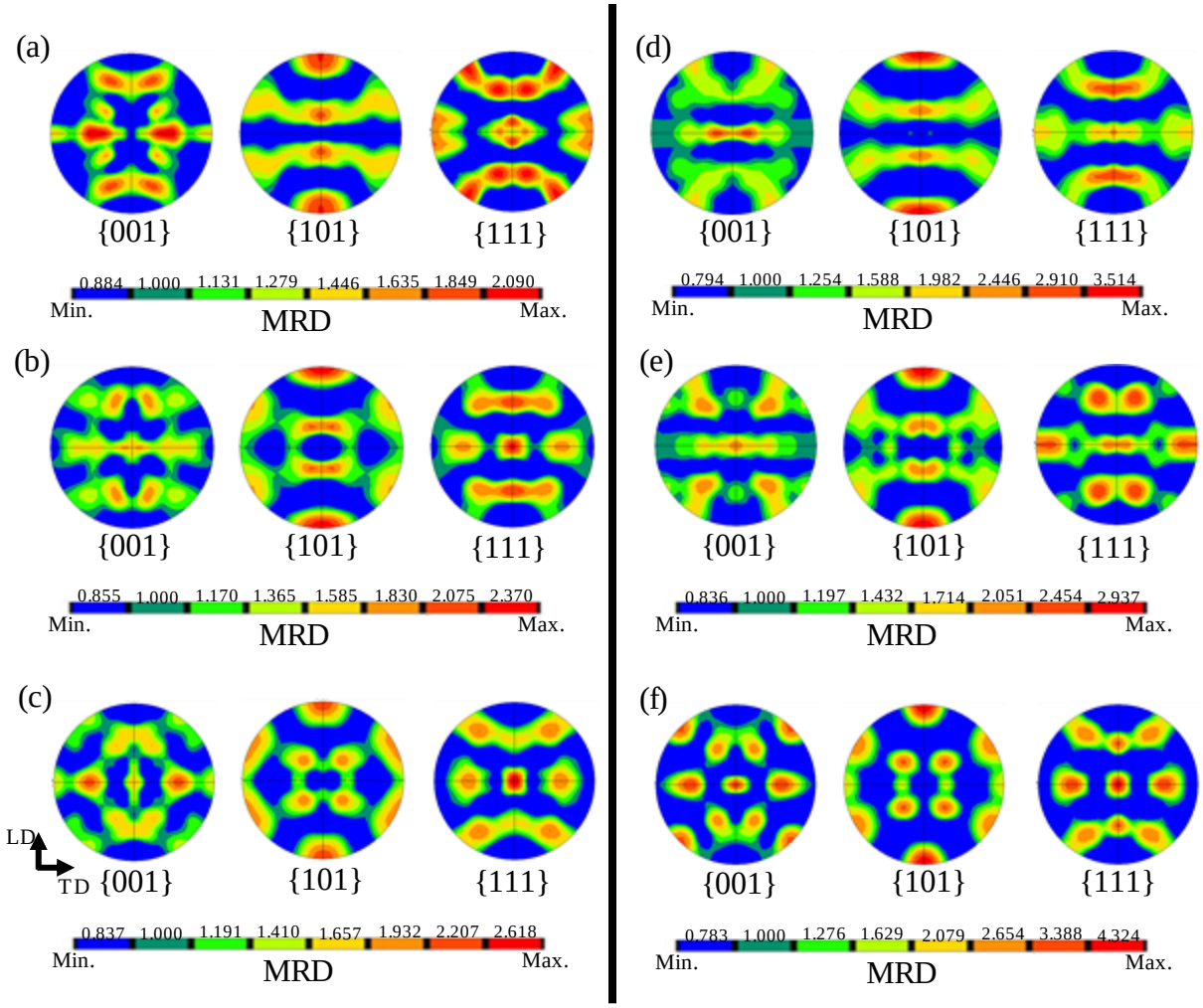

Figure 7.6 Pole figures of DP590 1.6mm specimens tested with and without MF in term of MRD: (**a**)-(**c**) specimen tested without MF at 0°, 45°, and 90° to RD and (**d**)-(**f**) specimen tested with MF at 0°, 45°, and 90° to RD.

The pole figures of specimen tested at 90° to the RD without and with MF (Figure 7.6 (c) and (f), respectively) shows the weak textures. It is also noticed that the effect of magnetic field

increased the texture strength of the material. The value of MRD increased from 2.618 to 4.324 which means the material developed stronger texture as compared to without MF. It can be concluded that the tested specimen with 20% of plastic strain with MF shows higher ductility as compared with results obtained without the MF.

7.2 Microstructural examination of ZC440 steel

7.2.1 Untested material ZC440 steel

The microstructures of the untested sheet obtained by electron backscattered diffraction (EBSD) technique are shown in Figure 7.7. The microstructure analysis through the IPF map with colour distribution triangle shown in Figure 7.7 (a) shows that the percentage distribution of the plane (001) is 45% followed by (111) and (101) as 38% and 17%, respectively. The grain sizes are observed to be in the range of approximately 9 μm to 11 μm. In order to get the details of distribution of low and high angle grain boundaries, a grain boundary map of the microstructure is shown in Figure 7.7 (b). The grains with grey shade represent the recrystallized strain free crystals with negligible dislocations. The blue boundary lines represent the high angle grain boundaries (HAGB) with misorientation angle larger than 15° and the low angle grain boundaries (LAGB) with misorientation angle in the range of 1°–5° are represented by the red boundary lines. The EBSD measurement indicates that the distribution fraction of HAGB is 67.4% and LAGB is 32.6%.

The pole figures of the sample of an untested sheet material are shown in Figure 7.7 (c) which gives the distribution of planes {001}, {110} and {111} corresponding to the EBSD map in Figure 7.7 (a). The pole figure of {001} planes show a higher intensity of peaks (4.589) in terms of multiples of random orientation (MRD) indicating a strong texture followed by the intensity of the peaks in {111} and {110} planes, respectively. It is noticed that the sheet material possesses a good texture. In a pole figure, the poles are taken with the normal to a

lattice plane for a given family of planes and plotted to a suitable reference axis i.e. longitudinal direction (LD) and transverse direction (TD) as shown in figure 8*C*.

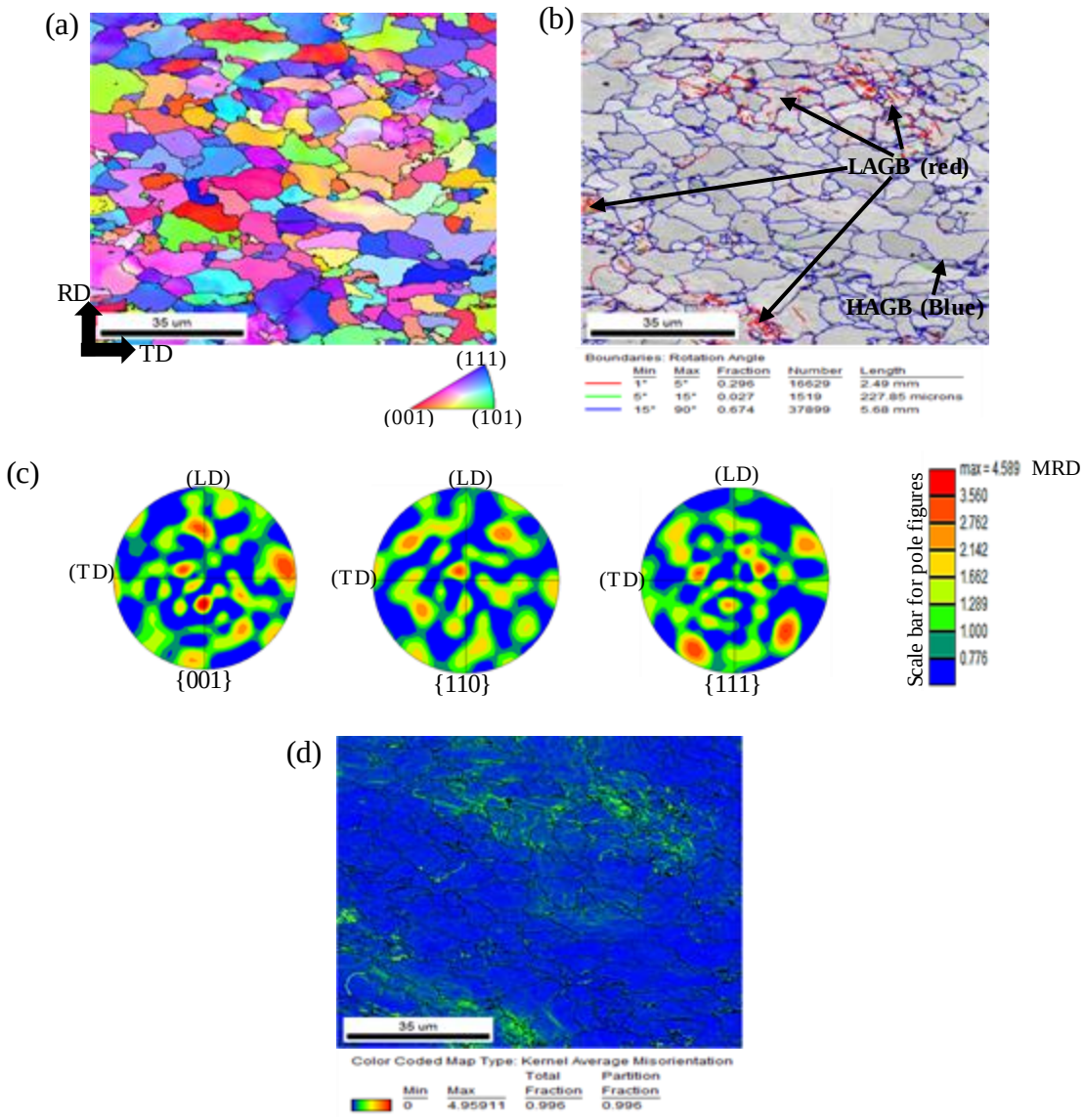

Figure 7.7 EBSD image of untested material of ZC440: (a) inverse pole figure map and key, (b) grain boundary map (c) kernel average misorientation map (d)misorientation angle distribution and (e) pole figures.

The Kernel Average Misorientation (KAM) map is frequently used as a tool in orientation imaging microscopy (OIM) analysis to subjectively evaluate local strain distribution and dislocation density [121]. In the KAM maps shown in Figure 7.7 (d), the grains with blue

colour represents a low KAM values and the green represents a higher value (in degree). It is observed that the untested sheet material has a majority of recrystallized strain free grains with an appreciable homogeneity within the grains along with the grains with few scattered dislocations at the grain boundaries.

7.2.2 Tested specimens of ZC440 steel without magnetic field

The IPF map with colour distribution in the microstructure of the samples taken from the tested specimen with 20% of plastic strain oriented at 0° to the RD is shown in Figure 7.8 (a). It is observed that the distribution of planes (111) is estimated to be 47% followed by (001) and (101) as 34% and 19%, respectively. Most of the grains are observed to lie on the planes of {111} and {001} after deformation. In the case of body-centered cubic (BCC) metals, due to the complex nature of the slip phenomenon during plastic deformation, slip occurs on plane (110) in the closed packed direction <111> [121]. The grain size is observed to be in the range of approximately 11 μm to 15 μm after plastic deformation. In order to get the details of distribution of low and high angle grain boundaries, a grain boundary map of the microstructure is shown in Figure 7.8 (b). The EBSD measurement shows that the fraction of HAGB (62.5%) is much higher than the fraction of LAGB (37.5%). During plastic deformation, a gradual change in grain orientation may take place which leads to a lattice rotation [125]. Rotation of a grain during plastic deformation results in a reduced grain misorientation [126]. On application of stress to a polycrystalline material, stress concentration occurs preferentially at the grain boundaries, which release the dislocations acting as dislocation sources and the grains undergo yielding by slip [127].

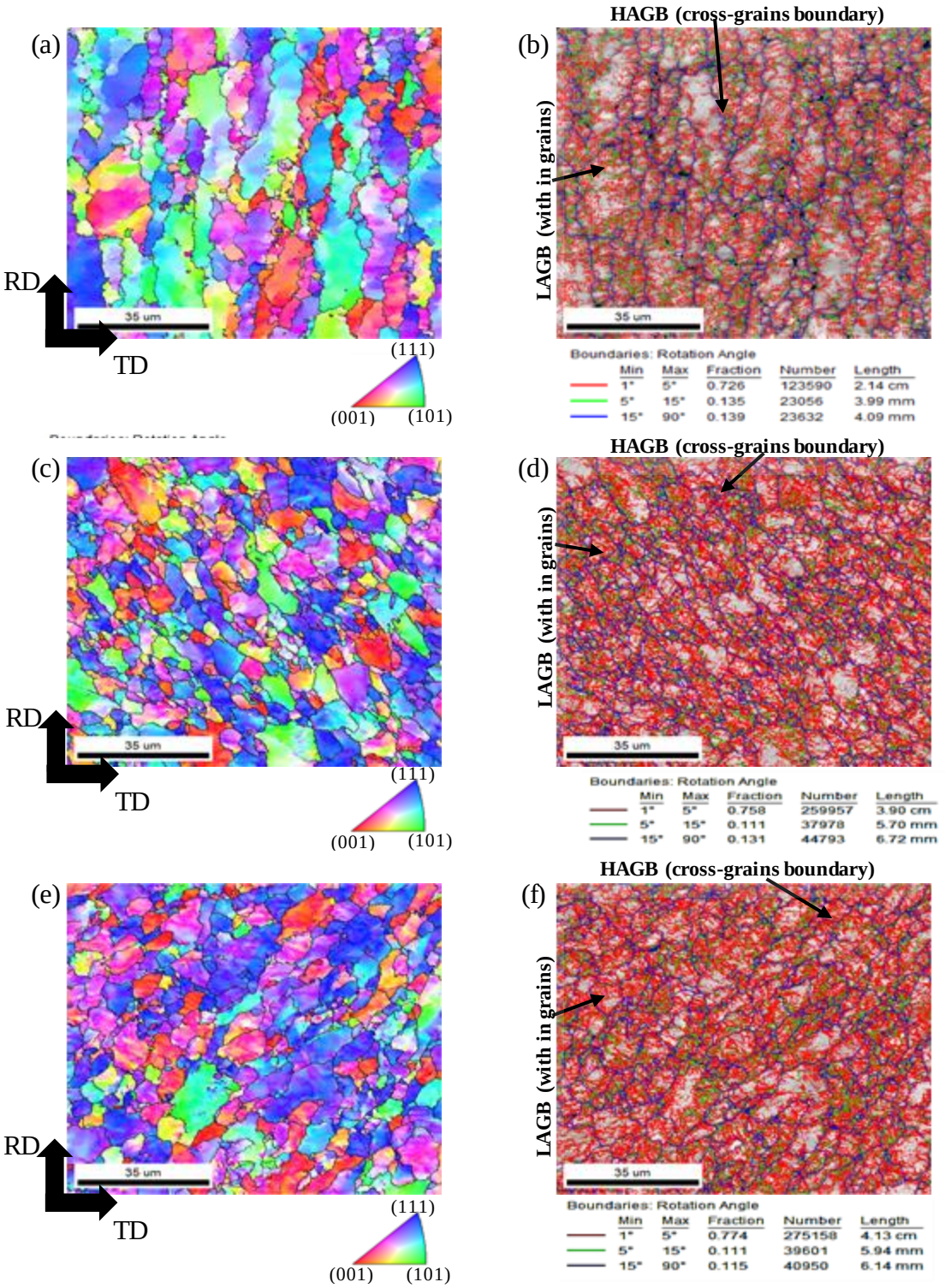

Figure 7.8 IPF maps and grain boundary maps without MF of ZC4400 1.4mm sheet at (a)-(a) 0°, (c)-(d) 45°, and (e)-(f) 90°.

The IPF map with colour distribution in the microstructure of the samples taken from the tested specimen oriented at 45° to the RD is shown in Figure 7.8 (c). It is observed that the percentage distribution of plane (111) is estimated to be 49% followed by (001) and (101) as 36% and 15%, respectively. The grain size is observed in the range of approximately 10 μm to 15 μm in the microstructure after plastic deformation. The distribution of low and high angle grain boundaries is given in a grain boundary map of the microstructure and is shown in Figure 7.8 (d). The EBSD measurement indicates that the fraction of HAGB is 72.6% which is much higher than the percentage of LAGB (27.4%). The grain boundary map results show that the LAGB affected marginally at 20% of the plastic strain as compare to the HAGB.

Figure 7.8 (e) shows IPF maps with colour distribution in the microstructure of the samples taken from the tested specimen oriented at 90° to the RD of the sheet. It is observed that the distribution of plane (111) is estimated to be 44% and followed by (001) and (101) as 38% and 18%, respectively. The grain size is observed in the range of approximately 13 μm to 17 μm. The EBSD measurement indicates that the fraction of HAGB is 55.5% and LAGB is 44.5%. The grain boundary map is shown in Figure 7.8 (f) which depicts a decrease in HAGB and an increase in LAGB indicating an easy movement of dislocations in the slip system as compared to the specimens tested at 45° to the RD.

The KAM distribution of sample taken from tested specimens oriented at the 0° to the RD of the sheet is shown in Figure 7.9 (a). The homogeneous deformation is observed in the majority of grains represented in green colour resulting in a high dislocation density. In a KAM map, both green and blue colours represent the local strain distribution. The green colour represents a higher magnitude of dislocation density within the grains and in the sub-region of the grains whereas, the blue shows a minimum of dislocation density. This also means that the grains with the blue regions are not deformed homogeneously as they offer higher resistance to deformation. The KAM distribution of the tested specimen oriented at 45° to the RD of the

sheet is shown in Figure 7.9 (b). A higher degree of homogeneous deformation is observed in the majority of grains represented in green colour that also possess higher magnitude of dislocation density. Whereas, a few of the grains represented in blue are observed to have a minimum localised strain distribution which is also higher in area than that of the distribution seen in the samples of tested specimens oriented at 0° to RD.

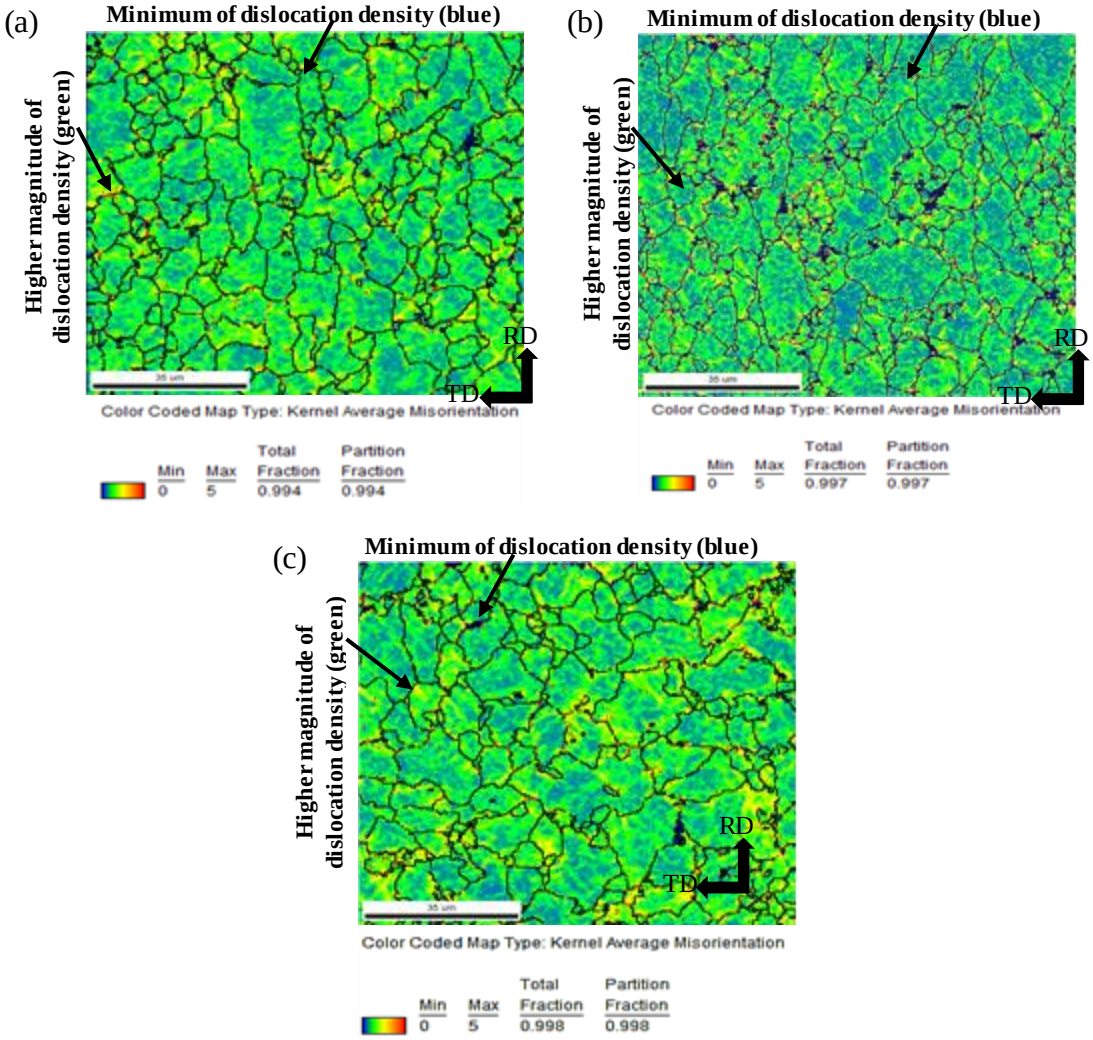

Figure 7.9 Distributions of KAM maps without MF for ZC440 1.4mm at (a) 0°, (b) 45°, and (c) 90°.

The KAM distribution of the tested specimen at 90° to the RD of the sheet is shown in Figure 7.9 (c). In this case, since the fraction of blue region in deformed grains decreases further indicating that the highest degree of homogeneous deformation takes place in the majority of grains represented in green colour when compared with the samples of tested specimens oriented in the 0° and 45° to the RD.

7.2.3 Specimens tested of ZC440 steel with magnetic field

The IPF map with colour distribution in the microstructure of the samples taken from a tested specimen with 20% of plastic strain oriented at 0° to the RD with the MF is shown in Figure 10 (a). It is observed that the distribution of planes (001) is estimated to be 45% followed by (111) and (101) as 38% and 17%, respectively. It is also noticed that the percentage distribution of plane (001) is increased whereas distribution of plane (111) decreased within the grains inhibiting the most favourable slip system when compared with the specimen tested for the same orientation without the MF. Plastic deformation of metals is generally governed by a collective motion and interaction of the dislocations on slip planes influenced by a lattice spacing [123]. The applied MF tends to align the magnetic domains in the direction of the applied field which offers hindrance to the movement of the dislocations. Moreover, microscopically all the magnetic dipoles are aligned parallel to their neighbours in a domain due to applied MF. It can be concluded that this phenomenon may have led to the development of elongated grains in the range of approximately 16 µm to 20 µm, as evidenced in the microstructure of the samples tested with the MF. The grain size is approximately 33% higher than the value obtained in the sample tested without the MF for the same orientation. The distribution of low and high angle grain boundaries is given in a grain boundary map of the microstructure and is shown in Figure 10 (b). The grain boundary map shows that the fraction of HAGB is 66.6% and LAGB is 33.4%. The fraction of HAGB is observed to be higher but for LAGB is lower due to the MF when compared with the microstructure of the samples

taken from the specimens tested without the MF with same plastic strain. The MF orients the spin in the direction of applied load along the length of the specimen and interacts with the slip directions and planes [124]. The grains with the similar orientation of spin directions are aligned parallel to the MF along the loading direction during testing thus leading is to the accumulation of dislocations within the grain and reducing the fraction of LAGB.

The IPF map of the samples taken from a tested specimen oriented at 45° to the RD of the sheet is shown in Figure 10 (c). It is observed that the distribution of planes (001) is estimated to be 46% followed by (111) and (101) as 40% and 13%, respectively. It is also noticed that after plastic deformation, the percentage distribution of plane (001) increased whereas distribution of plane (111) decreased within the grains when compared with the specimen tested without the MF for the same orientation. It can be seen that the grains lying in the family of planes {001} are elongated significantly due to plastic deformation when compared with the specimens tested without the MF. A range of elongated grains of approximately 15 μm to 19 μm size is observed in the microstructure with the MF which is 26% higher than the size obtained without the MF. The distribution of low and high angle grain boundaries is given in a grain boundary map of the microstructure and is shown in Figure 10 (d). The grain boundary map shows that the fraction of HAGB is 64.9% and LAGB is 35.1%. The fraction of LAGB is observed to be increased with the MF when compared with the microstructure of the samples taken from the specimens tested without the MF for the same orientation.

The IPF map with colour distribution in the microstructure of the samples taken from a tested specimen oriented at 90° to the RD of the sheet is shown in Figure 10 (e). It is observed that the distribution of plane (101) is estimated to be 39% followed by (111) and (001) as 35% and 26%, respectively. It is also observed that the percentage distribution of plane (101) increased, plane of (111) and (001) decreased within the grains when compared with the microstructure of the samples taken from the specimens tested without the MF.

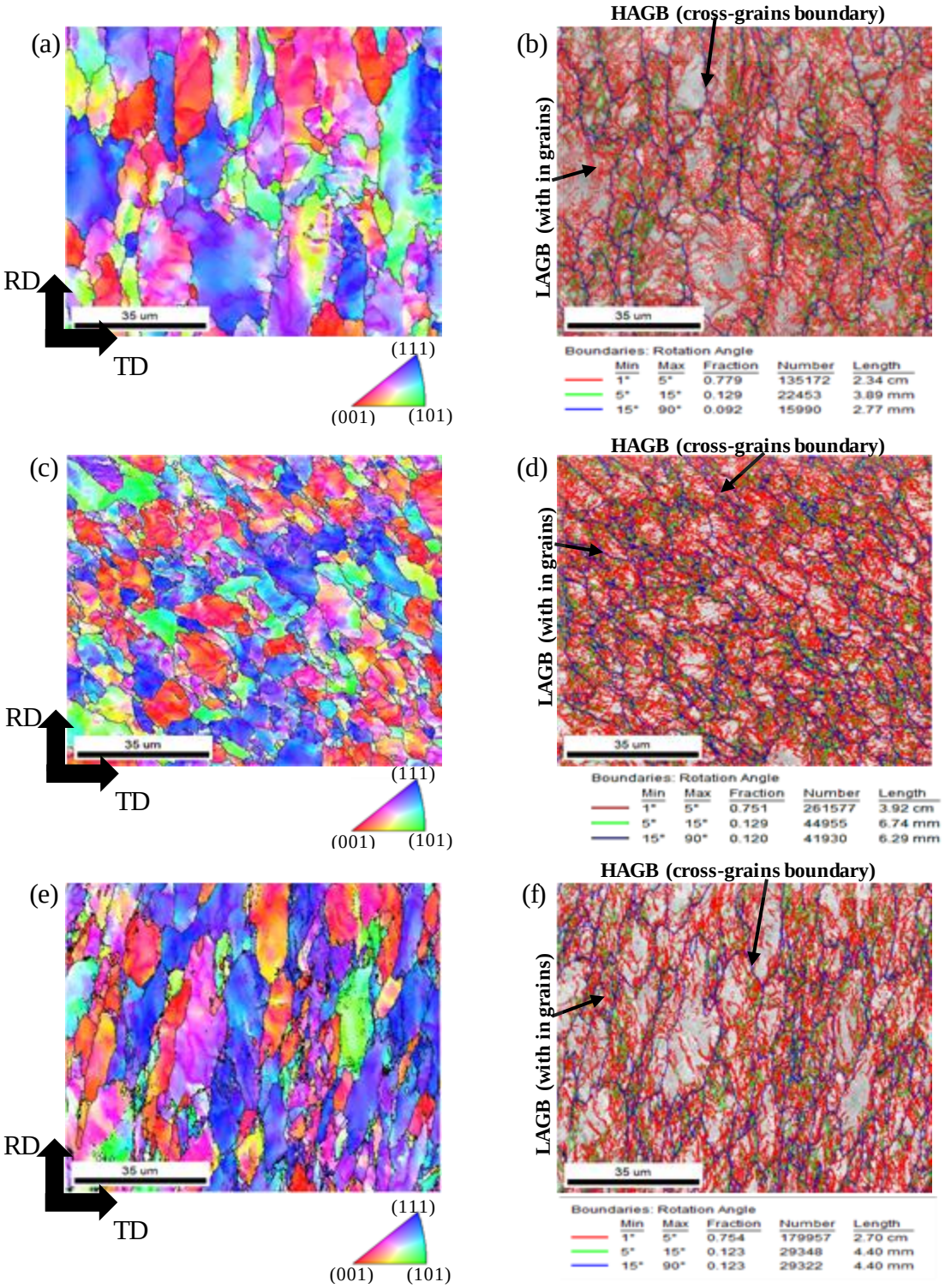

Figure 7.10 IPF maps and grain boundary maps with MF of ZC4400 1.4mm sheet at (a)- (a) 0°, (c)-(d) 45°, and (e)-(f) 90°.

A range of elongated grains size is observed approximately 16 μm to 22 μm in the microstructure with the effect of MF. The increase in grain size with the MF is almost 29% of the size seen in the samples tested without MF for the same orientation. The distribution of low and high angle grain boundaries is given in a grain boundary map of the microstructure and is shown in Figure 10 (f). The grain boundary map shows that the fraction of HAGB is 64.8% and LAGB is 35.2%. The fraction of HAGB is observed to be increased but for LAGB it is lower due to the MF when compared with the microstructure of the samples taken from the specimens tested for the same orientation without the MF.

The KAM distribution of samples taken from a tested specimen with MF oriented at 0° to the RD of the sheet is shown in Figure 7.11 (a). It represents a non-uniform and inhomogeneous plastic strain distribution within the grains when compared with the results obtained without the MF. The fraction of area in blue patches increased and appears to scatter at random within the grains in the microstructure when compared with the KAM map of the samples taken from the specimen tested without the MF. It may be concluded that although the grains are elongated and texture evolves to a greater extent but an increased resistance to deformation is offered by the grains due to the applied MF which enhances the tensile strength and anisotropy of the sheet in a particular direction.

The KAM distribution of samples taken from a tested specimen with MF at an orientation of 45° to the RD of the sheet is shown in Figure 7.11 (b). The fraction of area in blue patches is decreased and appears to scatter at random in the microstructure when compared with the KAM map of the samples taken from the specimen tested without the MF. The green shade seems to be distributed uniformly throughout the microstructure representing a higher dislocation density within the grain. It may be concluded that although the grains are elongated to a greater extent but an increase in LAGB (>8% when compared in the samples tested without the MF for the same orientation) enhances the tensile strength due to the MF.

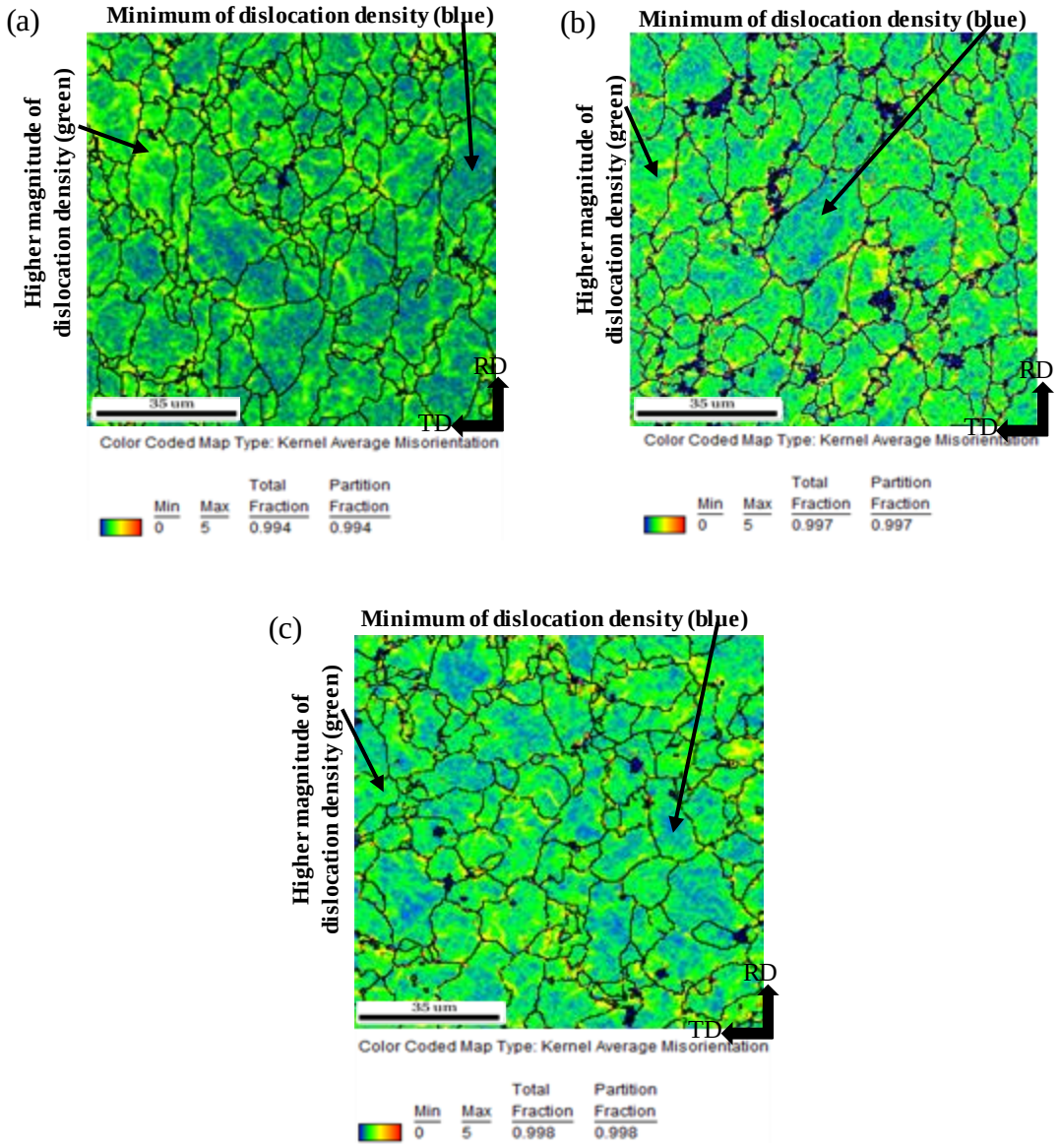

Figure 7.11 Distributions of KAM maps with MF for ZC440 1.4mm at (a) 0°, (b) 45°, and (c) 90°.

The KAM distribution of samples taken from a tested specimen with the MF at 90° to the RD of the sheet is shown in Figure 7.11 (c). It represents a highest degree of inhomogeneous plastic strain distribution within the grains and the grain size is elongated to a largest value in length along the loading axis when compared with the results in other directions. A highest fraction of area in blue patches is observed in the elongated grains shown in the microstructure

when compared with the KAM map of a sample taken from the specimen tested without the MF in the same orientation. It may be concluded that although the grains are elongated to a greater extent but an increased resistance to deformation is also offered by the grains due to the MF which enhances the tensile strength and anisotropy of the sheet in a particular direction. The highest values of tensile strength and anisotropy are observed in the specimens tested with an orientation of 90° to the RD of the sheet than that of the values obtained in the specimens tested with orientation in the other two directions due to the effect of MF.

7.2.4 Texture Evaluations of ZC440 steel with and without magnetic field

Figure 7.12 shows the comparison of the pole figures for the planes {001}, {110} and {111} of the samples taken from the specimens tested without the MF at the 0°, 45° and 90° to the RD of the sheet and corresponding EBSD maps are shown in Figure 7.12 (a), (b) and (c), respectively. The pole figures of the samples with orientations at 0°, 45° and 90° to the RD show a lower intensity of peaks of 2.819, 2.838 and 2.880 MRD, respectively when compared with untested samples. This indicates that as dislocation density increases due to plastic deformation, the MRD values decrease. A weak texture is observed in the sample taken from the tested specimen at the 0°, 45° and 90° to the RD of the sheet as seen in Figure 7.12 (a), (b) and (c), respectively.

Figure 7.13 depicts the comparisons of the pole figures for the planes {001}, {110} and {111} of tested specimens at the 0°, 45° and 90° w.r.t the RD of the sheet with the MF and corresponding to the EBSD maps shown in Figures 7.10 (a), (c) and (e), respectively. The peaks are distributed at random refers to a weak texture observed in the samples taken from the tested specimen at the 0° w.r.t the RD of the sheet with MF as the peak intensity of 3.479 MRD is seen in Figure 7.13 (a). It can be concluded that the peaks, distributed at random, are observed to increase in the plane of {001} and decrease in the plane of {111} and {101} with

the MF, which results in a stronger texture than that of specimens tested without MF for the same orientation.

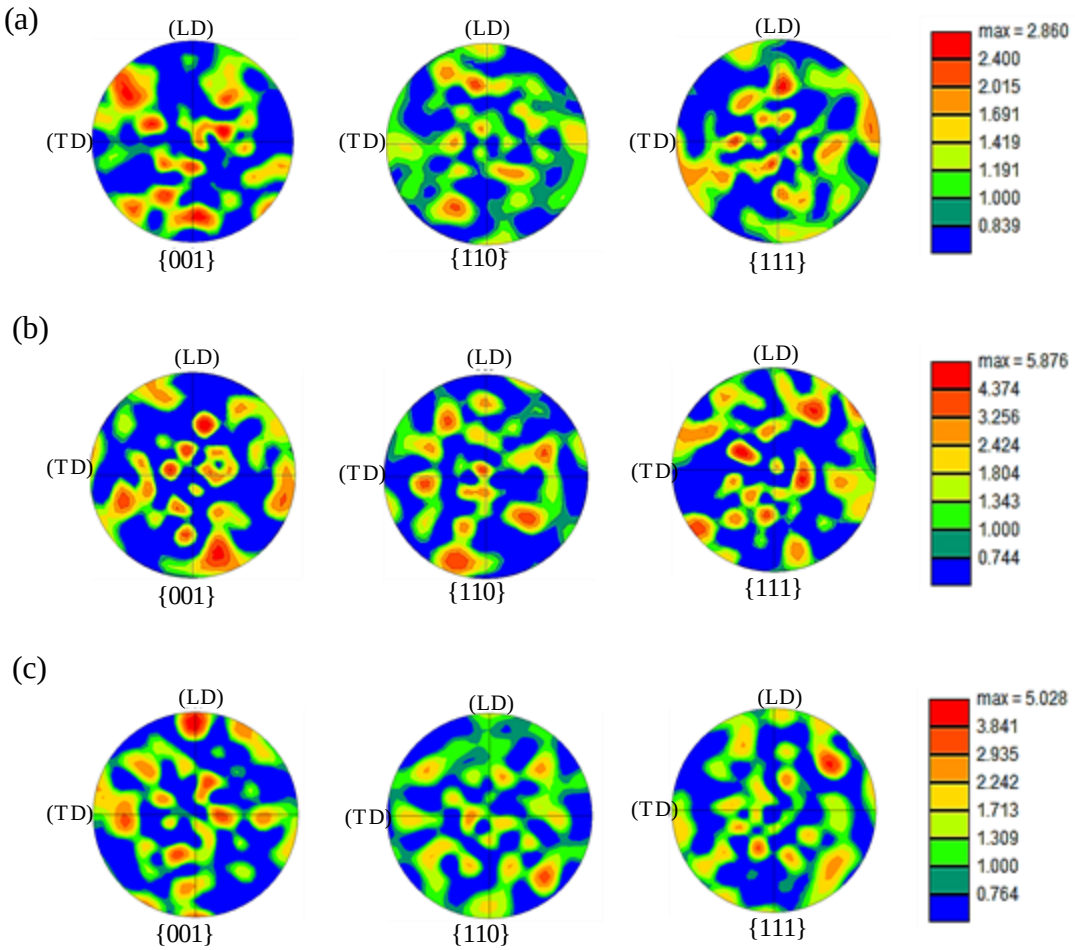

Figure 7.12 Pole figures of ZC440 1.4 mm specimen tested without MF at (a) 0°, (b) 45°, and (c) 90°.

Figure 7.13 depicts the comparisons of the pole figures for the planes {001}, {110} and {111} of tested specimens at the 0°, 45° and 90° w.r.t the RD of the sheet with the MF and corresponding to the EBSD maps shown in Figures 7.10 (a), (c) and (e), respectively. The peaks are distributed at random refers to a weak texture observed in the samples taken from the tested specimen at the 0° w.r.t the RD of the sheet with MF as the peak intensity of 3.479 MRD is seen in Figure 7.13 (a). It can be concluded that the peaks, distributed at random, are

observed to increase in the plane of {001} and decrease in the plane of {111} and {101} with the MF, which results in a stronger texture than that of specimens tested without MF for the same orientation.

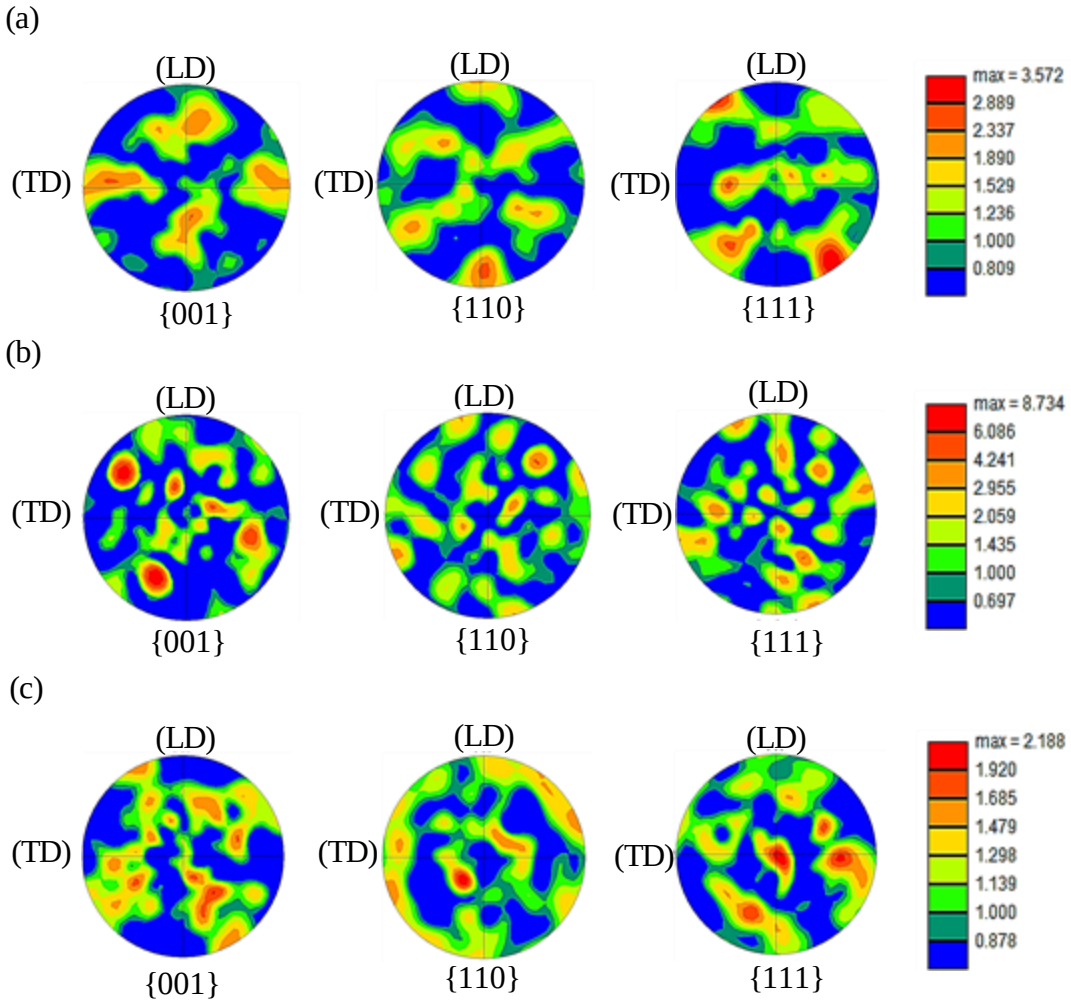

Figure 7.13 Pole figures of ZC440 1.4 mm specimen tested with MF at (a) 0°, (b) 45°, and (c) 90°.

Figure 7.13 (b), shows an evenly distributed weak texture (2.489 MRD) in the samples of tested specimen at 45° w.r.t the RD of the sheet tested with the MF when compared to the samples tested without MF for the same orientation. It is also noticed that the peaks with random orientation are decreased due to the MF. Figure 7.13 (c), shows a strong texture of

tested specimen at 90° w.r.t the RD of the sheet with MF (with a peak intensity of 5.110 MRD). In this case, the grains oriented in {001} plane are observed with a texture of sharp peaks concentrated in some areas when compared to the pole figures in the planes of {111} and {110} where the peaks are distributed at random. It is also observed that the effect of MF changes the texture significantly for the specimen tested at 90° to the RD when compared to the samples tested without MF for the same orientation. The change in the values of plastic strain ratio at any value of plastic strain could be attributed to the change in the texture after plastic deformation when tested with the MF.

7.3 Summary

On the basis of the results and discussion presented in this chapter, the microstructural study of the samples taken from the center of the specimens tested with and without the MF of DP590 steel shows that the average grain size is comparatively larger due to the MF especially in the specimens oriented at 0° and 90° to the RD. However, the grains are observed to be affected the least due to the MF in the specimens oriented at 45° to the RD. The average grain size increased in the case of DP590 steel sheet is 30% for the specimens oriented at 0° and 90° to the RD due to MF. The microstructural study of the samples taken from the center of the specimens tested with and without the MF of ZC440 steel shows that the average grain size is comparatively larger due to the MF especially in the specimens oriented at 0° and 90° to the RD. However, the grains are observed to be affected the least due to the MF in the specimens oriented at 45° to the RD. The average grain size increased in the case of ZC440 steel sheet is 45% for the specimens oriented at 0° and 90° to the RD due to MF. The texture study of DP590 steel indicated that the value of MRD increased in the cases of the specimens tested with orientation of 0° and 90° to the RD with MF and thereby produced a stronger texture when compared to the texture obtained without MF. The value of MRD gets least affected in case of the tested specimen oriented at 45° to the RD. The texture study of ZC440

steel indicated that the value of MRD increased in the cases of the specimens tested with orientation of 0° and 45° to the RD with MF and thereby produced a stronger texture when compared to the texture obtained without MF. The value of MRD gets decreased in case of the tested specimen oriented at 45° to the RD due to MF.

CHAPTER 8

RESULTS AND DISCUSSION: FAILURE PREDICTION IN ERICHSEN CUPPING USING FE SIMULATIONS

The Erichsen cupping test were performed for three different thicknesses of the ZC440 steel (1.0, 1.2 and 1.4mm) and DP590 steel (1.0, 1.2 and 1.6mm). In the stretching test the formability of the sheet is predicted by the FE simulations in term of the section sheet thickness, punch force and displacement of the punch which is correlated with Erichsen index or height of the cup. The results are also corelated with Erichsen cupping experiments.

8.1 Erichsen cupping of DP590 steel using FE simulation

8.1.1 FE simulation for sheet thickness of DP590 steel

The results of FE simulation of section sheet thinness for different sheet thicknesses of the DP590 steel observed with plastic strain data with and without the application of MF are shown in Figure 8.1. The FE results of 1.6 mm thickness observed with plastic strain data with and without the application of MF are shown in Figure 8.1 (a). It is observed that the material gets more thinning in case of applied MF as compared to without MF as seen from the flange to the punch center. The location of the necking was observed away from the punch center and slight changed due to MF. At the necking, the sheet thickness is observed to be 0.53mm in case of without MF and 0.43mm in case of with MF. The difference in thinning of the sheet is observed to be higher side at the punch center in case of MF. This may be attributed to the elongated grains of the sheet due to MF as seen in the chapter 7 microstructural analysis of DP590. The section thickness contour plots of 1.6mm thickness without and with MF are shown in Figure 8.2 (a) and (b), respectively. It shows that the failure of the material occurs and thinning of the sheet due to stretch forming. The effect of MF during the testing shows the material result higher in thinning of sheet.

The FE results of 1.2 mm thickness observed with plastic strain data with and without the application of MF are shown in Figure 8.1 (b). It is observed that the material gets more thinning in case of applied MF as compared to without MF as seen from the flange to the punch center. The location of the necking was observed away from the punch center and slight changed due to MF. At the necking, the sheet thickness is observed to be 0.41mm in case of without MF and 0.34mm in case of with MF. The difference in thinning of the sheet is observed to be higher side at the punch center in case of MF. This may be attributed to the elongated grains of the sheet due to MF. The section thickness contour plots of 1.2mm thickness without and with MF are shown in Figure 8.3 (a) and (b), respectively. It shows that the failure of the material occurs and thinning of the sheet due to stretch forming. The effect of MF during the testing shows the material result higher in thinning of sheet.

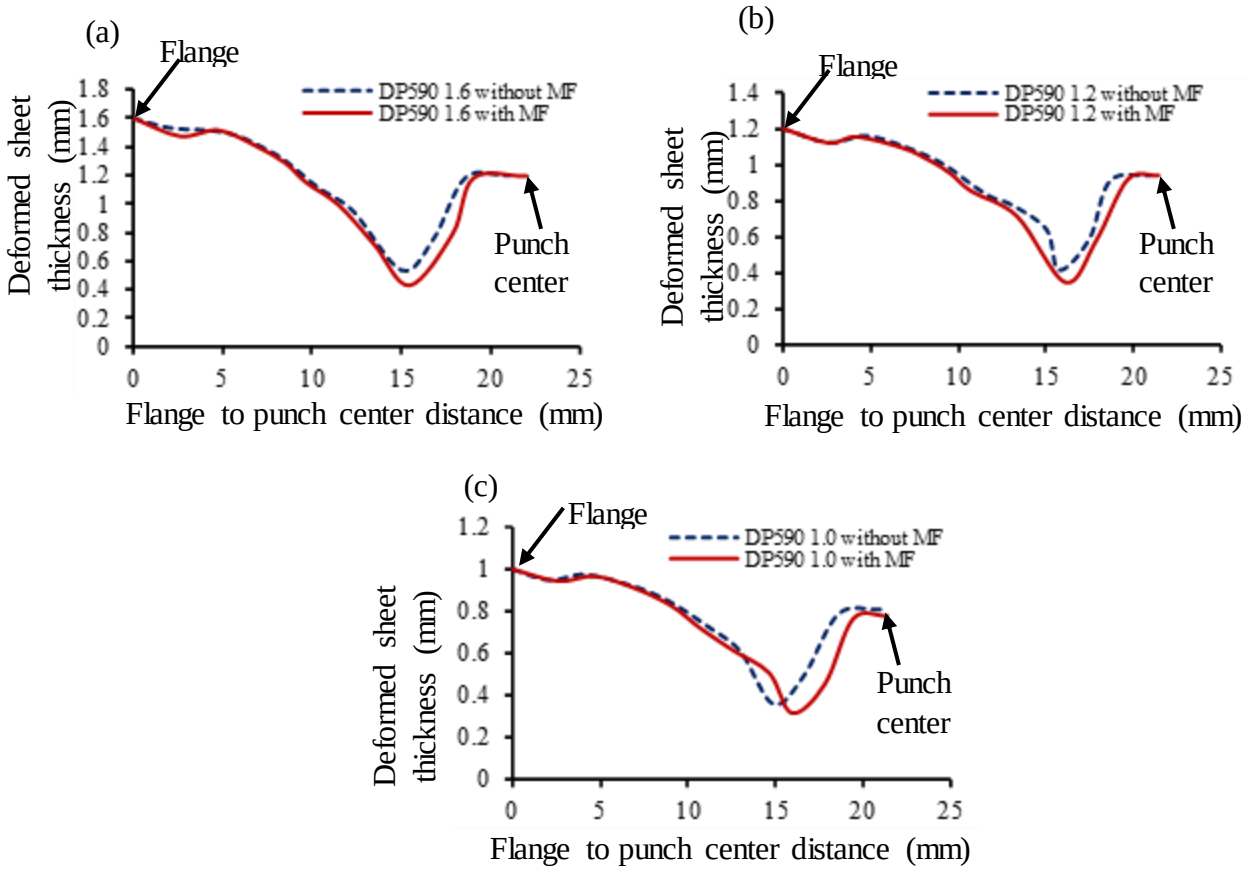

Figure 8.1 FEA results for change in sheet thickness with distance from flange to punch center for DP590, (a) 1.6 mm, (b) 1.2 mm, and (c) 1.0 mm.

The FE results of 1.0 mm thickness observed with plastic strain data with and without the application of MF are shown in Figure 8.1 (c). It is observed that the material gets more thinning in case of applied MF as compared to without MF as seen from the flange to the punch center. The location of the necking was observed away from the punch center and slight changed due to MF. The section thickness contour plots of 1.0mm thickness without and with MF are shown in Figure 8.4 (a) and (b), respectively. At the necking, the sheet thickness is observed to be 0.36mm in case of without MF and 0.31mm in case of with MF. The difference in thinning of the sheet is observed to be higher side at the punch center in case of MF. This may be attributed to the elongated grains of the sheet due to MF.

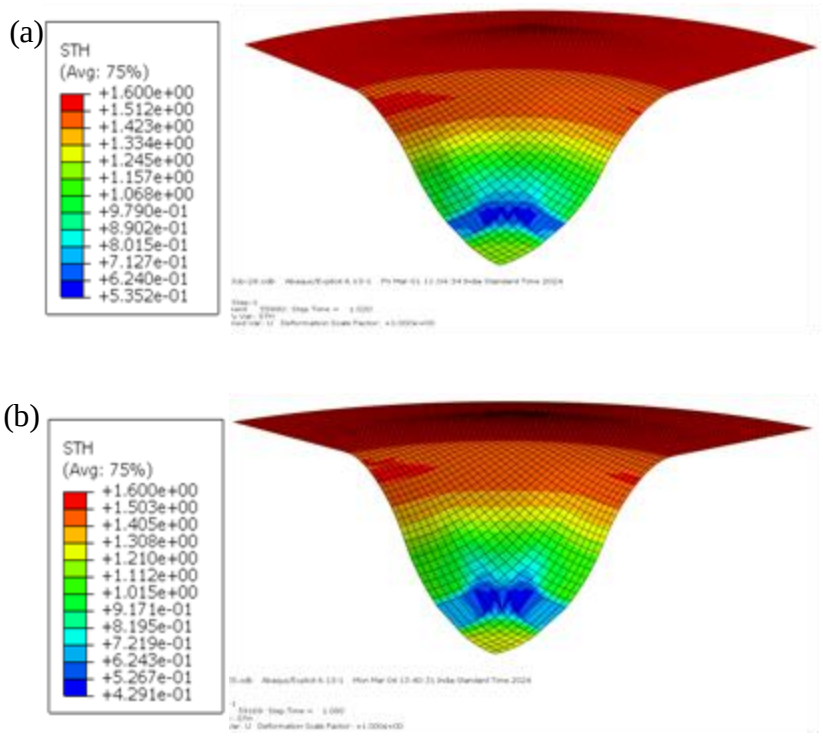

Figure 8.2 FE results of section thickness contour plots for the DP590 sheet, (a) 1.6 mm without MF and (b) 1.6 mm with MF.

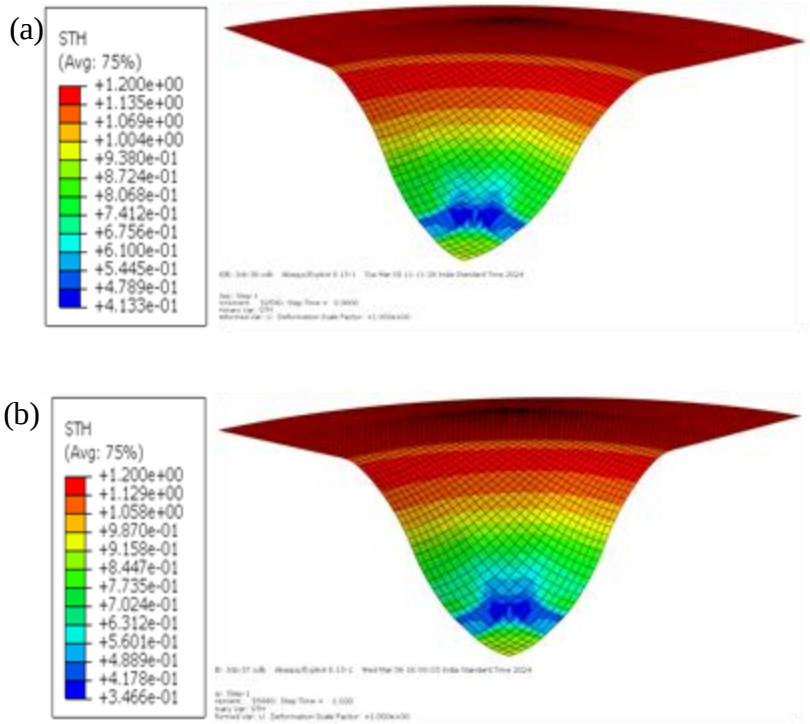

Figure 8.3 FE results of section thickness contour plots for the DP590 sheet, (a) 1.2 mm without MF and (b) 1.2 mm with MF.

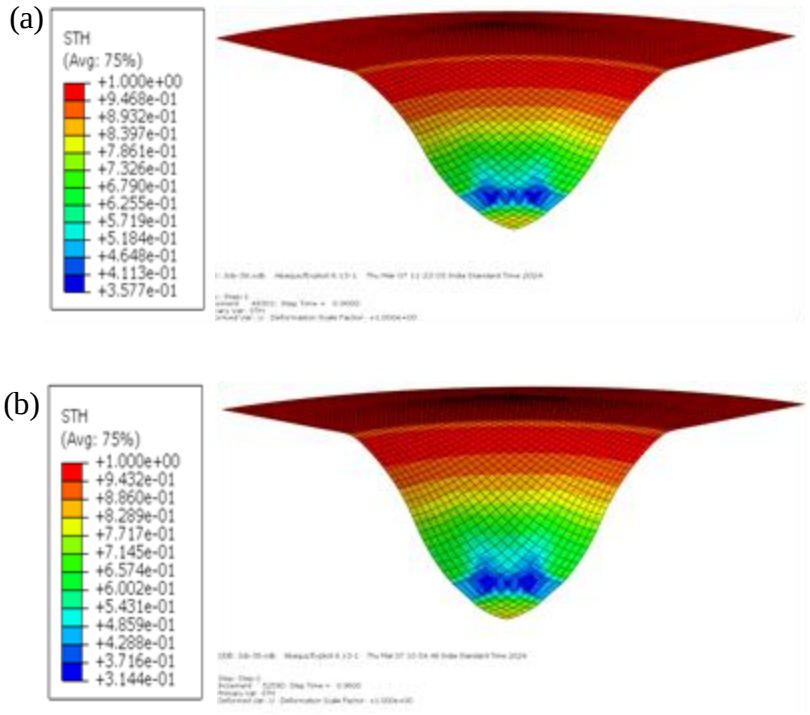

Figure 8.4 FE results of section thickness contour plots for the DP590 sheet, (a) 1.2 mm without MF and (b) 1.2 mm with MF.

8.1.2 FE simulation for punch force-displacement plots of DP590 steel

The results of FE simulation of punch force vs punch displacement plots for different sheet thicknesses of the DP590 steel observed with plastic strain data with and without the application of MF are shown in Figure 8.5.

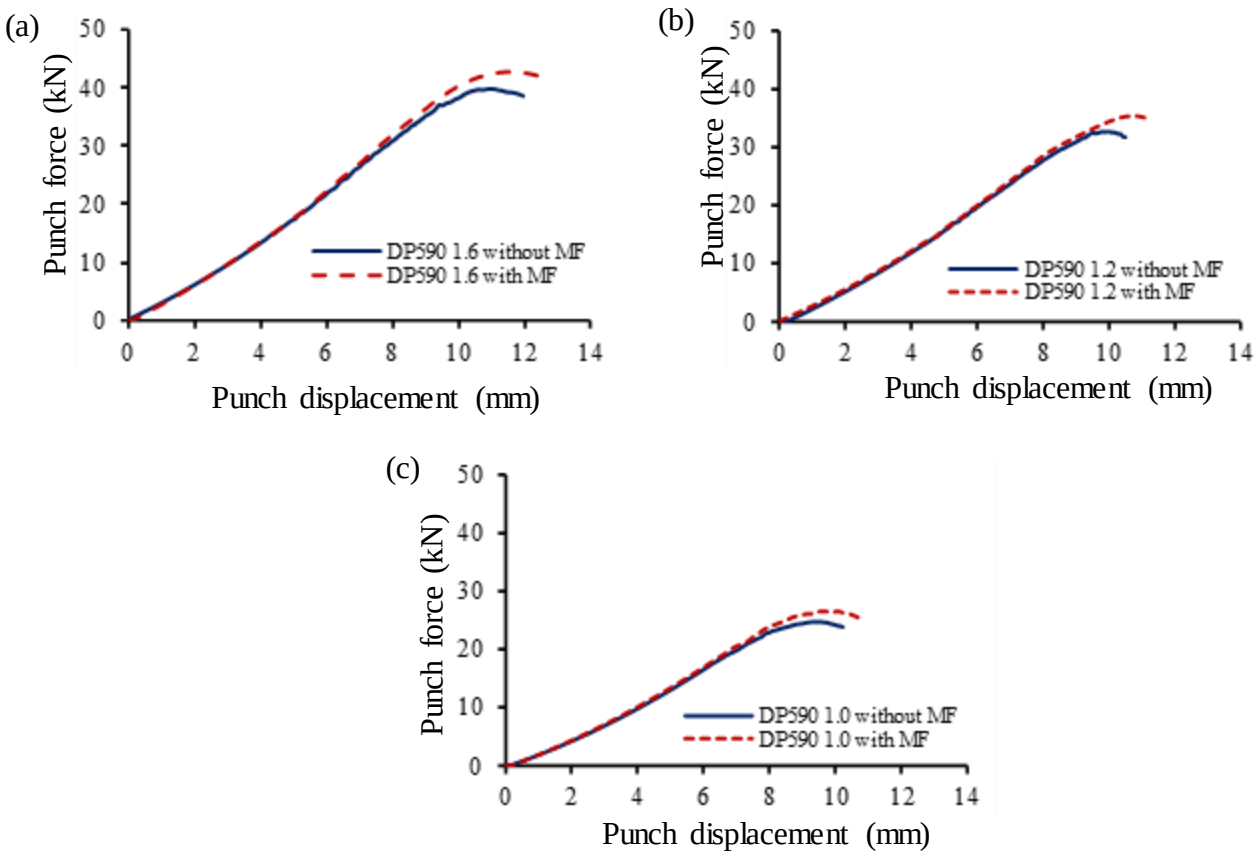

Figure 8.5 FE results of punch force vs. punch displacement plots for the DP590 sheet, (a) 1.6 mm, (b) 1.2 mm, and (c) 1.0 mm.

The FE results of punch force vs punch displacement plots for DP590 1.6mm thickness observed with plastic strain data with and without the application of MF are shown in Figure 8.5 (a). It is observed that the punch force increased with the application of MF from 39.70kN to 42.70kN. The punch force plots shows that initially the line of force and displacement is plots are almost same in both the case but at mid of the test punch force start rising due to the

yield stress ratio. The value of yield stress ratio is higher in case of MF (see Table 5.1). It is noticed that if the punch force is higher it affects the formability of the sheet.

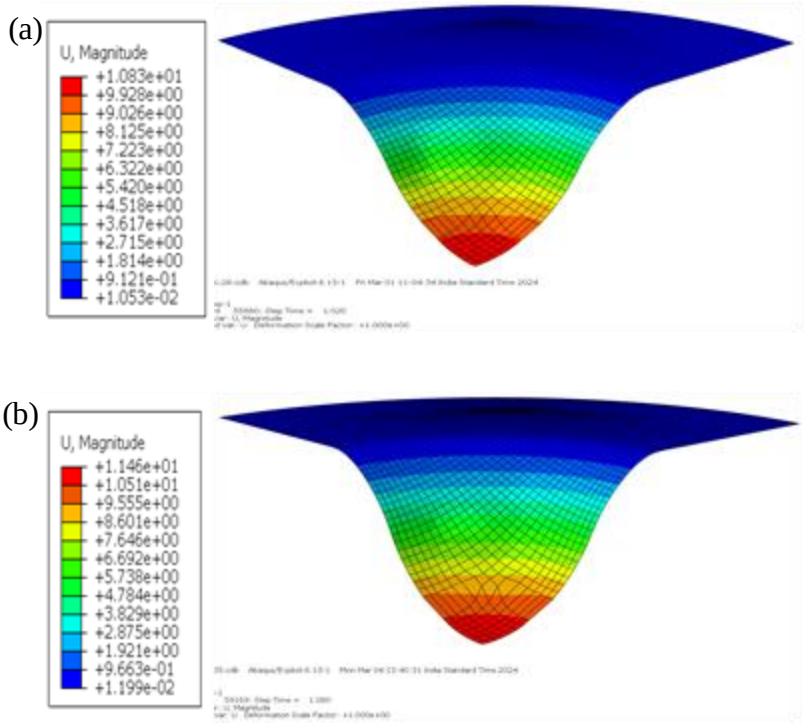

Figure 8.6 FE results of Erichsen cupping depth contour plots for the DP590 sheet, (a) 1.6 mm without MF and (b) 1.6 with MF.

The contour plot of punch displacement without and with the application of MF for DP590 steel sheet 1.6mm thickness are shown in Figure 8.6 (a) and (b), respectively. It shows that the displacement of the punch linearly moves from start point of the test to the necking of the sheet. It is noticed that the displacement of the punch is more in case of MF for the same kind of necking. The punch force displacement is considered as a Erichsen index and validated the results with the experimental data. The FE results of punch force vs punch displacement plots for DP590 1.2mm thickness observed with plastic strain data with and without the application of MF are shown in Figure 8.5 (b). It is observed that the punch force increased with the application of MF from 31.80kN to 35.06kN. The punch force plots shows that the line of

force and displacement in plots are just above the plots of test performed without MF. The value of yield stress ratio is higher in case of MF (see Table 5.1). It is noticed that higher punch force affects the formability of the sheet.

The contour plot of punch displacement without and with the application of MF for DP590 steel sheet 1.2mm thickness are shown in Figure 8.7 (a) and (b), respectively. It shows that the displacement of the punch linearly moves from start point of the test to the necking of the sheet. It is noticed that the displacement of the punch is more in case of MF for the same kind of necking appeared. The punch force displacement is considered as a Erichsen index and validated the results with the experimental data.

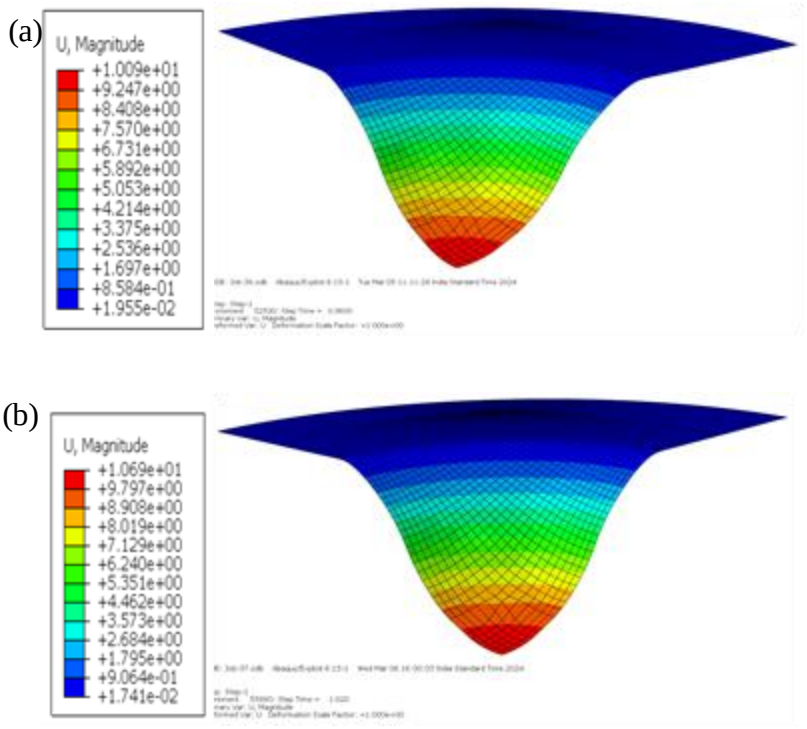

Figure 8.7 FE results of Erichsen cupping depth contour plots for the DP590 sheet, (a) 1.2 mm without MF and (b) 1.2 mm with MF.

The FE results of punch force vs punch displacement plots for DP590 1.0mm thickness observed with plastic strain data with and without the application of MF are shown in Figure 8.5 (c). It is observed that the punch force increased with the application of MF from 24.16kN to 26.51kN. The punch force plots shows that the line of force and displacement in plots are

just above the plots of test performed without MF. The value of yield stress ratio is higher in case of MF (see Table 5.1). It is noticed that higher punch force affect the formability of the sheet. The contour plot of punch displacement without and with the application of MF for DP590 steel sheet 1.0mm thickness are shown in Figure 8.8 (a) and (b), respectively. It shows that the displacement of the punch linearly moves from start point of the test to the necking of the sheet. It is noticed that the displacement of the punch is more in case of MF for the same kind of necking. The punch force displacement is considered as an Erichsen index and validated the results with the experimental data.

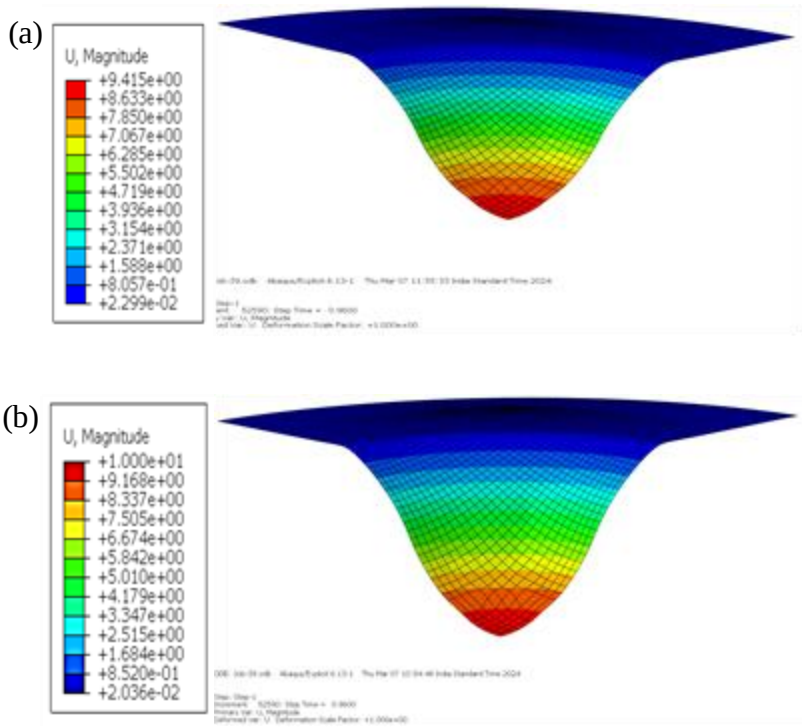

Figure 8.8 FE results of Erichsen cupping depth contour plots for the DP590 sheet, (a) 1.0 mm without MF and (b) 1.0 mm with MF.

8.1.3 FE simulation results vs experimental results of DP590 steel

The experimental and FE simulations result of DP590 steel sheet of Erichsen cupping test are observed in term of punch force, punch displacement and section sheet thickness are reported in Table 8.1. It is observed that the value of experimental maximum punch force is higher than the FEA maximum punch force approximately 1.5kN in case of 1.6mm sheet thickness

tested without MF. In case of MF, the value of experimental maximum punch force is higher than the FEA maximum punch force approximately 3.5kN for 1.6mm sheet thickness. It is observed that the value of experimental maximum punch force is lesser than the FEA maximum punch force approximately 0.5kN in case of 1.2mm sheet thickness tested without MF. In case of MF, the value of experimental maximum punch force is slightly higher than the FEA maximum punch force approximately 0.2kN for 1.2mm sheet thickness. It is observed that the value of experimental maximum punch force is slightly higher than the FEA maximum punch force approximately 1.0kN in case of 1.0mm sheet thickness tested without MF. In case of MF, the value of experimental maximum punch force is higher than the FEA maximum punch force approximately 2.0kN for 1.0mm sheet thickness. The experimental punch force results are validated the FE simulation punch force results.

Table 8.1 Erichsen cupping experimental vs. simulation results for DP590 sheet (performed with and without MF)

Sheet thickness (mm)		Punch force (kN)		Punch displacement (U) mm		Section thickness of sheet (STH) in (mm)	
		Experimental	Simulation	Experimental	Simulation	Experimental	Simulation
1.6	Without MF	41.30	39.70	11.32	10.83	0.60	0.53
	With MF	46.30	42.60	12.82	11.46	0.48	0.43
1.2	Without MF	31.31	31.80	10.27	10.09	0.46	0.41
	With MF	35.25	35.06	11.18	10.69	0.40	0.34
1.0	Without MF	25.27	24.16	9.81	9.45	0.41	0.36
	With MF	28.53	26.51	10.28	10.00	0.37	0.31

It is observed that the value of experimental punch displacement is higher than the FEA maximum punch displacement approximately 0.5mm in case of 1.6mm sheet thickness tested without MF. In case of MF, the value of experimental punch displacement is higher than the FEA maximum punch displacement approximately 1.4mm in case of 1.6mm sheet thickness. It is observed that the value of experimental punch displacement is higher than the FEA

maximum punch displacement approximately 0.2mm in case of 1.2mm sheet thickness tested without MF. In case of MF, the value of experimental punch displacement is higher than the FEA maximum punch displacement approximately 0.5mm in case of 1.2mm sheet thickness. It is observed that the value of experimental punch displacement is higher than the FEA maximum punch displacement approximately 0.4mm in case of 1.0mm sheet thickness tested without MF. In case of MF, the value of experimental punch displacement is higher than the FEA maximum punch displacement approximately 0.2mm in case of 1.0mm sheet thickness. The experimental punch displacement results validated the FE simulation punch displacement results. It is observed that the value of experimental section thickness of sheet is higher than the FEA section thickness of sheet approximately 0.05mm in all the case of sheet thickness of DP590.

8.2 Erichsen cupping of ZC440 steel using FE simulation

8.2.1 FE simulation for sheet thickness of ZC440 steel

The results of FE simulation of section sheet thinness for different sheet thicknesses of the ZC440 steel observed with plastic strain data with and without the application of MF are shown in Figure 8.9. The FE results of 1.4 mm thickness observed with plastic strain data with and without the application of MF are shown in Figure 8.9 (a). It is observed that the material gets more thinning in case of applied MF as compared to without MF as seen from the flange to the punch center. At the necking, the sheet thickness is observed to be 0.49mm in case of without MF and 0.46mm in case of with MF. The difference in thinning of the sheet is observed to be higher side at the punch center in case of MF. This may be attributed to the elongated grains of the sheet due to MF as seen in the chapter 7 microstructural analysis of ZC440. The section thickness contour plots of 1.4mm thickness without and with MF are shown in Figure 8.10 (a) and (b), respectively. It shows that the failure of the material occurs

and thinning of the sheet due to stretch forming. The effect of MF during the testing shows the material result higher in thinning of sheet.

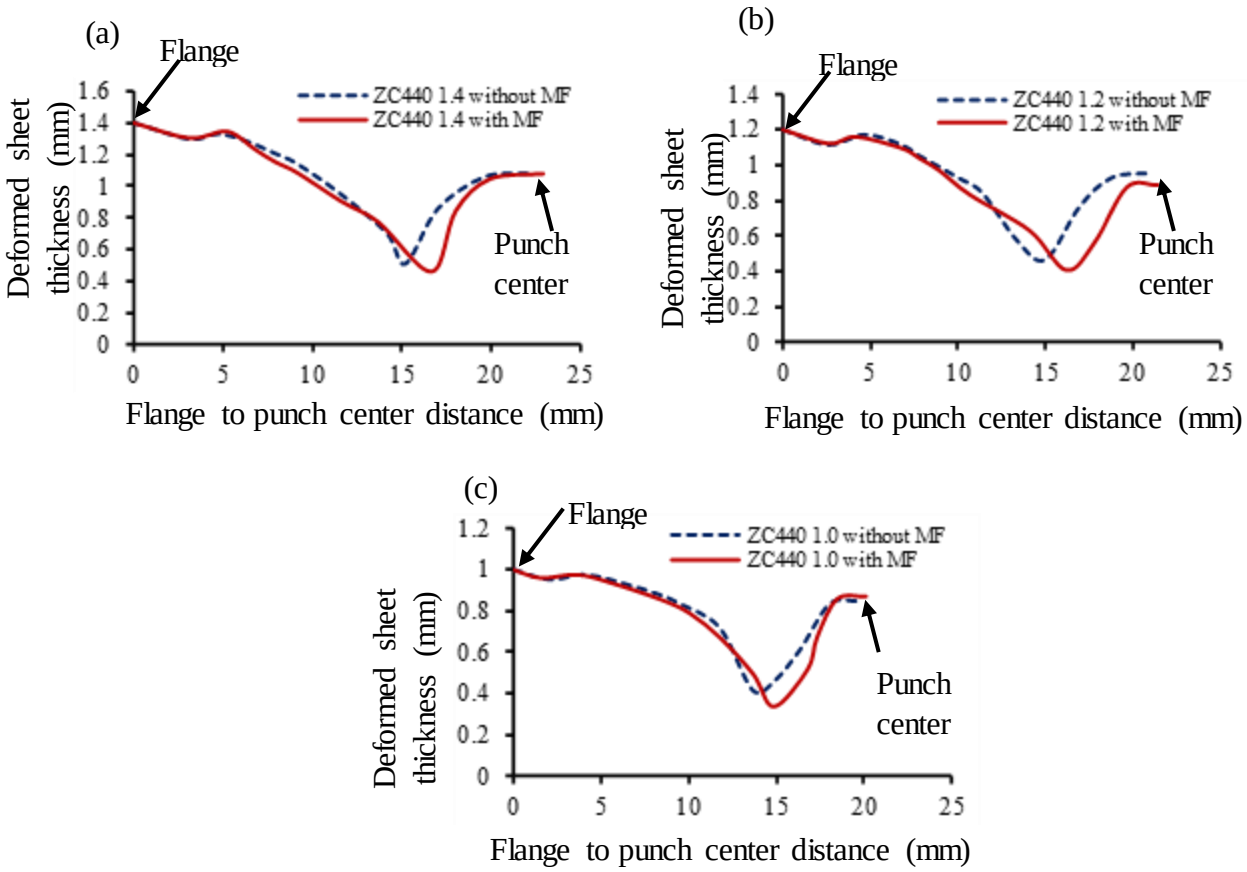

Figure 8.9 FEA results for change in sheet thickness with distance from flange to punch center for ZC440, (a) 1.4 mm, (b) 1.2 mm, and (c) 1.0 mm.

The FE results of 1.2 mm thickness observed with plastic strain data with and without the application of MF are shown in Figure 8.9 (b). It is observed that the material gets more thinning in case of applied MF as compared to without MF as seen from the flange to the punch center. At the necking, the sheet thickness is observed to be 0.46mm in case of without MF and 0.40mm in case of with MF. The difference in thinning of the sheet is observed to be higher side at the punch center in case of MF. This may be attributed to the elongated grains of the sheet due to MF.

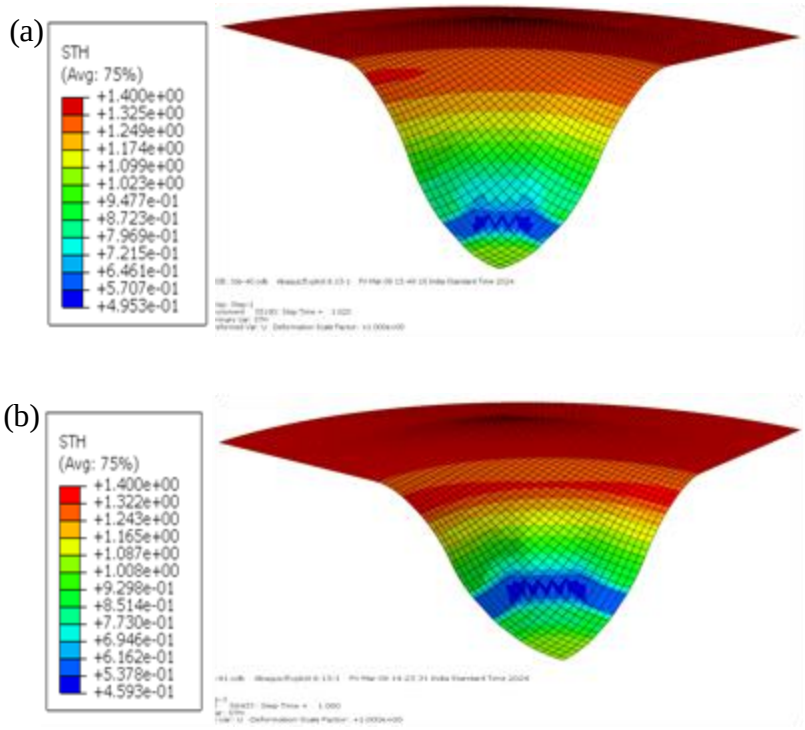

Figure 8.10 FE results of section thickness contour plots for the ZC440 sheet, (a) 1.4 mm without MF and (b) 1.4 mm with MF.

The section thickness contour plots of 1.2mm thickness without and with MF are shown in Figure 8.11 (a) and (b), respectively. It shows that the failure of the material occurs and thinning of the sheet due to stretch forming. The effect of MF during testing the material to get the result in thinning of sheet. The FE results of 1.0 mm thickness observed with plastic strain data with and without the application of MF are shown in Figure 8.9 (c). It is observed that the material gets more thinning in case of applied MF as compared to without MF as seen from the flange to the punch center.

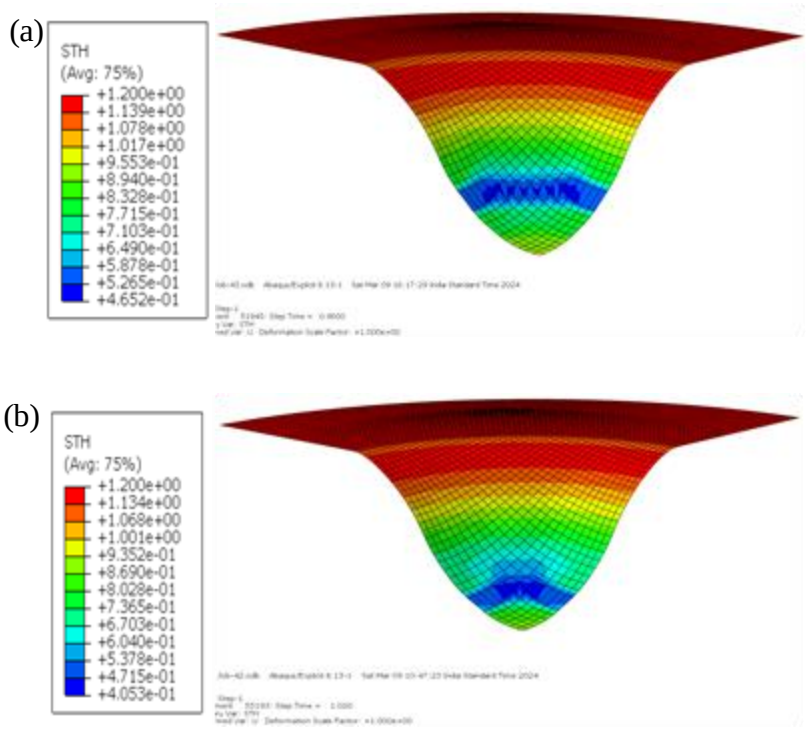

Figure 8.11 FE results of section thickness contour plots for the ZC440 sheet, (a) 1.2 mm without MF and (b) 1.2 mm with MF.

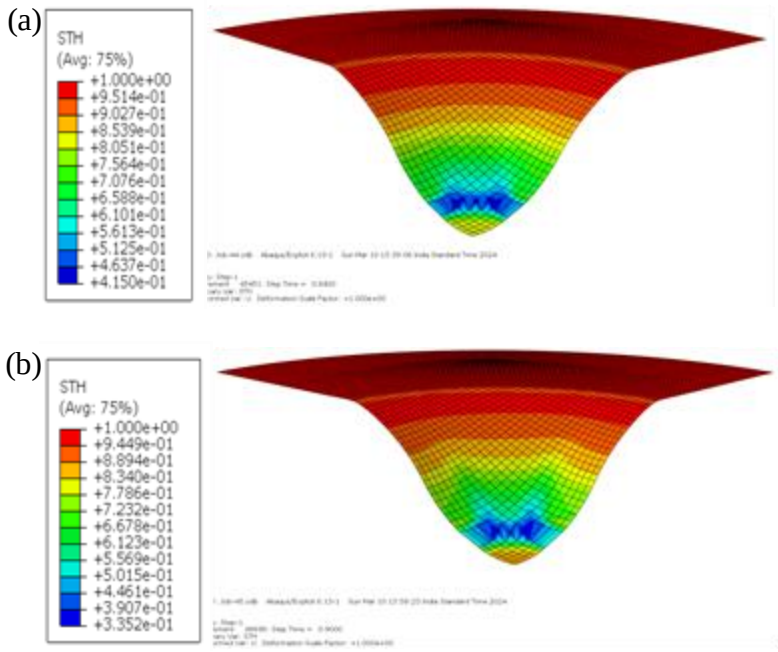

Figure 8.12 FE results of section thickness contour plots for the ZC440 sheet, (a) 1.0 mm without MF and (b) 1.0 mm with MF.

The section thickness contour plots of 1.0mm thickness without and with MF are shown in Figure 8.12 (a) and (b), respectively. At the necking, the sheet thickness is observed to be 0.41mm in case of without MF and 0.33mm in case of with MF. The difference in thinning of the sheet is observed to be on higher side at the punch center in case of MF. This may be attributed to the elongated grains of the sheet due to MF.

8.2.2 FE simulation for punch force-displacement plots of ZC440 steel

The results of FE simulation of punch force vs punch displacement plots for different sheet thicknesses of the ZC440 steel observed with plastic strain data with and without the application of MF are shown in Figure 8.13. The FE results of punch force vs punch displacement plots for ZC440 1.4mm thickness observed with plastic strain data with and without the application of MF are shown in Figure 8.13 (a). It is observed that the punch force increased with the application of MF from 28.44kN to 32.24kN. The punch force plots shows that initially the line of force and displacement is plots are almost same in both the case but at mid of the test punch force start rising due to the yield stress ratio. The value of yield stress ratio is higher in case of MF (see Table 5.2). It is noticed that higher punch force affect the formability of the sheet.

The contour plot of punch displacement without and with the application of MF for ZC440 steel sheet 1.4mm thickness are shown in Figure 8.14 (a) and (b), respectively. It shows that the displacement of the punch linearly moves from start point of the test to the necking of the sheet. It is noticed that the displacement of the punch is more in case of MF for the same kind of necking appeared. The FE results of punch force vs punch displacement plots for ZC440 1.2mm thickness observed with plastic strain data with and without the application of MF are shown in Figure 8.13 (b). It is observed that the punch force increased with the application of MF from 23.26kN to 25.66kN. The punch force plots shows that the line of force and displacement plots are just above the plots of test performed without MF. The value of yield

stress ratio is higher in case of MF (see Table 5.2). It is noticed that higher punch force affect the formability of the sheet.

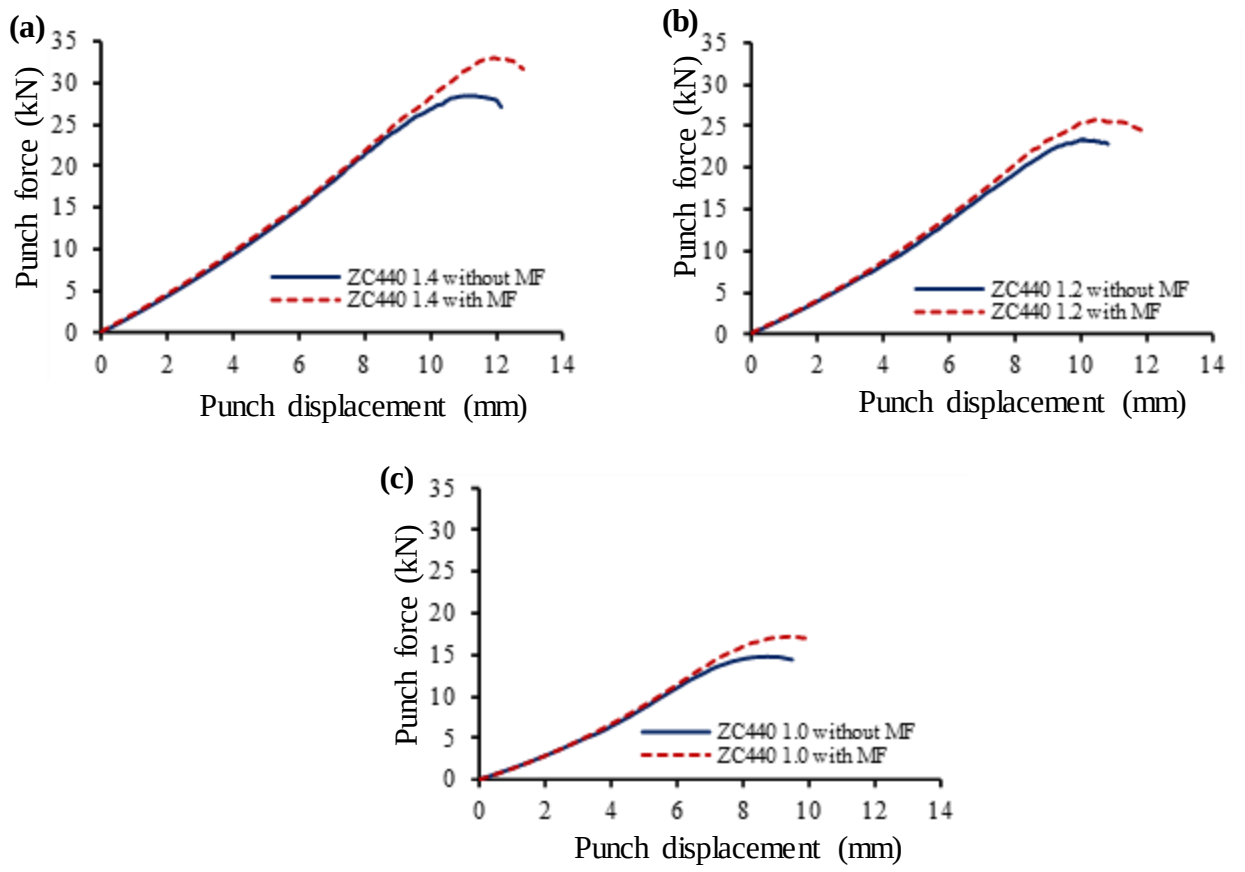

Figure 8.13 FE results of punch force vs. punch displacement plots for the ZC440 sheet, (a) 1.4 mm, (b) 1.2 mm, and (c) 1.0 mm.

The contour plot of punch displacement without and with the application of MF for ZC440 steel sheet 1.2mm thickness are shown in Figure 8.15 (a) and (b), respectively. It shows that the displacement of the punch linearly moves from start point of the test to the necking of the sheet. It is noticed that the displacement of the punch is more in case of MF for the same kind of necking.

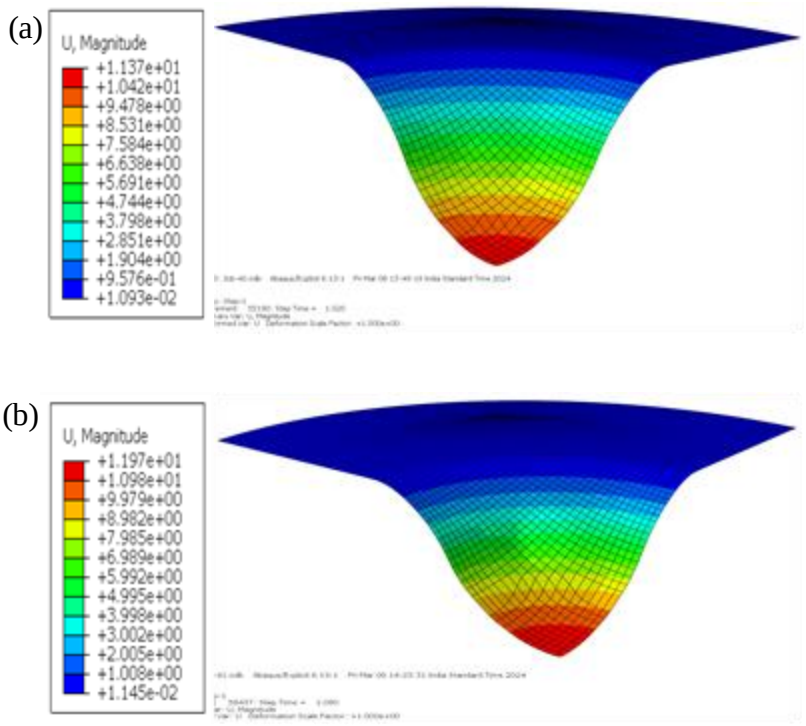

Figure 8.14 FE results of Erichsen cupping depth contour plots for the ZC440 sheet, (a) 1.4 mm without MF and (b) 1.4 with MF.

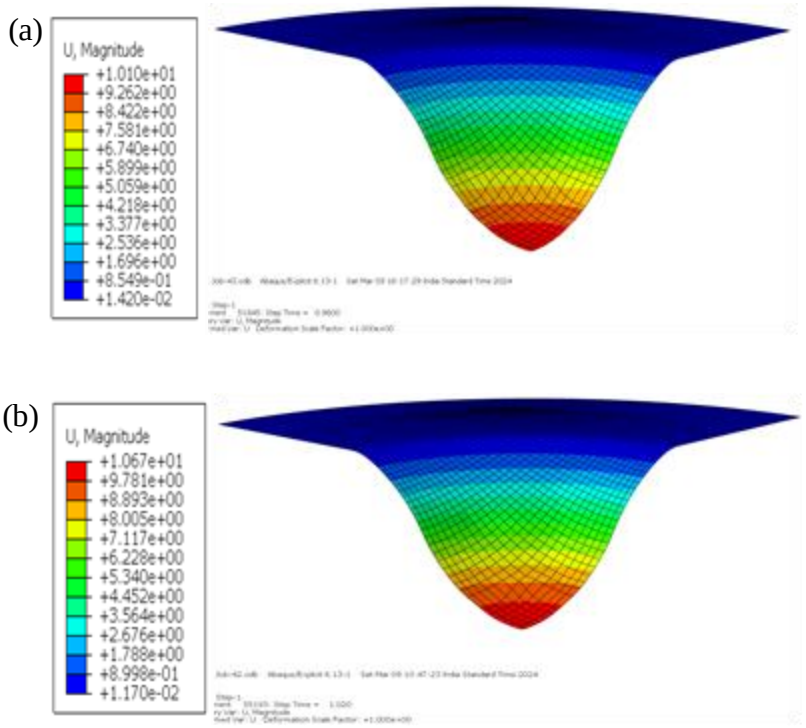

Figure 8.15 FE results of Erichsen cupping depth contour plots for the ZC440 sheet, (a) 1.2 mm without MF and (b) 1.2 mm with MF.

The FE results of punch force vs punch displacement plots for ZC440 1.0mm thickness observed with plastic strain data with and without the application of MF are shown in Figure 8.13 (c). It is observed that the punch force increased with the application of MF from 14.76kN to 17.19kN. The punch force plots shows that the line of force and displacement plots are just above the plots of test performed without MF. The value of yield stress ratio is higher in case of MF (see Table 5.2). It is noticed that higher punch force affects the formability of the sheet. The contour plot of punch displacement without and with the application of MF for ZC440 steel sheet 1.0mm thickness are shown in Figure 8.16 (a) and (b), respectively. It shows that the displacement of the punch linearly moves from start point of the test to the necking of the sheet. It is noticed that the displacement of the punch is more in case of MF for the same kind of necking appeared. The punch force displacement is considered as a Erichsen index and validated the results with the experimental data.

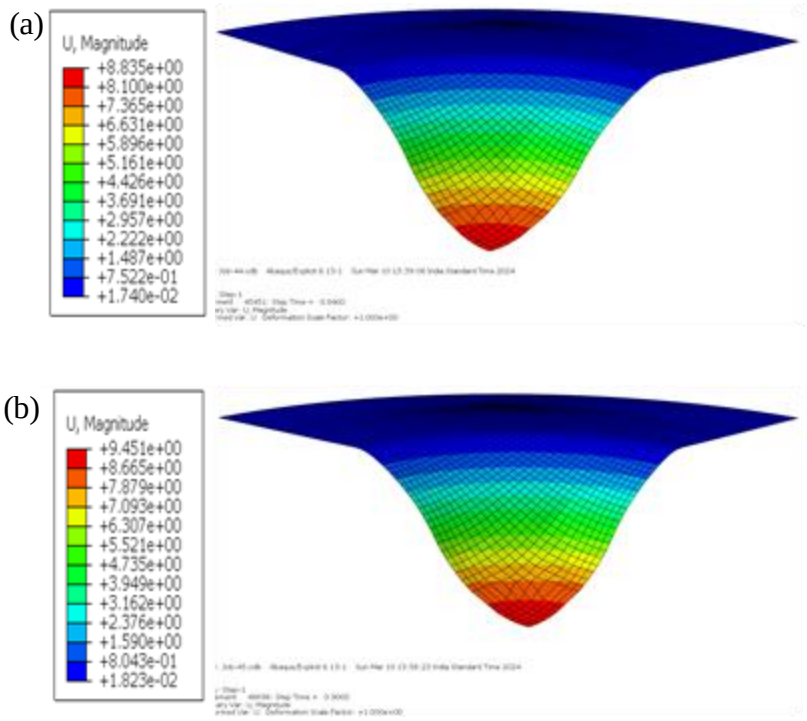

Figure 8.16 FE results of Erichsen cupping depth contour plots for the ZC440 sheet, (a) 1.0 mm without MF and (b) 1.0 mm with MF.

8.2.3 FE simulation results vs experimental results of ZC440 steel

The experimental and FE simulations result of ZC440 steel sheet of Erichsen cupping test are observed in term of punch force, punch displacement and section sheet thickness are reported in Table 8.2. It is observed that the value of experimental maximum punch force is higher than the FEA maximum punch force approximately 3kN in case of 1.4mm sheet thickness tested without MF. In case of MF, the value of experimental maximum punch force is higher than the FEA maximum punch force by approximately 4kN for 1.4mm sheet thickness. It is observed that the value of experimental maximum punch force is lesser than the FEA maximum punch force by approximately 0.4kN in case of 1.2mm sheet thickness tested without MF. In case of MF, the value of experimental maximum punch force is slightly higher than the FEA maximum punch force approximately 1.5kN for 1.2mm sheet thickness. It is observed that the value of experimental maximum punch force is slightly higher than the FEA maximum punch force by approximately 2.0kN in case of 1.0mm sheet thickness tested without MF. In case of MF, the value of experimental maximum punch force is higher than the FEA maximum punch force by approximately 2.0kN for 1.0mm sheet thickness. The experimental punch force results validated the FE simulation punch force results.

It is observed that the value of experimental punch displacement is higher than the FEA maximum punch displacement by approximately 0.2mm in case of 1.4mm sheet thickness tested without MF. In case of MF, the value of experimental punch displacement is higher than the FEA maximum punch displacement by approximately 1.3mm in case of 1.4mm sheet thickness. It is observed that the value of experimental punch displacement is higher than the FEA maximum punch displacement by approximately 0.2mm in case of 1.2mm sheet thickness tested without MF. In case of MF, the value of experimental punch displacement is higher than the FEA maximum punch displacement by approximately 0.6mm in case of 1.2mm sheet thickness.

Table 8.2 Erichsen cupping experimental vs. simulation results for ZC440 sheet (performed with and without MF)

Sheet thickness (mm)		Punch force kN		Punch displacement (U) mm		Section thickness of sheet (STH) in (mm)	
		Experimental	Simulation	Experimental	Simulation	Experimental	Simulation
1.4	Without MF	31.72	28.44	11.51	11.37	0.51	0.49
	With MF	36.61	32.24	13.12	11.97	0.49	0.46
1.2	Without MF	23.79	23.36	10.29	10.01	0.50	0.46
	With MF	27.33	25.66	11.36	10.67	0.45	0.40
1.0	Without MF	16.69	14.76	8.91	8.83	0.42	0.41
	With MF	19.24	17.19	9.42	9.45	0.38	0.33

It is observed that the value of experimental punch displacement is slightly higher than the FEA maximum punch displacement approximately 0.1mm in case of 1.0mm sheet thickness tested without MF. In case of MF, the value of experimental punch displacement is almost same than the FEA maximum punch displacement in case of 1.0mm sheet thickness. The experimental punch displacement results validated the FE simulation punch displacement results. It is observed that the value of experimental section thickness of sheet is higher than the FEA section thickness of sheet approximately 0.04mm in all the case of sheet thickness of DP590.

8.3 Summary

On the basis of the results and discussion presented in this chapter, it can be concluded that the prediction of sheet failure in the Erichsen cupping tester by using simulations in term of change in section sheet thickness, punch force and punch displacement can be concluded. It is noticed that the thinning of the sheet is increased due to the application of MF in the case of DP590 steel for all thicknesses. The FE results of punch force for DP590 sheet increased by approximately 3kN, 3.2kN and 2kN in the sheet thickness of 1.6mm, 1.2mm and 1.0mm,

respectively due to MF. The FE results of punch displacement for DP590 sheet increased by approximately 0.5mm, 0.6mm and 0.5mm in the sheet thickness of 1.6mm, 1.2mm and 1.0mm, respectively due to MF. It noticed that the thinning of the sheet is increased due to the application of MF in the case of ZC440 steel for all thicknesses. The FE results of punch force for ZC440 sheet increased by approximately 4kN, 3kN and 2kN in the sheet thickness of 1.4mm, 1.2mm and 1.0mm, respectively due to MF. The FE results of punch displacement for ZC440 sheet get increased by approximately 0.6mm, 0.6mm and 0.5mm in the sheet thickness of 1.4mm, 1.2mm and 1.0mm, respectively due to MF. The experimental data of the punch force validated with the FE simulations data shows that the value of punch force gets higher by 2kN in case of 1.6mm thickness and very slight change in the case of 1.2mm and 1.0mm of DP590 steel sheets tested without MF. In case of MF, the value of punch force is higher by 4kN and 2kN in case of 1.6mm and 1.0mm thickness and very slight change in the case of 1.2mm of DP590 steel sheets. The experimental data of the punch force validated with the FE simulations data shows that the value of punch force incresed by 2kN in case of 1.4mm and 1.0mm thickness and very slight change was observed in the case of 1.2mm of ZC440 steel sheets tested without MF. In case of MF, the value of punch force incresed by 3kN and 2kN in case of 1.4mm and 1.0mm thickness and very slight change in the case of 1.2mm of ZC440 steel sheets. The results of FE simulations are higher in the punch force, sheet thickness and punch displacement are dominated by the yield stress ratio of the sheet that is higher due to MF.

CHAPTER 9

CONCLUSIONS AND SUGGESTIONS FOR FURTHER WORK

9.1 Conclusions

In the present work, a novel electromagnetic uniaxial tensile test (EMUTT) tool is designed on the basis of distribution of magnetic flux density in the gauge length of the tensile specimen. The effectiveness of the designed EMUTT tools is confirmed experimentally on the tensile properties of the DP590 with sheet thickness of (1.0-, 1.2- and 1.6-mm) and ZC440 with sheet thickness of (1.0-, 1.2- and 1.4-mm) steel sheet. The magnetostatic finite element analysis predicts that the novel electromagnetic tools such as *tool-A* to *tool-E* give a continuously increasing magnetic flux density in the parallel length of a tensile specimen. Hence, the presented uniaxial tensile test with the magnetic field shows a promising process to improve some of the tensile properties of the steel sheet. After analyzing the EMUTT tools performance on a 50 kN UTM, a modified electromagnetic tool was designed as an attachment with sheet samples for conducting experiments on an Erichsen cupping machine to evaluate its forming behavior. The following specific conclusions show the usefulness and effectiveness of the magnetic field (MF).

1. Higher values of YS and UTS are observed in the specimens tested with the magnetic field of DP590 and ZC440 steel in all thicknesses. The values of strain hardening exponent are affected marginally due to the MF in all the cases. The change in the tensile properties may be attributed to the hindrance to the movement of dislocations caused due to the MF.

2. The average values of plastic strain ratio of specimens tested with the MF for a plastic strain of 20% in three different orientations of DP590 and ZC440 steel w.r.t. RD, are observed to be higher than the results obtained without the MF. The value of normal anisotropy of the DP590 sheet increased by 23.4%, 22.0% and 11.5% in the sheet thickness of 1.6mm, 1.2mm and 1.0mm, respectively due to MF. The normal anisotropy of the ZC440 sheet increased by 25.1%, 21.2% and 17.5% in the sheet thickness of 1.4mm, 1.2mm and 1.0mm, respectively due to MF.
3. Higher values of plastic strain ratio are observed specifically in the specimens oriented at 0° and 90° to the rolling directions tested with the MF in both the materials. The change in the values of plastic strain ratio at any direction of the sheet could be attributed to a significant change in the texture after plastic deformation when tested with the MF.
4. The microstructural study of the samples taken from the center of the specimens tested with and without the MF for a plastic strain of 20% shows that the average grain size is comparatively larger due to the effect of the MF specifically in the specimens oriented at 0º and 90º to the rolling direction. The average grain size increased in the case of DP590 steel sheet is 30% for the specimens oriented at 0° and 90° to the RD due to MF. The average grain size increased in the case of ZC440 steel sheet is 45% for the specimens oriented at 0° and 90° to the RD due to MF. However, the grains are observed to be affected least due to the MF in the specimens oriented at 45º to the rolling direction.
5. The texture study of DP590 steel indicated that the value of MRD increased in the cases of the specimens tested with orientation of 0° and 90° to the RD with MF and thereby produced a stronger texture when compared to the texture obtained without MF. The value of MRD gets least affected in case of the tested specimen oriented at

45° to the RD. The texture study of ZC440 steel indicated that the value of MRD increased in the cases of the specimens tested with orientation of 0° and 45° to the RD with MF and thereby produced a stronger texture when compared to the texture obtained without MF. The value of MRD gets decreased in case of the tested specimen oriented at 45° to the RD due to MF.

6. A strong surface texture is observed in the cases of the samples oriented at 0° and 90° to the rolling direction of sheet due to the MF as compared with the surface texture observed without MF. A weak texture is observed in the case of the samples oriented at 45° to the rolling direction due to the MF in case of DP590 and ZC440 steel sheet.
7. Comparisons the experimental versus simulations results of Erichsen cupping test confirmed that the MF increased the formability of sheet. It also confirmed that the MF has more influence on the ZC440 material as compared to the DP590 material. This newly developed electromagnetic tool setup worked on the basic of the magnetization behaviour of the material as well the sheet thickness of the material.
8. The FE results of punch force for DP590 sheet get increased by approximately 10% in all the sheet thickness due to MF. The FE results of punch displacement for DP590 sheet increased by approximately 8% due to MF. The FE results of punch force for ZC440 sheet showed an increased by approximately 11% due to MF. The FE results of punch displacement for ZC440 sheet get increased by approximately 8% due to MF.
9. The experimental data of the punch force validated with the FE simulations data shows that the value of punch force increased by approximately 5% for DP590 steel sheets tested without MF. In case of MF, the value of punch force increased by approximately 6% for DP590 steel sheets. The experimental data of the punch force validated with the FE simulations data shows that the value of punch force increased by

approximately 4% for ZC440 steel sheets tested without MF. In case of MF, the value of punch force increased by approximately 6% for ZC440 steel sheets.

9.2 Suggestions for future work

A few suggestions are outlined below which can be explored further to get more insight into understanding the effect of magnetic field on formability of various steel sheets to realize their potential in various applications.

1. Investigations on effect of magnetic field on formability of very high strength materials and low strength materials are important because of their increasing applications in automobile, semiconductors and structural frame.
2. Effect of magnetic field in transverse direction for the uniaxial and biaxial stretching of tensile specimens to predict the formability of the sheet.
3. Hydraulic bulge test is an important method to find the forming limit curve in which the magnetic can be applied on the sheet. This will give the correct information about the formability of the sheet.
4. An applied magnetic field can be studied on the simulations software with formability test for predicting the actually formability of the sheet.
5. Influence of important process parameters in forming of the sheet can be studied to applied higher value of magnetic field or lower value of magnetic field during drawing of the cup.

REFERENCES

[1] M. Takahashi, H. Arai, T. Tanaka, and T. Wakiyama, "Magnetocrystalline anisotropy for Fe-Al-Si (Sendust) single crystals with DO<inf>3</inf>ordered structure," *IEEE Trans Magn*, vol. 22, no. 5, pp. 638–640, Sep. 1986, doi: 10.1109/TMAG.1986.1064587.

[2] B. Lee, S. K. Lee, and D. N. Lee, "Formulation of the A2/B2/D03 atomic ordering energy and a thermodynamic analysis of the Fe-Si system," *Calphad*, vol. 11, no. 3, pp. 253–270, Jul. 1987, doi: 10.1016/0364-5916(87)90044-7.

[3] C. Bolfarini, P. P. Gusson, M. C. A. da Silva, and C. S. Kiminami, "Magnetic Properties of Spray Formed Fe-3%Si, Fe-5%Si and Fe-6.5%Si Alloys," *Materials Science Forum*, vol. 416–418, pp. 113–118, Feb. 2003, doi: 10.4028/www.scientific.net/MSF.416-418.113.

[4] F. Faudot, J. F. Rialland, and J. Bigot, "Study of order-disorder effect on magnetic properties of rapidly quenched Fe-6.5 wt% Si alloys," *Phys Scr*, vol. 39, no. 2, pp. 263–267, Feb. 1989, doi: 10.1088/0031-8949/39/2/013.

[5] J. S. Shin *et al.*, "Ordering–disordering phenomena and micro-hardness characteristics of B2 phase in Fe–(5–6.5%)Si alloys," *Materials Science and Engineering: A*, vol. 407, no. 1–2, pp. 282–290, Oct. 2005, doi: 10.1016/j.msea.2005.07.012.

[6] D. A. Molodov and P. J. Konijnenberg, "Grain boundary and grain structure control through application of a high magnetic field," *Scr Mater*, vol. 54, no. 6, pp. 977–981, Mar. 2006, doi: 10.1016/j.scriptamat.2005.11.038.

[7] R. Kushibiki, K. K. Tham, S. Hinata, and S. Saito, "Magnetic Properties and Columnar Structure for CoPt Alloy Granular Media With Grain Boundary Oxides of Various

Melting Points," *IEEE Trans Magn*, vol. 53, no. 11, pp. 1–4, Nov. 2017, doi: 10.1109/TMAG.2017.2706959.

[8] Z. P. Cai, J. A. Lin, L. A. Zhou, and H. Y. Zhao, "Evaluation of effect of magnetostriction on residual stress relief by pulsed magnetic treatment," *Materials Science and Technology*, vol. 20, no. 12, pp. 1563–1566, Dec. 2004, doi: 10.1179/026708304X4286.

[9] Y. Hong *et al.*, "Influencing mechanisms of atomic diffusion and compositional distribution on the magnetic anisotropy of Cr/SmCo/(Cu)/Cr thin films," *Acta Mater*, vol. 164, pp. 627–635, Feb. 2019, doi: 10.1016/j.actamat.2018.11.005.

[10] X. Li, Z. Ren, and Y. Fautrelle, "Effect of a high gradient magnetic field on the distribution of the solute Si and the morphology of the primary Si phase," *Mater Lett*, vol. 63, no. 15, pp. 1235–1238, Jun. 2009, doi: 10.1016/j.matlet.2009.02.030.

[11] I. Glavatskyy, N. Glavatska, A. Dobrinsky, J.-U. Hoffmann, O. Söderberg, and S.-P. Hannula, "Crystal structure and high-temperature magnetoplasticity in the new Ni–Mn–Ga–Cu magnetic shape memory alloys," *Scr Mater*, vol. 56, no. 7, pp. 565–568, Apr. 2007, doi: 10.1016/j.scriptamat.2006.12.019.

[12] P. Müllner, V. A. Chernenko, and G. Kostorz, "A microscopic approach to the magnetic-field-induced deformation of martensite (magnetoplasticity)," *J Magn Magn Mater*, vol. 267, no. 3, pp. 325–334, Dec. 2003, doi: 10.1016/S0304-8853(03)00400-1.

[13] M. I. Molotskii, "Theoretical basis for electro- and magnetoplasticity," *Materials Science and Engineering: A*, vol. 287, no. 2, pp. 248–258, Aug. 2000, doi: 10.1016/S0921-5093(00)00782-6.

[14] R. B. Morgunov and A. L. Buchachenko, “Magnetoplasticity and magnetic memory in diamagnetic solids,” *Journal of Experimental and Theoretical Physics*, vol. 109, no. 3, pp. 434–441, Sep. 2009, doi: 10.1134/S1063776109090076.

[15] A. A. Skvortsov and A. V. Karizin, “Magnetoplasticity and diffusion in silicon single crystals,” *Journal of Experimental and Theoretical Physics*, vol. 114, no. 1, pp. 85–88, Jan. 2012, doi: 10.1134/S1063776111160096.

[16] H. Blank, “Plastisches Verhalten von Nickelkristallen unter Magnetisierung,” *Naturwissenschaften*, vol. 43, no. 21, pp. 494–494, 1956, doi: 10.1007/BF00632517.

[17] V. I. Alshits, E. V. Darinskaya, and E. A. Petrzhik, “Effects of magnetic fields on the dislocation unlocking from paramagnetic centers in non-magnetic crystals,” in *Fundamental Aspects of Dislocation Interactions*, Elsevier, 1993, pp. 322–326. doi: 10.1016/B978-1-4832-2815-0.50053-X.

[18] V. I. Alshits, E. V. Darinskaya, M. V. Koldaeva, and E. A. Petrzhik, “Magnetoplastic effect: Basic properties and physical mechanisms,” *Crystallography Reports*, vol. 48, no. 5, pp. 768–795, Sep. 2003, doi: 10.1134/1.1612598.

[19] Y.-T. Zhao, S.-L. Zhang, G. Chen, X.-N. Cheng, and C.-Q. Wang, “In situ (Al2O3+Al3Zr)np/Al nanocomposites synthesized by magneto-chemical melt reaction,” *Compos Sci Technol*, vol. 68, no. 6, pp. 1463–1470, May 2008, doi: 10.1016/j.compscitech.2007.10.036.

[20] A. A. Skvortsov, D. E. Pshonkin, M. N. Luk’yanov, and M. R. Rybakova, “Influence of permanent magnetic fields on creep and microhardness of iron-containing aluminum alloy,” *Journal of Materials Research and Technology*, vol. 8, no. 3, pp. 2481–2485, May 2019, doi: 10.1016/j.jmrt.2019.02.002.

[21] R.C. O'handley, "Modern magnetic materials: principles and applications," *Wiley-VCH* , p. 768, Nov. 1999.

[22] A. Aharoni, *Introduction to the Theory of Ferromagnetism* , vol. 109. Clarendon Press, 2000.

[23] D. Clarke, O. A. Tretiakov, and O. Tchernyshyov, "Stripes in thin ferromagnetic films with out-of-plane anisotropy," *Phys Rev B*, vol. 75, no. 17, p. 174433, May 2007, doi: 10.1103/PhysRevB.75.174433.

[24] "https://ece.northeastern.edu/fac-ece/nian/mom/domains.html."

[25] A. Hubert and R. Schäfer, *Magnetic domains: the analysis of magnetic microstructures*. Springer Science & Business Media, 1998.

[26] S. Chikazumi, *Physics of Magnetism* . John Wiley & Sons, Inc., 1964.

[27] H. Kronmüller and M. Fähnle, *Magnetism and the Microstructure of Ferromagnetic Solids*. Cambridge: Cambridge University Press, 2003.

[28] M. Kleiner, M. Geiger, and A. Klaus, "Manufacturing of Lightweight Components by Metal Forming," *CIRP Annals*, vol. 52, no. 2, pp. 521–542, 2003, doi: 10.1016/S0007-8506(07)60202-9.

[29] W.F. Hosford and R.M. Caddell, *Metal forming: Mechanics and Metallurgy*. Cambridge University Press: New York, 2011.

[30] S. Kalpakjian and S. Schmid, *Manufacturing Processes for Engineering Materials*, 4th ed. New Delhi, India: Pearson Education, 2009.

[31] S. GmbH, *Metal Forming Handbook*. Germany: Springer-Verlag Berlin Heidelberg , 1998.

[32] H. Swift, “The mechanism of a simple deep-drawing operation ,” *Sheet Met Ind*, vol. 31, no. 330, pp. 817–828, 1954.

[33] A. Bhaduri, “Deep Drawing,” 2018, pp. 693–719. doi: 10.1007/978-981-10-7209-3_15.

[34] A. Erichsen, “ A new test for thin sheets,” *Stahl and Eisen* , vol. 34, pp. 879–882, 1914.

[35] A. Handbook, *Metalworking: Sheet Forming*, vol. 14B. Ohia, USA: ASM International, 2006. doi: 10.31399/asm.hb.v14b.9781627081863.

[36] M. P. Miles, J. L. Siles, R. H. Wagoner, and K. Narasimhan, “A better sheet formability test,” *Metallurgical Transactions A*, vol. 24, no. 5, pp. 1143–1151, May 1993, doi: 10.1007/BF02657245.

[37] J. Duncan, J. Kolodziejski, and G. Glover, “Bulge testing as an aid to formability assessment. ,” *Sheet Metal Forming and Energy Conservation*, vol. 9, pp. 131–150, 1976.

[38] V. Prakash, D. R. Kumar, A. Horn, H. Hagenah, and M. Merklein, “Modeling material behavior of AA5083 aluminum alloy sheet using biaxial tensile tests and its application in numerical simulation of deep drawing,” *The International Journal of Advanced Manufacturing Technology*, vol. 106, no. 3–4, pp. 1133–1148, Jan. 2020, doi: 10.1007/s00170-019-04587-0.

[39] W. F. Hosford and J. L. Duncan, “Sheet metal forming: A review,” *JOM*, vol. 51, no. 11, pp. 39–44, Nov. 1999, doi: 10.1007/s11837-999-0221-5.

[40] J. Hu, Z. Marciniak, and J. Duncan, *Mechanics of sheet metal forming*. Elsevier, 2002.

[41] W.F Hosford and R.M. Caddell, *Metal Forming. Mechanikcs and Metallurgy*. . Cambridgy University Press, 2007.

[42] G.E. Dieter and D. Bacon, *Mechanical metallurgy* , vol. 3. New York: McGraw-hill., 1976.

[43] B. Van, "Anisotropic Work-Hardening and Strain Path Effects in an AlMn Alloy," *Grenoble INP*, 2010.

[44] Z. J. Li, G. Winther, and N. Hansen, "Anisotropy in rolled metals induced by dislocation structure," *Acta Mater*, vol. 54, no. 2, pp. 401–410, Jan. 2006, doi: 10.1016/j.actamat.2005.09.011.

[45] S. Matthies, H.-R. Wenk, and G. W. Vinel, "Some basic concepts of texture analysis and comparison of three methods to calculate orientation distributions from pole figures," *J Appl Crystallogr*, vol. 21, no. 4, pp. 285–304, Aug. 1988, doi: 10.1107/S0021889888000275.

[46] I. Samajdar, P. Ratchev, B. Verlinden, and E. Aernoudt, "Hot working of AA1050—relating the microstructural and textural developments," *Acta Mater*, vol. 49, no. 10, pp. 1759–1769, Jun. 2001, doi: 10.1016/S1359-6454(01)00083-0.

[47] O. Engler, "Comparison of X-ray and electron backscatter diffraction textures for back-annealed Al–Mg alloys," *J Appl Crystallogr*, vol. 42, no. 6, pp. 1147–1157, Dec. 2009, doi: 10.1107/S0021889809041685.

[48] T. A. Bennett, R. H. Petrov, and L. A. I. Kestens, "Texture-induced surface roping in an automotive aluminium sheet," *Scr Mater*, vol. 61, no. 7, pp. 733–736, Oct. 2009, doi: 10.1016/j.scriptamat.2009.06.016.

[49] V. Randle, "Applications of electron backscatter diffraction to materials science: status in 2009," *J Mater Sci*, vol. 44, no. 16, pp. 4211–4218, Aug. 2009, doi: 10.1007/s10853-009-3570-0.

[50] O. Engler, X. W. Kong, and K. Lücke, "Influence of precipitates on the microstructure and texture during the rolling of Al-Cu and Al-Mn single crystals with rolling texture orientations," *Philosophical Magazine A*, vol. 81, no. 3, pp. 543–570, Mar. 2001, doi: 10.1080/01418610108212159.

[51] O.-G. Lademo, K. O. Pedersen, T. Berstad, T. Furu, and O. S. Hopperstad, "An experimental and numerical study on the formability of textured AlZnMg alloys," *European Journal of Mechanics - A/Solids*, vol. 27, no. 2, pp. 116–140, Mar. 2008, doi: 10.1016/j.euromechsol.2007.06.003.

[52] O. Engler and V. Randle, *Introduction to texture analysis: macrotexture, microtexture and orientation mapping* , 2nd edn. USA: Taylor and Francis, 2009.

[53] K. O. Pedersen, O.-G. Lademo, T. Berstad, T. Furu, and O. S. Hopperstad, "Influence of texture and grain structure on strain localisation and formability for AlMgSi alloys," *J Mater Process Technol*, vol. 200, no. 1–3, pp. 77–93, May 2008, doi: 10.1016/j.jmatprotec.2007.08.040.

[54] D. V. Wilson, "Strain-rate sensitivity and effects of strain rate in sheet forming," *Metals Technology*, vol. 7, no. 1, pp. 282–292, Jan. 1980, doi: 10.1179/030716980803287297.

[55] L. P. Ma, Z. Q. Liang, X. Bin Wang, W. X. Zhao, T. F. Zhou, and H. M. Yao, "Effect of Low-Frequency Pulsed Magnetic Treatment on Micro-Hardness of High Speed Steel," *Adv Mat Res*, vol. 797, pp. 663–666, Sep. 2013, doi: 10.4028/www.scientific.net/AMR.797.663.

[56] M. Shimotomai, "Influence of Magnetic-Field Gradients on the Pearlitic Transformation in Steels," *Mater Trans*, vol. 44, no. 12, pp. 2524–2528, 2003, doi: 10.2320/matertrans.44.2524.

[57] R. A. Vorob'ev and V. N. Dubinskii, "Effect of treatment by a pulsed magnetic field on the hardness and fracture strength of a hypereutectoid tool steel," *The Physics of Metals and Metallography*, vol. 115, no. 8, pp. 805–808, Aug. 2014, doi: 10.1134/S0031918X1408016X.

[58] M. Kraiev, "Analysis of the magnetoplasticity of steel by constructing the absorption spectrum of mechanical energy at magnetic resonance," *Multiscale and Multidisciplinary Modeling, Experiments and Design*, vol. 6, no. 4, pp. 573–577, Dec. 2023, doi: 10.1007/s41939-023-00167-8.

[59] M. Hou *et al.*, "Effects of Pulsed Magnetic Fields of Different Intensities on Dislocation Density, Residual Stress, and Hardness of Cr4Mo4V Steel," *Crystals (Basel)*, vol. 10, no. 2, p. 115, Feb. 2020, doi: 10.3390/cryst10020115.

[60] Y. Q. Wang, M. Gorley, S. Kabra, and E. Surrey, "Influence of a 1.5 T magnetic field on the tensile properties of Eurofer-97 steel," *Fusion Engineering and Design*, vol. 141, pp. 68–72, Apr. 2019, doi: 10.1016/j.fusengdes.2019.02.081.

[61] D. Zagulyaev, S. Konovalov, V. Shlyarov, and X. Chen, "Influence of constant magnetic field on plastic characteristics of paramagnetic metals," *Mater Res Express*, vol. 6, no. 9, p. 096523, Jul. 2019, doi: 10.1088/2053-1591/ab2c8a.

[62] Y. Zhang, N. Gey, C. He, X. Zhao, L. Zuo, and C. Esling, "High temperature tempering behaviors in a structural steel under high magnetic field," *Acta Mater*, vol. 52, no. 12, pp. 3467–3474, Jul. 2004, doi: 10.1016/j.actamat.2004.03.044.

[63] P. E. Goins, H. A. Murdoch, E. Hernández-Rivera, and M. A. Tschopp, "Effect of magnetic fields on microstructure evolution," *Comput Mater Sci*, vol. 150, pp. 464–474, Jul. 2018, doi: 10.1016/j.commatsci.2018.04.034.

[64] A. A. E. Sidhom, S. A. A. Sayed, and S. A. R. Naga, "The influence of magnetic field on the mechanical properties & microstructure of plain carbon steel," *Materials Science and Engineering: A*, vol. 682, pp. 636–639, Jan. 2017, doi: 10.1016/j.msea.2016.11.083.

[65] M. Domenjoud and L. Daniel, "Effects of plastic strain and reloading stress on the magneto-mechanical behavior of electrical steels: Experiments and modeling," *Mechanics of Materials*, vol. 176, p. 104510, Jan. 2023, doi: 10.1016/j.mechmat.2022.104510.

[66] Y. Zhang, J. Wang, M. Li, Z. Ren, and Y. He, "Magneto-Plasticity Behavior of Fe-3.2 wt.%Si Single Crystal under Transverse Static Magnetic Field," *J Mater Eng Perform*, vol. 32, no. 10, pp. 4749–4756, May 2023, doi: 10.1007/s11665-022-07429-5.

[67] Yu. I. Golovin, "Magnetoplastic effects in solids," *Physics of the Solid State*, vol. 46, no. 5, pp. 789–824, May 2004, doi: 10.1134/1.1744954.

[68] G. Kostorz and P. Müllner, "Magnetoplasticity," *International Journal of Materials Research*, vol. 96, no. 7, pp. 703–709, Feb. 2022, doi: 10.1515/ijmr-2005-0124.

[69] P. Müllner, V. A. Chernenko, and G. Kostorz, "A microscopic approach to the magnetic-field-induced deformation of martensite (magnetoplasticity)," *J Magn Magn Mater*, vol. 267, no. 3, pp. 325–334, Dec. 2003, doi: 10.1016/S0304-8853(03)00400-1.

[70] T. G. Kovaleva and A. D. Shevchuk, "Effect of a magnetic field on the elasticity characteristics for certain steels and alloys," *Strength of Materials*, vol. 15, no. 5, pp. 701–703, May 1983, doi: 10.1007/BF01523222.

[71] Yu. V. Osinskaya, S. S. Petrov, A. V. Pokoev, and V. V. Runov, "Small-angle neutron scattering study of the magnetoplastic effect in the beryllium bronze aged in magnetic fields," *Physics of the Solid State*, vol. 52, no. 3, pp. 523–526, Mar. 2010, doi: 10.1134/S1063783410030121.

[72] M. A. Verzhakovskaya, S. S. Petrov, and A. V. Pokoev, "Heterodiffusion of aluminum in α-iron in a pulsed magnetic field," *Technical Physics Letters*, vol. 33, no. 11, pp. 961–963, Nov. 2007, doi: 10.1134/S1063785007110211.

[73] J. Huber, J. Vogler, and E. Werner, "Multiscale modeling of the mechanical behavior of brazed Ni-based superalloy sheet metals," *Continuum Mechanics and Thermodynamics*, vol. 35, no. 1, pp. 211–229, Jan. 2023, doi: 10.1007/s00161-022-01172-x.

[74] Y. Wang, H. Ding, H. Zhang, R. Chen, J. Guo, and H. Fu, "Microstructures and fracture toughness of Ti–(43–48)Al–2Cr–2Nb prepared by electromagnetic cold crucible directional solidification," *Mater Des*, vol. 64, pp. 153–159, Dec. 2014, doi: 10.1016/j.matdes.2014.06.073.

[75] D. Atherton and J. Szpunar, "Effect of stress on magnetization and magnetostriction in pipeline steel," *IEEE Trans Magn*, vol. 22, no. 5, pp. 514–516, Sep. 1986, doi: 10.1109/TMAG.1986.1064373.

[76] E. Silva *et al.*, "Detection of the Magnetic Easy Direction in Steels Using Induced Magnetic Fields," *Metals (Basel)*, vol. 6, no. 12, p. 317, Dec. 2016, doi: 10.3390/met6120317.

[77] G. Mian and T. Yamaguchi, "Stress effect on the magnetization process in Ni-Cu-Zn ferrite in a weak field," *J Magn Magn Mater*, vol. 68, no. 3, pp. 351–357, Sep. 1987, doi: 10.1016/0304-8853(87)90013-8.

[78] A. Misra, "Theoretical study of the fracture-induced magnetic effect in ferromagnetic materials," *Phys Lett A*, vol. 62, no. 4, pp. 234–236, Aug. 1977, doi: 10.1016/0375-9601(77)90781-2.

[79] V. Permiakov, L. Dupré, A. Pulnikov, and J. Melkebeek, "2D magnetization of grain-oriented 3%-Si steel under uniaxial stress," *J Magn Magn Mater*, vol. 290–291, pp. 1495–1498, Apr. 2005, doi: 10.1016/j.jmmm.2004.11.558.

[80] T. Matsuo, "Magnetization process analysis using a simplified domain structure model," *J Appl Phys*, vol. 109, no. 7, Apr. 2011, doi: 10.1063/1.3556923.

[81] S. Ito, T. Mifune, T. Matsuo, and C. Kaido, "Macroscopic magnetization modeling of silicon steel sheets using an assembly of six-domain particles," *J Appl Phys*, vol. 117, no. 17, May 2015, doi: 10.1063/1.4915105.

[82] D. C. Jiles, "Theory of the magnetomechanical effect," *J Phys D Appl Phys*, vol. 28, no. 8, pp. 1537–1546, Aug. 1995, doi: 10.1088/0022-3727/28/8/001.

[83] R. R. Birss, C. A. Faunce, and E. D. Isaac, "Magnetomechanical effects in iron and iron-carbon alloys," *J Phys D Appl Phys*, vol. 4, no. 7, p. 322, Jul. 1971, doi: 10.1088/0022-3727/4/7/322.

[84] D. J. Craik and M. J. Wood, "Magnetization changes induced by stress in a constant applied field," *J Phys D Appl Phys*, vol. 3, no. 7, p. 303, Jul. 1970, doi: 10.1088/0022-3727/3/7/303.

[85] C. Saka, K. Shiiki, and K. Shinagawa, "Simulation of domain structure for magnetic thin film in an applied field," *J Appl Phys*, vol. 68, no. 1, pp. 263–268, Jul. 1990, doi: 10.1063/1.347126.

[86] S. Ren and X. Ren, "Studies on laws of stress-magnetization based on magnetic memory testing technique," *J Magn Magn Mater*, vol. 449, pp. 165–171, Mar. 2018, doi: 10.1016/j.jmmm.2017.09.050.

[87] O. Perevertov, "Influence of the residual stress on the magnetization process in mild steel," *J Phys D Appl Phys*, vol. 40, no. 4, pp. 949–954, Feb. 2007, doi: 10.1088/0022-3727/40/4/004.

[88] J. Li, M. Xu, J. Leng, and M. Xu, "Modeling plastic deformation effect on magnetization in ferromagnetic materials," *J Appl Phys*, vol. 111, no. 6, Mar. 2012, doi: 10.1063/1.3695460.

[89] R. Langman, "The effect of stress on the magnetization of mild steel at moderate field strengths," *IEEE Trans Magn*, vol. 21, no. 4, pp. 1314–1320, Jul. 1985, doi: 10.1109/TMAG.1985.1063901.

[90] H. Kusanagi, H. Kimura, and S. Sasaki, "Stress effect on the magnitude of acoustic emission during magnetization of ferromagnetic materials," *J Appl Phys*, vol. 50, no. 4, pp. 2985–2987, Apr. 1979, doi: 10.1063/1.326183.

[91] D. Atherton and D. Jiles, "Effects of stress on the magnetization of steel," *IEEE Trans Magn*, vol. 19, no. 5, pp. 2021–2023, Sep. 1983, doi: 10.1109/TMAG.1983.1062784.

[92] V. Permiakov, A. Pulnikov, L. Dupre, and J. Melkebeek, "Rotational Magnetization in Nonoriented Fe-Si Steel Under Uniaxial Compressive and Tensile Stresses," *IEEE Trans Magn*, vol. 40, no. 4, pp. 2760–2762, Jul. 2004, doi: 10.1109/TMAG.2004.832265.

[93] D. Lihong, X. Binshi, D. Shiyun, C. Qunzhi, and W. Dan, "Variation of stress-induced magnetic signals during tensile testing of ferromagnetic steels," *NDT & E*

International, vol. 41, no. 3, pp. 184–189, Apr. 2008, doi: 10.1016/j.ndteint.2007.10.003.

[94] S. Kim, J. Lee, F. Barlat, and M. G. Lee, "Formability prediction of advanced high strength steels using constitutive models characterized by uniaxial and biaxial experiments," *J Mater Process Technol*, vol. 213, no. 11, pp. 1929–1942, 2013, doi: 10.1016/j.jmatprotec.2013.05.015.

[95] A. Vinogradov, I. S. Yasnikov, H. Matsuyama, M. Uchida, Y. Kaneko, and Y. Estrin, "Controlling strength and ductility: Dislocation-based model of necking instability and its verification for ultrafine grain 316L steel," *Acta Mater*, vol. 106, pp. 295–303, Mar. 2016, doi: 10.1016/j.actamat.2016.01.005.

[96] S. Panich, F. Barlat, V. Uthaisangsuk, S. Suranuntchai, and S. Jirathearanat, "Experimental and theoretical formability analysis using strain and stress based forming limit diagram for advanced high strength steels," *Mater Des*, vol. 51, pp. 756–766, 2013, doi: 10.1016/j.matdes.2013.04.080.

[97] A. Kumar Singh, S. Jha, and P. M. Pandey, "Design and development of nanofinishing process for 3D surfaces using ball end MR finishing tool," *Int J Mach Tools Manuf*, vol. 51, no. 2, pp. 142–151, Feb. 2011, doi: 10.1016/j.ijmachtools.2010.10.002.

[98] A. K. Sawhney, *Electrical Machine Design*. New Delhi, India.: Dhanpat Rai Publishing Co., 2016.

[99] C. Du, X. Chen, Y. Wang, J. Li, and D. Yu, "An Adaptive 6-DOF Tracking Method by Hybrid Sensing for Ultrasonic Endoscopes," *Sensors*, vol. 14, no. 6, pp. 9961–9983, Jun. 2014, doi: 10.3390/s140609961.

[100] X. Guo, G. Yan, and W. He, "A position telemetric method for implantable microcapsules in the gastrointestinal tract," *Meas Sci Technol*, vol. 19, no. 4, p. 045201, Apr. 2008, doi: 10.1088/0957-0233/19/4/045201.

[101] R. D. Yadav and A. K. Singh, "A novel magnetorheological gear profile finishing with high shape accuracy," *Int J Mach Tools Manuf*, vol. 139, pp. 75–92, Apr. 2019, doi: 10.1016/j.ijmachtools.2019.02.001.

[102] ASTM 517-00, "Standard Test Method for Plastic Strain Ratio R for Sheet Metal ," *ASTM Book of Standards*, pp. 1–8, 2010.

[103] J. Fish and T. Belytschko, *A first course in finite elements* . John Wiley & Sons, 2007.

[104] M. Singh, A. K. Choubey, and C. Sasikumar, "Formability Analysis of Aluminium Alloy by Erichsen Cupping Test Method," *Mater Today Proc*, vol. 4, no. 2, pp. 805–810, 2017, doi: 10.1016/j.matpr.2017.01.089.

[105] M. R. N. Reddy, M. S. Theja, and M. G. Tilak, "Modified Erichsen Cupping Test for Copper, Brass, Aluminium and Stainless Steel," *The SIJ Transactions on Industrial, Financial & Business Management*, vol. 06, no. 02, pp. 01–06, Apr. 2018, doi: 10.9756/SIJIFBM/V6I2/0102550102.

[106] A. S. Hamada, A. Kisko, A. Khosravifard, M. A. Hassan, L. P. Karjalainen, and D. Porter, "Ductility and formability of three high-Mn TWIP steels in quasi-static and high-speed tensile and Erichsen tests," *Materials Science and Engineering: A*, vol. 712, pp. 255–265, Jan. 2018, doi: 10.1016/j.msea.2017.11.111.

[107] F. S. Sorce, S. Ngo, C. Lowe, and A. C. Taylor, "Quantification of coating surface strains in Erichsen cupping tests," *J Mater Sci*, vol. 54, no. 10, pp. 7997–8009, May 2019, doi: 10.1007/s10853-019-03392-0.

[108] J. Singh *et al.*, "Heterogeneity in deformation and twinning behaviors through the thickness direction in E-form Mg alloy sheets during an Erichsen test," *Materials Science and Engineering: A*, vol. 729, pp. 370–384, Jun. 2018, doi: 10.1016/j.msea.2018.05.072.

[109] C. G. Dengiz and K. Yıldızlı, "Experimental and numerical study of process limits for deep drawing of dome-structured sheet metals," *The International Journal of Advanced Manufacturing Technology*, vol. 92, no. 9–12, pp. 4457–4472, Oct. 2017, doi: 10.1007/s00170-017-0450-7.

[110] R. WAGONER and M. LI, "Simulation of springback: Through-thickness integration," *Int J Plast*, vol. 23, no. 3, pp. 345–360, Mar. 2007, doi: 10.1016/j.ijplas.2006.04.005.

[111] R. H. Wagoner, "Advances in Springback," in *AIP Conference Proceedings*, AIP, 2005, pp. 209–214. doi: 10.1063/1.2011219.

[112] W. L. Xu, C. H. Ma, C. H. Li, and W. J. Feng, "Sensitive factors in springback simulation for sheet metal forming," *J Mater Process Technol*, vol. 151, no. 1–3, pp. 217–222, Sep. 2004, doi: 10.1016/j.jmatprotec.2004.04.044.

[113] D. Banabic, *Sheet metal forming processes: constitutive modelling and numerical simulation*. Springer Science & Business Media, 2010.

[114] D. Hibbit, B. Karlsson, and P Sorensen, *ABAQUS/Standard Analysis User's Manual* . USA.: Hibbit, Karlsson, Sorensen Inc, Providence, 2010.

[115] S. Chatti and N. Hermi, "The effect of non-linear recovery on springback prediction," *Comput Struct*, vol. 89, no. 13–14, pp. 1367–1377, Jul. 2011, doi: 10.1016/j.compstruc.2011.03.010.

[116] L. Papeleux and J.-P. Ponthot, "Finite element simulation of springback in sheet metal forming," *J Mater Process Technol*, vol. 125–126, pp. 785–791, Sep. 2002, doi: 10.1016/S0924-0136(02)00393-X.

[117] J.-W. Yoon, F. Pourboghrat, K. Chung, and D.-Y. Yang, "Springback prediction for sheet metal forming process using a 3D hybrid membrane/shell method," *Int J Mech Sci*, vol. 44, no. 10, pp. 2133–2153, Oct. 2002, doi: 10.1016/S0020-7403(02)00165-0.

[118] T. Diehl, D. Carroll, B.K Nagaraj, and P. Motorola, " Using digital signal processing (DSP) to significantly improve the interpretation of ABAQUS/Explicit results," *ABAQUS Users Conference Proceedings*, pp. 25–28, May 1999.

[119] M. Levy and D. Karki, "Nonreciprocal Transverse Photonic Spin and Magnetization-Induced Electromagnetic Spin-Orbit Coupling," *Sci Rep*, vol. 7, no. 1, p. 39972, Jan. 2017, doi: 10.1038/srep39972.

[120] J. H. Simpson, *NMR case studies: data analysis of complicated molecules*. Elsevier , 2017.

[121] A. Ghandi, M. Shamanian, A. Rezaeian, M. R. Salmani, and J. A. Szpunar, "Study of DP590 Microstructure Welded with Resistance Spot Welding Method by Using EBSD Technique," *Metallography, Microstructure, and Analysis*, vol. 10, no. 2, pp. 266–275, Apr. 2021, doi: 10.1007/s13632-021-00727-9.

[122] J.-A. Yan, C.-Y. Wang, and S.-Y. Wang, "Generalized-stacking-fault energy and dislocation properties in ***bcc*** Fe: A first-principles study," *Phys Rev B*, vol. 70, no. 17, p. 174105, Nov. 2004, doi: 10.1103/PhysRevB.70.174105.

[123] B. Devincre, T. Hoc, and L. P. Kubin, "Collinear interactions of dislocations and slip systems," *Materials Science and Engineering: A*, vol. 400–401, pp. 182–185, Jul. 2005, doi: 10.1016/j.msea.2005.02.071.

[124] N. Aravas and E. C. Aifantis, "On the geometry of slip and spin in finite plastic deformation," *Int J Plast*, vol. 7, no. 3, pp. 141–160, Jan. 1991, doi: 10.1016/0749-6419(91)90028-W.

[125] P. Chen *et al.*, "In-situ EBSD study of the active slip systems and lattice rotation behavior of surface grains in aluminum alloy during tensile deformation," *Materials Science and Engineering: A*, vol. 580, pp. 114–124, Sep. 2013, doi: 10.1016/j.msea.2013.05.046.

[126] S. Li, C. Guo, L. Hao, Y. Kang, and Y. An, "In-situ EBSD study of deformation behaviour of 600 MPa grade dual phase steel during uniaxial tensile tests," *Materials Science and Engineering: A*, vol. 759, pp. 624–632, Jun. 2019, doi: 10.1016/j.msea.2019.05.083.

[127] N. Saeidi, F. Ashrafizadeh, B. Niroumand, and F. Barlat, "EBSD study of micromechanisms involved in high deformation ability of DP steels," *Mater Des*, vol. 87, pp. 130–137, Dec. 2015, doi: 10.1016/j.matdes.2015.07.134.

PUBLICATIONS BASED ON THE PRESENT WORK

The followings are the publications in journals and conferences based on the present work.

International Journals: -

1. Ravi Datt Yadav, and Vijay Gautam, "Effect of Magnetic Field on Deformation Behavior of a Steel Sheet in Uniaxial Tension." *Journal of Testing and Evaluation* ASTM 52.1 (2023).
2. Ravi Datt Yadav, and Vijay Gautam, "Effect of magnetic field on mechanical properties of an advanced high strength steel sheet." *Materials Letters* (2024): 136087.

Conferences: -

1. Ravi Datt Yadav, and Vijay Gautam, 2022, A hybrid method for assigning containers to automated guided vehicle in automated container terminal, Recent Advances in Materials, Manufacturing and Thermal Engineering (RAMMTE 2022), Id –181.
2. Ravi Datt Yadav, and Vijay Gautam, 2023, Mechanical Behaviour of Dual Phase Steel Sheets, International Conference on Computational and Experimental Methods in Mechanical Engineering (ICCEMME 2023), Id-870.

BIO DATA

Mr. Ravi Datt Yadav was born in Haryana on 5th December 1988. He graduated from Maharishi Dayanand University in 2010 and did his post-graduation in Production Engineering from Thapar University, Patiala, in 2018. Currently, he is Submitted a Ph.D. thesis at Delhi Technological University, He is a full-time scholar in the Department of Mechanical Engineering, DTU Delhi, under the guidance of Prof. Vijay Gautam.

He has five years of industrial experience in the field of Manufacturing Processes, quality control and vendor development (Munjal Showa Limited). He has also worked in DRDO as research scientist scholar in the DIAT Pune. He has also worked as SRF in the Thapar University, Patiala. He has published his work in high PhD work in the ASTAND impact international journals and international conferences.